OPTICAL SPECTRAL PROPERTIES OF ACTIVE GALACTIC NUCLEI AND QUASARS

Thesis by

Howard Kwong Chew Yee

In Partial Fulfillment of the Requirements

for the Degree of

Doctor of Philosophy

California Institute of Technology

Pasadena, California

1981

(Submitted October 30, 1980)

To

Mother and Father

and

To

Grandmother (1892-1980)

who fought valiantly

ACKNOWLEDGEMENTS

To my advisor Dr. J. B. Oke, my deepest gratitude for not only providing most of the data for this thesis, but also spending endless hours discussing various ideas, pouring over my many "fierce" drafts of each chapter, and disentangling my convoluted logic.

To all those who helped along the way, especially John Hoessel and Steve Kent for teaching me how to observe with that fine piece of instrument on Palomar Mountain; Bill Sebok for providing the computer program for reduction of the direct-SIT data; and Doug Rabin for showing me the fine arts of troffing one's thesis, a sincere thank you.

And last, but certainly not least, to my many fellow graduate students -- cellar dwellers of past and present, my special thanks for providing friendship, help, and comic relief, making life in the abyss of Robinson tolerable, and even pleasant at times.

ABSTRACT

Four separate investigations dealing with the properties of optical continuum and emission-lines of active galactic nuclei (AGN) and quasars are presented.

Multichannel scans of 3CR radio galaxies are decomposed by using a two-component model -- an elliptical galaxy and a power-law nonthermal component. It is found that there is a strong correlation between the luminosity of the power-law component and the strength of the Balmer emission-lines. In most cases, by extrapolating to the Lyman continuum, the power-law models derived provide enough ionizing radiation to account for the Balmer line strengths.

Extending the study of radio galaxies to include Seyfert galaxies and quasars, it is found that there is a strong continuity between broad-line AGN's and quasars in terms of similarities in the correlations between line luminosities and nonthermal continuum luminosity. There is a tight correlation between Hβ and nonthermal luminosity for all objects, suggesting that the Balmer lines arise from recombination after photoionization by the central continuum, and that parameters such as the overall spectral index and the covering factor are similar. Relative to the nonthermal continuum, the forbidden lines of the broad-line objects are approximately one order of magnitude weaker than those of the narrow-line objects. This is consistent with the view that forbidden lines are suppressed in the dense broad-line region of the broad-line objects.

Next, a study of the variability of absolute optical energy distribution and emission-lines of the N-galaxies 3C 382 and 3C 390.3 is made. By assuming that the nuclear component retains its spectral shape despite the variation, consistent decomposition of the spectrum into its nuclear and ellitipcial galaxy component can be made. Within each object, the narrow forbidden lines have remained constant, but the broad Balmer lines vary with the luminosity of the central com-

ponent (L_{NT}) as a power-law: L_{NT}^{Γ} with $\Gamma < 0.5$. This relation can be explained by having two components of broad-line gas clouds – one having a time-scale for variability of a few months, the other, years. Variability of Balmer line profiles in these two objects are also discussed.

Lastly, a preliminary study of surface photometry of Markarian Seyfert galaxies are presented. It is found that the properties of the underlying galaxies such as scale-length and surface brightness of the disk, color, and total brightness, do not depart systematically from those of luminous normal spiral galaxies. In addition, along with the results from the study of radio galaxies, it is found that there is no correlation between the luminosity of nuclear component and the brightness of the host-galaxy.

TABLE OF CONTENTS

INTRODUCTION

This thesis contains four separate but related studies of the properties of optical continuum and emission-lines of active galactic nuclei and quasars. Each of these forms a self-contained chapter. The first three are articles either published in, or submitted to the Astrophysical Journal. Chapters one and three were done in collaboration with J. B. Oke.

A large part of the work described in this thesis concerns the nuclear continuum energy distribution and its relationship to the emission-line spectrum of extragalaxctic active objects. A major problem in dealing with the nonthermal continuum of these objects is the contamination of the spectra by the underlying galaxy. Various solutions to circumvent this problem are explored.

In chapter one, multichannel spectrophotometry (MCSP) of 3CR radio galaxies are studied. The optical energy distributions are modelled by using a standard elliptical galaxy and power-law nonthermal component. Chapter two is basically an extention of the work of chapter one to encompass all types of active objects -- radio galaxies, Seyfert galaxies and quasars, allowing comparisons of the properties of different classes of active objects to be made. In chapter three, variability of the absolute energy distribution and emission-lines is studied, using data of two N-galaxies covering a period of ~ 10 years. The variability of these two objects offers much insight into the relationship between the continuum and the emission-lines, and it also provided an unambiguous method for decomposing the spectrum. Chapter four is a preliminary study of the host-galaxy of these objects using digital surface photometry of a number of Markarian Seyfert galaxies. It is hoped that by studying the galaxy component of the active galaxies, not only can one compare their properties with those of the normal galaxies, but also obtain some constraints for decomposing the spectrum of these objects.

CHAPTER 1

PHOTOELECTRIC SPECTROPHOTOMETRY OF RADIO GALAXIES

THE ASTROPHYSICAL JOURNAL, 226:753–769, 1978 December 15

PHOTOELECTRIC SPECTROPHOTOMETRY OF RADIO GALAXIES

H. K. C. YEE AND J. B. OKE
Hale Observatories, California Institute of Technology, Carnegie Institution of Washington
Received 1977 December 28; accepted 1978 June 27

ABSTRACT

The multichannel spectrometer of the Hale 5 m telescope has been used to obtain spectrophotometric observations of 26 3CR radio galaxies. The spectral characteristics of these objects range from N galaxies with very strong and broad emission lines to normal E-type galaxies with only absorption lines. Emission lines are usually correlated with accompanying excess radiation in the ultraviolet. Each spectral energy distribution is decomposed into two components; one component is a power-law spectrum, while the other is an underlying normal E-type galaxy spectrum. The Balmer emission line intensity is well correlated with the power-law luminosity in the optical spectrum, suggesting that photoionization by Lyman continuum photons followed by recombination is the dominating mechanism. In most cases, the power-law models derived provide enough ionizing photons to account for the Balmer line strengths; in those few cases which do not fit, there is probably another ultraviolet source of radiation, which is hinted at by the observations. There is a weak correlation between radio emission and the power-law optical emission; this correlation is improved if only the central compact radio source is included in the radio flux.

Subject headings: radio sources: general — spectrophotometry

I. INTRODUCTION

Since the first optical identification of extragalactic radio sources was made by Baade and Minkowski (1954), 3CR radio sources have been found to be associated with all classes of galaxies. They include strong emission line objects such as Seyfert and N galaxies, and normal quiescent objects such as elliptical galaxies. While the peculiar emission line sources such as 3C 84 (NGC 1275) and 3C 405 (Cyg A) have attracted much attention and are well studied, it is of interest to obtain a homogeneous set of optical data on all types of radio galaxies. With such a sample, one can investigate general radio and optical properties of active galactic nuclei. Such a program to study the emission line and continuum characteristics has been carried out using the multichannel spectrophotometer on the Hale 5 m telescope.

II. OBSERVATION AND DATA REDUCTION

The absolute energy distributions from 3200 to 10000 Å of 26 radio galaxies were obtained during the period of 1971 to 1976. This modest sample contains a representative half of the list given by Schmidt (1965), plus nine others. The galaxies observed are listed in Table 1. Also tabulated are their redshifts, galactic latitudes, morphological types, and references, in columns (2), (3), (8), and (11), respectively. The spectral energy distributions were obtained with the multichannel spectrometer. The majority of them were obtained with a bandwidth of 80 Å for $\lambda \lesssim 5800$ Å, and 160 Å for $\lambda \gtrsim 5800$ Å. A few have bandwidths which are half as large. The entrance aperture diameters used are listed in Table 1. Integration time for each observation was typically 600 seconds.

The absolute fluxes are based on the calibration of α Lyrae by Oke and Schild (1970). In cases where several exposures of the same source were made, they have been averaged, weighted according to the integration time to form a single final energy distribution. The final flux densities (before reddening correction), f_ν (ergs s^{-1} cm^{-2} Hz^{-1}), are listed in Table 2 in the form of $AB = -2.5 \log f_\nu - 48.60$. Representative standard deviations on the energy distributions are listed in Table 3. The AB values at 5460 Å ($\log \nu = 14.740$) give the approximate visual magnitudes V_{AB} of the sources and are listed in Table 1.

The data are corrected for reddening before analysis, using the reddening-free polar-cap model of Sandage (1973*b*) for galactic latitude dependence (except for Cyg A), and Whitford's relation (Whitford 1958) for the wavelength dependence. The equivalent E_{B-V} values are listed in column (7) of Table 1. The value of AB corresponding to the redshifted position of $\lambda_0 = 5460$ Å and corrected for reddening is listed as V_I in Table 1.

The reddening of Cyg A (3C 405) deserves special comment. Sandage (1972*a*) used $A_B = 1.20$, derived from his photometric measurement. However, Osterbrock and Miller (1975), using the Balmer decrement which they obtained from the nucleus, and assuming a photoionization-recombination model with $T = 10^4$ K and $N_e = 10^4$ cm^{-3}, obtained an extinction of $A_B = 2.85$. Van den Bergh (1976) used an elliptical galaxy near Cyg A to obtain an extinction of $A_B \approx 1.7$. In view of the large discrepancies in the existing values, we derived a reddening value by yet another method. We obtained a scan with the multichannel spectrometer using a 5″ aperture at an angular distance of 8″ north of the nucleus. This observed energy distribution was compared with that of a typical elliptical

TABLE 1

PROPERTIES OF THE RADIO GALAXIES OBSERVED

Object (1)	z (2)	b^{II} (3)	Aperture (arcsec) (4)	V_{AB} (5)	V_I (6)	E_{B-V} (7)	Morphological Type (8)	log L_B (9)	Radio Structure* (10)	Ref. (11)
3C 17.....	0.2197	−65	7	18.53	18.05	0.00	E, N	43.99	U	1
3C 28.....	0.1952	−37	7	18.30	17.78	0.02	E	43.43	CD	1
3C 31.....	0.017	−30	14	13.63	13.53	0.03	E	41.58	S	5
3C 33.....	0.0595	−50	9.9	16.31	16.10	0	D	43.11	T	1
3C 76.1.....	0.0326	−36	14	15.71	15.55	0.02	D	41.94	D	3, 4
3C 78.....	0.0288	−44	9.9	14.13	14.05	0.015	D	42.24	S	1
3C 79.....	0.2559	−34	7	18.89	18.15	0.03	N	44.01	D	1
3C 88.....	0.0302	−43	9.9	15.79	15.70	0.015	D	42.09	D	1
3C 98.....	0.0306	−31	9.9	15.65	15.20	0.03	E	42.50	CD	1
3C 109.....	0.3056	−28	7	17.93	17.00	0.04	N	44.14	T	3
3C 171.....	0.2384	+22	5	19.45	18.80	0.06	N	43.80	D	1
3C 192.....	0.0596	+26	14	16.27	15.78	0.04	E	42.73	C	2
3C 198.....	0.0815	+23	7	17.42	17.25	0.05	E	42.54	D	1
3C 219.....	0.1744	+45	7	17.80	17.10	0.01	D	43.84	D	1
3C 234.....	0.1848	+53	9.9	17.64	17.23	0	N	43.76	T	1
3C 264.....	0.0208	+73	9.9	14.31	14.30	0	E	41.81	S	1
3C 277.3.....	0.0857	+89	9.9	16.43	16.25	0	D	42.82	CT†	1
3C 293.....	0.045	+76	9.9	15.87	15.70	0	D	42.38	S	2, 3
3C 296.....	0.0237	+64	9.9	13.85	13.83	0	E	41.79	D	2
3C 305.....	0.0416	+49	9.9	14.90	14.78	0.01	Sa?	42.14	D†	2
3C 382.....	0.0578	+18	7	15.38	15.05	0.07	D	42.75	CT	1
3C 390.3.....	0.0569	+27	9.9	15.44	15.25	0.04	N	43.02	T	2
3C 405.....	0.0570	+5	9.9	16.90	15.20	0.5	D	45.11	T	6
3C 445.....	0.0569	−46	9.9	16.49	16.40	0.01	N	42.71	D	1
3C 456.....	0.2330	−46	7	19.30	18.60	0.01	E?	43.58	U	1
3C 459.....	0.2199	−52	7	17.64	17.43	0	N	43.81	U	1, 3

* Radio structure: S = single, D = double, T = triple, C = complex, U = unresolved at 1.4 GHz at 20″.

† Radio structure embedded in galaxy.

REFERENCES.—(1) Schmidt 1965; (2) Sandage 1966; (3) Burbidge 1967; (4) Sandage 1967; (5) Wyndham 1966; (6) Baade and Minkowski 1954.

galaxy (described later) to determine the reddening. The energy distributions match quite well and yield $A_B = 2.0 \pm 0.1$, corresponding to $E_{B-V} \approx 0.50$; this value is close to that of van den Bergh's nearby elliptical galaxy. Note that this value does not allow for any internal reddening within the nucleus itself. Since internal reddening corrections are not made for the other galaxies, we adopt $A_B = 2.0$.

III. RADIO PROPERTIES

All of the sources in our sample show the typical power-law spectrum in the radio region. Defining flux $\propto \nu^{\alpha}$, then in all cases a relatively steep spectral index, $\alpha < -0.5$, is obtained. The radio flux data used here are those of Kellermann, Pauliny-Toth, and Williams (1969). A radio luminosity was computed for each source, using the data with an arbitrarily chosen bandwidth between 30 MHz and 15 GHz at the rest frame of the emitter, and using $q_0 = 0$ and $H_0 = 55$ km s^{-1} Mpc^{-1}. Our sample contains rather bright radio sources with radio luminosities ranging from $10^{41.6}$ to over 10^{45} ergs s^{-1}. The values are tabulated in column (9) of Table 1. In general, N galaxies dominate the upper range of the luminosity, while elliptical galaxies tend to occupy the lower end.

Almost all of these sources have been observed by interferometry, so that structures are available in the literature (see Macdonald, Kenderdine, and Neville 1968; Mackay 1969; Elsmore and Mackay 1969; Fomalont 1971). Many show the classical double structure, while some are single components, often unresolved at $<20''$. The structure of each source is described schematically in column (10) of Table 1.

IV. OPTICAL PROPERTIES

a) Emission Lines

There is a very wide range of emission line strengths seen in the sample, ranging from the very strong emission lines of N galaxies with equivalent widths of hundreds of angstroms to the extremely weak or even undiscernible lines in some elliptical galaxies. Due to the poor resolution of the multichannel data, lines such as Hα and [N II] $\lambda\lambda$6548, 6584 and [O III] λ4363 and Hγ are often blended. Line profiles are unobtainable. Representative scans are shown in Figures 1 and 2. The emitted luminosities (after galactic reddening correction) of the measurable lines, using $q_0 = 0$ and $H_0 = 55$, are listed in Table 4. Also listed are the equivalent widths of Hβ. The errors quoted for the line strength come from two sources. One is the uncertainty in the actual data of the channel where the

TABLE 2A

OBSERVATIONS

λ	3C17	3C28	3C31	3C33	3C79	3C171	3C277.3	3C296	3C456	λ	3C88	3C219	3C234
3260...	19.92	20.27	16.62	18.53	19.86	20.95	...	17.00	20.23	3260...	19.11	20.05	18.55
3340...	20.01	20.64	16.38	18.57	20.31	20.92	18.85	16.59	20.32	3330...	18.89	20.12	18.16
3420...	19.31	20.65	16.39	18.52	20.99	20.68	19.00	16.48	20.00	3410...	18.75	20.24	18.43
3500...	19.86	20.72	16.21	18.22	19.91	20.81	18.85	16.42	20.42	3490...	18.38	20.08	18.42
3580...	19.97	20.48	16.10	18.28	20.27	21.35	18.68	16.32	20.27	3570...	18.20	19.77	18.48
3660...	20.00	20.25	16.05	18.02	20.41	21.09	18.41	16.25	20.63	3650...	18.27	19.79	18.28
3740...	20.26	20.53	15.81	18.10	20.21	20.75	18.56	16.00	20.27	3730...	18.14	19.68	18.26
3820...	20.17	20.31	15.86	18.13	20.24	20.92	18.20	16.03	20.23	3810...	17.86	19.95	18.28
3900...	19.87	20.47	15.98	17.94	20.13	20.87	18.43	16.05	20.22	3890...	18.09	20.00	18.36
3980...	19.95	20.23	15.63	17.25	20.06	20.73	18.05	15.86	20.15	3970...	17.95	19.55	18.09
4060...	19.75	19.86	15.19	17.53	19.72	20.61	18.00	15.52	19.89	4050...	17.76	19.34	18.14
4140...	19.76	19.89	14.93	17.61	19.90	20.66	18.14	15.09	19.85	4130...	17.23	19.48	18.11
4220...	19.89	19.77	14.93	17.33	19.51	20.42	18.15	15.03	19.68	4210...	17.10	19.52	18.07
4300...	19.67	19.83	14.79	17.11	19.26	20.53	17.79	14.99	19.85	4290...	17.01	19.05	17.62
4380...	19.54	19.76	14.75	17.16	19.66	20.51	17.36	14.94	20.24	4370...	16.94	18.67	17.57
4460...	19.42	19.30	14.54	17.08	19.65	20.40	17.32	14.72	19.99	4450...	16.86	19.08	17.58
4540...	18.69	19.57	14.36	17.07	19.62	20.23	17.26	14.55	19.75	4530...	16.63	18.77	17.98
4620...	19.36	19.49	14.19	16.80	19.49	18.48	17.23	14.40	18.48	4610...	16.42	18.94	17.53
4700...	19.17	19.47	14.10	16.75	18.57	20.34	17.17	14.28	19.66	4690...	16.42	18.59	17.80
4780...	19.38	19.03	14.06	16.60	19.74	19.61	16.98	14.25	19.13	4770...	16.25	18.35	17.99
4860...	18.91	18.97	13.94	16.51	18.96	20.01	16.81	14.15	19.57	4850...	16.16	18.45	17.79
4940...	18.91	18.95	13.94	16.49	19.74	19.81	16.69	14.11	19.41	4930...	16.10	18.47	17.95
5020...	18.83	18.87	13.89	16.41	19.05	19.87	16.64	14.10	19.22	5010...	16.06	18.33	17.95
5100...	18.96	18.83	13.91	16.38	19.15	19.72	16.64	14.07	19.41	5090...	15.98	18.07	17.78
5180...	18.86	18.70	13.90	16.29	19.10	19.90	16.58	14.05	19.38	5170...	15.95	18.06	17.30
5260...	18.64	18.60	13.94	15.72	19.21	19.80	16.49	14.01	19.19	5250...	15.98	18.01	17.75
5340...	18.48	18.72	13.77	15.72	19.12	19.47	16.45	14.02	19.09	5330...	16.03	17.91	17.65
5420...	18.60	18.31	13.63	16.32	18.83	19.39	16.36	13.87	19.16	5410...	15.85	17.84	17.68
5500...	18.45	18.30	13.64	16.29	18.96	19.50	16.52	13.82	19.47	5490...	15.75	17.76	17.60
5580...	18.57	18.27	13.60	16.21	18.77	19.51	16.52	13.80	19.09	5570...	15.72	17.71	17.29
5660...	18.43	18.18	13.55	16.12	18.75	19.50	16.51	13.77	18.99	5650...	15.70	17.66	17.48
5740...	18.42	18.20	13.52	16.11	18.82	19.28	16.34	13.72	18.94	5730...	15.68	17.59	17.43
5760...	18.38	18.23	13.49	16.17	18.76	19.43	16.37	13.79	18.96	5800...	15.60	17.38	16.62
5920...	18.15	18.27	13.44	16.09	18.65	19.19	16.21	13.68	18.85	5880...	15.57	...	15.84
6080...	17.74	18.06	13.35	15.98	18.28	18.42	16.16	13.69	17.97	5900...	...	17.52	15.46
6240...	18.30	18.02	13.27	15.86	16.74	17.89	16.02	...	17.46	6060...	15.50	17.70	17.30
6400...	18.14	17.89	13.26	15.79	18.47	19.15	16.02	13.60	18.65	6220...	15.36	17.49	17.28
6560...	18.05	17.80	13.18	15.76	18.38	18.93	15.99	13.47	18.63	6380...	15.36	17.38	17.25
6720...	18.00	17.72	13.20	15.66	18.27	18.97	16.01	13.45	18.65	6540...	15.24	17.36	17.17
6880...	18.00	17.64	13.09	15.38	18.16	18.88	15.90	13.45	18.57	6700...	15.13	17.31	17.12
7040...	17.86	17.64	13.00	15.44	18.14	18.91	15.85	13.33	18.46	6860...	15.11	17.23	17.13
7200...	17.88	17.56	13.01	15.51	18.04	18.65	15.80	13.23	18.43	7020...	15.12	17.19	17.07
7360...	17.80	17.57	12.95	15.49	18.02	18.84	15.77	13.30	18.47	7180...	15.07	17.12	16.90
7520...	17.78	17.47	12.83	15.49	17.93	18.56	15.78	13.22	18.32	7340...	15.05	17.03	16.96
7680...	17.60	17.41	12.72	15.40	18.12	18.68	15.71	13.08	18.35	7500...	14.95	16.93	16.76
7840...	17.66	17.19	12.75	15.36	17.82	18.14	15.74	13.28	18.12	7660...	14.86	16.59	16.59
8000...	16.94	17.29	12.73	15.26	17.80	18.36	15.70	13.24	17.68	7820...	14.79	16.74	15.30
8160...	17.21	17.22	12.62	15.26	17.26	17.21	15.53	13.10	16.84	7980...	14.79	16.88	16.35
8320...	17.59	17.18	12.52	15.16	17.03	17.84	15.58	12.90	17.54	8140...	14.74	16.91	16.57
8480...	17.43	17.24	12.53	15.12	17.31	18.62	15.52	12.92	17.86	8300...	14.62	16.82	16.60
8640...	17.43	17.15	12.59	15.11	17.48	18.18	15.55	13.00	18.07	8460...	14.56	16.87	16.62
8800...	17.54	17.08	12.46	15.10	17.52	18.38	15.43	12.91	17.94	8620...	14.54	16.58	16.59
8960...	17.09	17.07	12.37	15.02	17.67	18.41	15.43	12.81	17.85	8780...	14.56	16.63	16.54
9120...	17.33	16.97	12.31	15.02	17.40	18.25	15.26	12.72	17.92	8940...	14.48	16.64	16.36
9280...	17.02	16.67	12.29	14.94	17.51	17.79	15.28	12.62	18.00	9100...	14.42	16.57	16.43
9440...	16.92	16.94	12.31	14.85	17.06	17.84	15.25	12.58	17.94	9260...	14.31	16.64	16.52
9600...	17.27	16.84	12.28	14.75	17.23	18.17	15.18	12.62	17.84	9420...	14.46	16.71	16.38
9760...	17.35	16.67	12.25	14.79	17.30	18.16	15.16	12.62	17.66	9580...	14.36	16.72	16.45
9920...	17.06	16.72	11.95	14.89	17.29	17.80	15.21	12.64	18.11	9740...	14.36	16.46	16.19
10080...	17.58	16.52	12.14	14.66	17.05	18.13	15.30	12.65	17.67	9900...	14.28	16.39	16.20
10240...	16.93	16.73	12.04	14.71	17.34	17.69	15.28	12.55	17.36	10060...	14.22	16.32	16.46
10400...	16.98	16.70	12.01	14.72	16.94	17.61	15.13	12.43	17.27	10220...	14.18	16.51	16.17
10560...	16.88	16.46	11.97	14.59	17.11	17.71	15.06	12.40	17.61	10380...	14.09	16.19	15.86
10720...	16.23	16.18	11.95	15.90	15.07	16.61	...	...	...	10540...	14.08	16.05	15.67
										10700...	13.91	15.91	...

TABLE 2B

OBSERVATIONS

λ	3C76.1	3C78	3C98	3C109	3C198	3C264	3C293	3C382	λ	3C459	λ	CYG A
3240...	...	17.52	...	...	...	...	...	...	3221...	18.95	3366...	19.47
3320...	18.66	16.92	18.23	19.89	19.54	16.88	18.86	15.96	3300...	18.95	3446...	19.20
3400...	18.61	16.75	18.70	19.46	18.95	16.81	18.27	15.91	3380...	18.87	3526...	18.61
3480...	18.48	16.83	18.11	19.47	18.99	16.71	18.00	15.90	3460...	18.83	3606...	18.52
3560...	18.22	16.64	18.15	19.53	18.79	16.67	18.03	15.91	3540...	18.84	3686...	18.69
3640...	18.08	16.57	18.07	19.08	18.62	16.63	17.95	15.83	3620...	18.85	3766...	18.88
3720...	18.20	16.45	18.42	19.21	18.69	16.43	18.06	15.95	3700...	18.74	3846...	18.81
3800...	17.86	16.35	17.81	19.30	18.89	16.38	17.92	15.93	3780...	18.82	3926...	17.45
3880...	17.80	16.29	17.72	19.06	18.73	16.35	17.32	15.97	3860...	18.78	4006...	18.65
3960...	17.85	16.35	17.79	19.08	18.60	16.29	17.59	15.84	3940...	18.76	4086...	18.01
4040...	17.57	16.07	17.63	19.10	18.13	16.09	17.47	15.99	4020...	18.69	4166...	18.33
4120...	17.18	15.58	17.11	18.74	18.46	15.57	17.36	15.87	4100...	18.59	4246...	18.16
4200...	16.94	15.43	16.94	18.65	18.29	15.51	16.89	15.96	4180...	18.62	4326...	17.94
4280...	16.90	15.44	16.91	18.70	18.32	15.48	16.86	15.81	4260...	18.60	4406...	18.02
4360...	16.83	15.27	16.81	18.63	18.06	15.44	16.80	15.94	4340...	18.49	4486...	18.04
4440...	16.82	15.24	16.71	18.43	18.05	15.20	16.76	15.86	4420...	18.53	4566...	17.66
4520...	16.59	15.01	16.50	18.53	18.03	15.05	16.65	15.77	4500...	18.30	4646...	17.66
4600...	16.41	14.83	16.36	18.47	18.00	14.89	16.49	15.56	4580...	17.89	4726...	17.56
4680...	16.32	14.71	16.23	18.35	17.85	14.82	16.38	15.64	4660...	18.21	4806...	17.45
4760...	16.15	14.61	16.11	18.27	17.79	14.77	16.26	15.57	4740...	17.98	4886...	17.3[illegible]
4840...	16.11	14.55	16.06	18.14	17.74	14.64	16.20	15.57	4820...	18.07	4966...	17.14
4920...	16.03	14.48	16.00	18.28	17.69	14.61	16.15	15.46	4900...	17.84	5046...	17.21
5000...	16.04	14.45	15.95	18.32	17.62	14.64	16.06	15.42	4980...	17.84	5126...	16.81
5080...	15.96	14.39	15.77	17.95	17.60	14.58	16.04	15.09	5060...	17.80	5206...	16.12
5160...	15.91	14.37	15.58	18.02	17.56	14.54	15.97	15.07	5140...	17.76	5286...	15.30
5240...	15.91	14.37	15.86	18.06	17.39	14.58	15.92	14.96	5220...	17.78	5366...	16.75
5320...	15.92	14.41	15.91	17.97	17.48	14.57	16.01	15.13	5300...	17.73	5446...	16.95
5400...	15.78	14.22	15.76	18.01	17.19	14.37	16.02	15.31	5380...	17.72	5526...	16.76
5480...	15.68	14.09	15.60	17.89	17.52	14.29	15.81	15.41	5460...	17.63	5606...	16.69
5560...	15.65	14.08	15.63	17.88	17.60	14.32	15.70	15.28	5540...	17.62	5686...	16.63
5640...	15.65	14.06	15.62	17.73	17.47	14.30	15.72	15.29	5620...	17.65	5766...	16.60
5720...	15.58	14.04	15.51	17.60	17.37	14.29	15.69	15.22	5700...	17.59	5846...	16.52
5800...	15.59	13.98	15.50	17.89	17.34	14.18	15.64	15.25	5780...	17.52	6133...	16.24
5880...	15.54	13.97	15.47	17.74	17.40	14.24	15.66	15.20	5841...	17.74	6293...	16.22
6040...	15.41	13.87	15.35	17.76	17.39	14.22	15.44	15.02	6000...	17.54	6453...	16.11
6200...	15.32	13.74	15.25	17.51	17.23	14.07	15.42	15.03	6160...	17.30	6613...	15.85
6360...	15.31	13.71	15.18	17.13	17.23	14.05	15.36	14.90	6320...	17.44	6773...	15.90
6520...	15.22	13.59	15.05	16.53	17.17	13.97	15.31	14.92	6480...	17.52	6933...	14.66
6680...	15.17	13.58	15.05	17.26	17.06	13.88	15.26	14.74	6640...	17.41	7093...	14.79
6840...	15.14	13.52	15.01	17.27	16.98	13.85	15.04	13.98	6801...	17.40	7253...	15.75
7000...	15.10	13.49	14.99	...	17.09	13.80	15.07	13.70	6960...	17.36	7413...	15.69
7160...	15.01	13.39	14.98	17.11	16.73	13.78	15.10	14.45	7121...	17.31	7573...	15.67
7320...	15.03	13.46	14.99	17.00	16.86	13.80	15.07	14.65	7280...	17.29	7733...	15.55
7480...	14.96	13.32	14.86	16.92	16.85	13.62	15.07	14.74	7441...	17.26	7893...	15.48
7640...	14.92	13.28	14.73	16.73	16.86	...	15.00	14.71	7600...	17.28	8053...	15.40
7800...	14.76	13.14	14.67	16.73	16.86	13.60	14.88	14.59	7761...	17.03	8213...	15.39
7960...	14.78	13.15	14.66	16.61	16.74	13.51	14.84	14.56	7921...	16.95	8373...	15.34
8120...	14.71	13.09	14.64	16.49	16.63	13.51	14.82	14.48	8080...	16.33	8533...	15.24
8280...	14.65	13.00	14.54	16.37	16.70	13.45	14.79	14.45	8240...	16.84	8693...	15.18
8440...	14.57	12.95	14.49	15.82	16.60	13.37	14.70	14.44	8400...	16.86	8853...	15.25
8600...	14.56	12.93	14.43	14.97	16.66	13.32	14.60	14.40	8560...	17.00	9013...	15.16
8760...	14.58	12.97	14.48	15.95	16.65	13.34	14.64	14.30	8720...	17.06	9173...	15.03
8920...	14.53	12.87	14.42	16.28	16.55	13.29	14.66	14.28	8881...	16.88	9333...	15.05
9080...	14.42	12.78	14.27	16.11	16.49	13.27	14.53	14.24	9040...	16.91	9493...	14.81
9240...	14.42	12.74	14.17	16.00	16.52	13.21	14.42	14.21	9201...	16.85	9653...	14.73
9400...	14.28	12.63	14.10	15.92	16.42	13.47	14.42	14.35	9361...	17.07	9813...	14.91
9560...	14.33	12.74	14.25	15.90	16.41	13.34	14.29	13.94	9520...	16.69	9973...	14.67
9720...	14.27	12.72	14.17	15.94	16.32	13.16	14.34	14.06	9681...	16.76	10133...	14.30
9880...	14.29	12.61	14.14	16.00	16.32	13.01	14.31	14.15	9840...	16.69	10293...	14.72
10040...	14.20	12.55	14.05	15.95	16.43	12.92	14.24	14.16	10000...	16.83	10453...	14.58
10200...	14.10	12.48	14.06	15.83	16.36	12.90	14.15	14.06	10160...	16.75	10613...	14.65
10360...	14.12	12.41	14.00	15.95	16.20	12.83	14.13	...	10321...	16.66	10773...	14.85
10520...	14.12	12.35	13.87	15.76	16.15	12.82	14.03	...	10480...	16.47		
10680...	...	...	14.01	...	...	12.76	13.82	...	10641...	16.56		

TABLE 2C

OBSERVATIONS

λ	3C192	3C390.3	3C445	λ	3C192	3C390.3	3C445	λ	3C305	λ	3C305
3241...	19.08	16.13	...	5761...	15.95	...	...	3337...	17.29	5993...	14.66
3281...	18.93	16.05	18.53	5801...	15.92	15.39	16.40	3377...	17.26	6073...	14.59
3321...	19.05	15.82	17.77	5881...	15.88	15.35	16.37	3417...	17.25	6153...	14.61
3361...	19.06	15.90	18.13	5961...	15.85	15.30	16.32	3457...	17.01	6233...	14.57
3401...	18.65	15.91	18.78	6041...	15.77	15.19	16.21	3497...	17.17	6313...	14.51
3441...	18.37	15.91	18.31	6121...	15.73	15.13	16.17	3537...	17.08	6393...	14.55
3481...	18.65	15.88	18.45	6201...	15.71	15.13	16.06	3577...	16.96	6473...	14.55
3521...	18.41	15.84	17.88	6281...	15.75	15.11	16.08	3617...	17.21	6553...	14.44
3561...	18.59	15.90	18.20	6361...	15.66	15.18	16.15	3657...	16.96	6633...	14.43
3601...	18.46	15.75	17.52	6441...	15.60	15.11	16.12	3697...	16.94	6713...	14.41
3641...	18.28	15.76	17.54	6521...	15.63	15.14	16.04	3737...	16.85	6793...	14.07
3681...	18.08	15.86	17.93	6601...	15.65	15.05	15.91	3777...	16.89	6873...	13.90
3721...	18.53	15.87	17.65	6681...	15.63	14.86	15.73	3817...	16.76	6953...	14.23
3761...	18.24	15.98	17.59	6761...	15.55	14.50	15.54	3857...	16.47	7033...	14.20
3801...	18.48	15.88	17.75	6841...	15.48	13.69	14.91	3897...	16.01	7113...	14.31
3841...	18.06	15.86	17.86	6921...	15.33	13.50	13.85	3937...	16.48	7193...	14.36
3881...	17.83	15.90	17.74	7001...	15.36	13.82	14.90	3977...	16.45	7273...	14.26
3921...	18.00	15.74	17.07	7081...	15.40	14.36	15.33	4017...	16.18	7353...	14.24
3961...	17.19	15.76	17.35	7161...	15.35	14.77	15.66	4057...	16.22	7433...	14.25
4001...	18.10	15.97	17.71	7241...	15.41	14.86	15.70	4097...	16.27	7513...	14.26
4041...	18.08	15.88	17.14	7321...	15.39	14.86	15.67	4137...	16.16	7593...	14.26
4081...	17.89	15.54	16.87	7401...	15.34	14.83	15.62	4177...	15.82	7673...	14.17
4121...	17.76	15.72	17.42	7481...	15.32	14.88	15.67	4217...	15.80	7753...	14.20
4161...	17.83	15.90	17.61	7561...	15.35	14.85	15.49	4257...	15.76	7833...	14.12
4201...	17.54	15.85	17.23	7641...	15.36	14.75	15.39	4297...	15.70	7913...	14.10
4241...	17.34	15.88	17.55	7721...	15.25	14.76	15.37	4337...	15.75	7993...	14.14
4281...	17.16	15.82	17.30	7801...	15.16	14.79	15.44	4377...	15.65	8073...	14.12
4321...	17.06	15.70	17.14	7881...	15.12	14.82	15.68	4417...	15.64	8153...	14.10
4361...	17.02	15.86	17.35	7961...	15.10	14.77	15.53	4457...	15.61	8233...	14.09
4401...	16.99	15.93	17.38	8041...	15.10	14.75	15.47	4497...	15.66	8313...	14.05
4441...	17.08	15.92	17.25	8121...	15.13	14.74	15.42	4537...	15.52	8393...	14.02
4481...	17.03	15.84	17.28	8201...	15.12	14.70	15.36	4577...	15.49	8473...	14.04
4521...	16.94	15.72	17.20	8281...	15.14	14.56	15.63	4617...	15.40	8553...	14.00
4561...	17.07	15.63	16.70	8361...	15.04	14.66	15.58	4657...	15.35	8633...	13.95
4601...	16.73	15.31	16.36	8441...	15.04	14.66	15.35	4697...	15.27	8713...	14.01
4641...	16.74	15.66	17.05	8521...	14.97	14.53	15.46	4737...	15.23	8793...	13.92
4681...	16.72	15.73	16.98	8601...	14.95	14.54	15.25	4777...	15.20	8873...	13.99
4721...	16.64	15.70	16.85	8681...	14.93	14.58	15.11	4817...	15.17	8953...	13.90
4761...	16.45	15.71	16.96	8761...	14.88	14.49	15.29	4857...	15.14	9033...	13.89
4801...	16.49	15.73	16.97	8841...	14.94	14.42	14.96	4897...	15.16	9113...	13.92
4841...	16.41	15.60	16.96	8921...	14.90	14.60	15.27	4937...	15.10	9193...	13.87
4881...	16.30	15.56	16.89	9001...	14.92	14.52	15.26	4977...	15.02	9273...	13.91
4921...	16.35	15.58	16.72	9081...	14.91	14.46	15.17	5017...	15.08	9353...	13.80
4961...	16.30	15.53	16.57	9161...	14.88	14.54	15.34	5057...	15.12	9433...	13.80
5001...	16.37	15.50	16.67	9241...	14.85	14.48	15.13	5097...	15.10	9513...	13.84
5041...	16.26	15.28	16.58	9321...	14.84	14.68	14.91	5137...	14.98	9593...	13.80
5081...	16.28	15.17	16.42	9401...	14.89	14.44	14.74	5177...	14.78	9673...	13.78
5121...	16.24	14.98	15.86	9481...	14.86	14.46	14.90	5217...	14.43	9753...	13.76
5161...	16.15	15.05	16.20	9561...	14.73	14.24	14.68	5257...	15.00	9833...	13.73
5201...	16.22	15.12	16.28	9641...	14.66	14.44	14.94	5297...	14.97	9913...	13.54
5241...	15.90	14.76	15.29	9721...	14.68	14.39	15.00	5337...	14.99	9993...	13.65
5281...	16.04	14.23	14.47	9801...	14.72	14.44	14.94	5377...	15.10	10073...	13.70
5321...	15.58	15.29	16.36	9881...	14.74	14.36	14.76	5417...	14.98	10153...	13.65
5361...	16.16	15.44	16.46	9961...	14.72	14.42	15.44	5457...	14.90	10233...	13.64
5401...	16.19	15.48	16.56	10041...	14.60	14.20	14.83	5497...	14.87	10313...	13.41
5441...	16.20	15.46	16.44	10121...	14.65	14.26	15.14	5537...	14.82	10393...	13.40
5481...	16.39	15.46	16.56	10201...	14.58	14.39	14.96	5577...	14.81	10473...	13.98
5521...	16.14	15.40	16.37	10281...	14.61	14.34	14.83	5617...	14.91	10553...	13.78
5561...	16.09	15.42	16.36	10361...	14.57	14.18	14.45	5657...	14.80	10633...	13.26
5601...	16.00	15.36	16.45	10441...	14.47	14.08	14.85	5697...	14.79		
5641...	15.96	15.36	16.44	10521...	14.55	14.16	14.77	5737...	14.76		
5681...	15.96	15.38	16.34	10601...	14.47	14.07	14.61	5777...	14.74		
5721...	15.97	15.42	16.43	10681...	14.17	...	...	5817...	14.79		
				10761...	14.07	...	...	5857...	14.76		
								5897...	14.76		

TABLE 3

STANDARD DEVIATIONS IN MAGNITUDES FOR THE TABULATED WAVELENGTH INTERVALS

Object	Wavelengths (standard deviations)							
3C 17.....	3260 (0.25)	3500 (0.14)	4460 (0.06)	4940 (0.04)	8320 (0.13)	10080 (0.20)	10560	...
3C 28.....	3260 (0.27)	3500 (0.17)	4060 (0.07)	4780 (0.03)	6400 (0.02)	7520 (0.03)	8320 (0.10)	10560
3C 31.....	3260 (0.02)	3740 (0.01)	10560 (0.02)	10720	...	...	...	...
3C 33.....	3260 (0.09)	3340 (0.05)	3980 (0.02)	3780 (0.01)	8320 (0.03)	9280 (0.05)	10240 (0.42)	10720
3C 76.1.....	3320 (0.16)	3560 (0.05)	4120 (0.02)	5400 (0.01)	8120 (0.02)	9240 (0.04)	10520	...
3C 78.....	3240 (0.27)	3320 (0.04)	3880 (0.02)	4200 (0.01)	10040 (0.07)	10520	...	...
3C 79.....	3260 (0.26)	3420 (0.14)	4060 (0.08)	4700 (0.05)	6080 (0.04)	7680 (0.09)	9280 (0.20)	10720
3C 88.....	3260 (0.15)	3570 (0.05)	4130 (0.03)	4770 (0.01)	7660 (0.02)	9740 (0.07)	10700	...
3C 98.....	3320 (0.13)	3800 (0.03)	4520 (0.01)	8120 (0.02)	9560 (0.05)	10680	...	...
3C 109.....	3320 (0.42)	3480 (0.14)	3720 (0.09)	4120 (0.04)	6840 (0.20)	7320 (0.04)	9400 (0.1)	10360
3C 171.....	3260 (0.25)	3420 (0.18)	4220 (0.10)	4940 (0.05)	6080 (0.04)	7680 (0.10)	9120	...
3C 192.....	3241 (0.30)	3401 (0.15)	3841 (0.09)	4361 (0.03)	5281 (0.02)	8281 (0.08)	10601 (0.29)	10761
3C 198.....	3320 (0.20)	3560 (0.05)	3960 (0.03)	4760 (0.02)	6680 (0.06)	9880 (0.14)	10520 (0.22)	10720
3C 219.....	3260 (0.30)	3570 (0.13)	4290 (0.05)	4770 (0.03)	5900 (0.02)	8140 (0.07)	10220 (0.14)	10700
3C 234.....	3260 (0.60)	3650 (0.04)	4690 (0.04)	7980 (0.07)	9260 (0.09)	10060 (0.14)	10700	...
3C 264.....	3320 (0.03)	3721 (0.01)	9240 (0.05)	9720 (0.01)	10520	...	...	...
3C 277.3.....	3340 (0.32)	3500 (0.18)	3820 (0.08)	4460 (0.04)	5580 (0.02)	8160 (0.07)	9280 (0.10)	10560
3C 293.....	3320 (0.12)	3560 (0.07)	3880 (0.03)	5240 (0.04)	6040 (0.02)	8440 (0.03)	9400 (0.06)	10520
3C 296.....	3260 (0.08)	3340 (0.03)	3660 (0.01)	9280 (0.02)	10560	...	...	...
3C 305.....	3337 (0.14)	3537 (0.07)	3817 (0.02)	5897 (0.01)	7593 (0.02)	8313 (0.05)	10393 (0.15)	10633
3C 382.....	3320 (0.02)	3640 (0.01)	8920 (0.02)	9400 (0.04)	10200 (0.02)	10680	...	...
3C 390.3.....	3241 (0.06)	3321 (0.04)	3921 (0.02)	4961 (0.01)	7001 (0.02)	7721 (0.05)	8761 (0.10)	10601
3C 405.....	3366 (0.35)	3526 (0.12)	3780 (0.05)	4646 (0.04)	6293 (0.02)	8373 (0.04)	10293 (0.07)	10773
3C 445.....	3281 (0.35)	3521 (0.12)	4560 (0.05)	4960 (0.02)	5360 (0.03)	6761 (0.02)	7651 (0.12)	10601
3C 456.....	3260 (0.21)	3740 (0.13)	4540 (0.05)	5660 (0.03)	8320 (0.13)	9280 (0.25)	10240 (0.32)	10720
3C 459.....	3321 (0.07)	3300 (0.02)	3860 (0.01)	5460 (0.02)	6000 (0.01)	8400 (0.06)	9361 (0.13)	10641

line is located, i.e., from statistics of photon counts. This generally will not contribute more than $\pm 5\%$ for moderately strong lines. The other contributor to the error, and often the major part, is the uncertainty in the continuum level. This is especially large for weak lines and lines such as [S II] $\lambda\lambda$4068, 4076, situated on a rapidly changing part of the continuum; here the uncertainty in the continuum level can account for almost all of the large error quoted. For the most part, the extensive coverage of the continuum obtainable with the multichannel spectrometer enables us to draw reasonably smooth continua easily.

Emission line intensities for 3C 234, 3C 382, 3C 390.3, 3C 405, and 3C 445 have also been measured by Osterbrock, Koski, and Phillips (1976), Osterbrock and Miller (1975), and Grandi and Osterbrock (1978). If we look at the ratio of intensities of the combined lines near Hα to [O II] + Hβ we find that they agree on the average to 10%. Since this ratio does not depend on deconvolution techniques, it demonstrates that the spectrophotometry over this spectral range is accurate. A comparison of the actual intensities shows that ours are systematically higher than those measured at Lick by up to 50%, presumably due to the small entrance aperture used at Lick compared with that used for our observations. A comparison of [O III] and Hβ shows that the deconvolution increases the errors; our estimated errors reflect these larger errors since, in this respect, the higher resolution Lick data are of better quality. For weak, broad lines such as Hγ and Hδ, the errors are larger than for the strong lines, due mainly to errors in placing the continuum. For λ3869 of [Ne III] and λ3727 of [O II] our intensities are larger than the Lick values by a factor 2.5 in 3C 390.3 and 5 in 3C 382. These large differences could be explained if there is a large contribution to these lines by material far from the nucleus since our aperture is much larger than the Lick one. It is also possible that there is a substantial light loss in the violet at Lick due to seeing and guiding effects in their small aperture; they make corrections for this light loss, however.

For purposes of discussion, we divide the sample objects crudely into three separate sets according to their emission line strengths. There is no sharp division between the groupings, since the emission line characteristics vary more or less continuously.

i) *Strong Line Objects*

This group includes 3C 17, 3C 79, 3C 109, 3C 171, 3C 234, 3C 382, 3C 390.3, 3C 405 (Cyg A), 3C 445, 3C 456, and 3C 459. These objects all have equivalent widths of the [N II]–Hα blend greater than 100 Å. With the exceptions of 3C 17 and 3C 456, which are classified as E galaxies, and 3C 382 and 3C 405, which are D galaxies, all the rest are N galaxies. The classifications of 3C 17 and 3C 456 are ambiguous, since they are of large redshift ($\sim$0.2); they have much stronger emission lines than the other ellipticals in the sample. In fact, 3C 17 is classified as an N galaxy by Burbidge (1970).

Both the permitted hydrogen lines and the forbidden lines are very prominent in these objects. The higher resolution spectra of 3C 382, 3C 390.3, and 3C 445 obtained by Osterbrock, Koski, and Phillips (1976) show that the Balmer lines have both a broad and a narrow component. In cases where the [O III] and Hβ lines appear as an unseparated group in the spectrum,

TABLE 4

LINE STRENGTHS (in units of 10^{42} ergs s^{-1})

A.

LINE	OBJECT											
	3C 17	3C 28	3C 33	3C 79	3C 88	3C 98	3C 109	3C 171	3C 192	3C 198	3C 219	3C 234
[S II] 6717, 6731 [N II] 6548, 6583 Hα 6562	6.9a*	0.9c	0.84c	12.c	0.1c	P	119a	13b	0.4c	P	4c	38a
[O I] 6300, 6363	P							2.2c				
[O III] 5007 [O III] 4959	3.5b	...	1.93a	22.a	P?	0.26b 0.1c	24.8a	6.54a 2.2b	0.76b 0.27b	0.4c	2.2b	40.2b
Hβ 4861	1.0c	P?	0.12c	1.6c	...	...	7.0b	0.93b	0.08c	0.15c	0.3c(?)	4.2b
[O III] 4363, Hγ 4364	P	...	...	0.3c	...	...	2.2c	0.7c	...	...	0.3c	2.1b
Hδ 4101 [S II] 4068, 4076	P	...	0.09c	P	...	P	...	P	...	...	0.5c	0.6c
[Ne III], Hε, 3967, 3970	P	...	...	1.1c	...	...	...	...	...	...	...	0.6c
[Ne III] 3869, He I, H8	P	...	0.1c	1.6b	...	...	2.5c	0.8c	...	P	0.36c	2.c
[O II] 3727	1.4b	0.44c	0.43b	3.15a	0.03c	0.06c	1.8c	4.24a	0.32b	0.28b	0.75c	4.c
[Ne V] 3425	...	...	...	1.c	...	...	...	...	...	0.13c	...	2.8b
[Ne V] 3345	...	...	...	P	...	...	...	...	...	0.2c	...	P
Mg II 2798	P?	...	...	P	...	...	P	...	...	...	...	1.7c
$W(H\beta)$ (Å)	32	...	8	46	...	...	51	52	4	14	8?	86

B.

LINE	OBJECT								
	3C 277.3	3C 293	3C 305	3C 382	3C 390.3	3C 405	3C 446	3C 456	3C 459
[S II] 6717, 6731 [N II] 6548, 6583 Hα 6562	...	0.6c	1.7b	20.9a	19.0a	18.6a	8.67a	15.c	17.5b
[O I] 6300, 6363						1.0b	0.51b		
[O III] 5007 [O III] 4959	0.5c	...	0.77a 0.35b	1.3c	3.28a 1.28a	10.1a 3.6b	2.76a 0.92a	8.1a 2.6b	2.6c
Hβ 4861	P	...	0.1c?	3.4b	2.16a	0.82c	1.3b	1.3b	3.5c
[O III] 4363, Hγ 4364	...	...	...	0.3c	1.4b	0.3c	0.4c	0.5c	...
Hδ 4101 [S II] 4068, 4076	...	...	...	0.44c	0.36c	...	...	0.3c	...
[Ne III], Hε, 3967, 3970	...	...	...	...	...	...	...	...	...
[Ne III] 3869, He I, H8	...	...	0.9c	0.38b	0.97b	1.1c	0.2c	0.78	0.7c
[O II] 3727	P	0.17b	0.32b	0.6c	0.5c	1.33b	0.26b	2.8a	1.7b
[Ne V] 3425	...	...	...	P	...	...	0.2c	P?	...
[Ne V] 3345	...	...	...						
Mg II 2798	...	...	...	...	...	...	...	P?	...
$W(H\beta)$ (Å)	6?	...	4?	74	61	26	127	60	50

* Lower-case letters denote uncertainties; a, ≤10%; b, 10 to 25%; c, 25 to 60%; *P*, present, but uncertainty >60%.

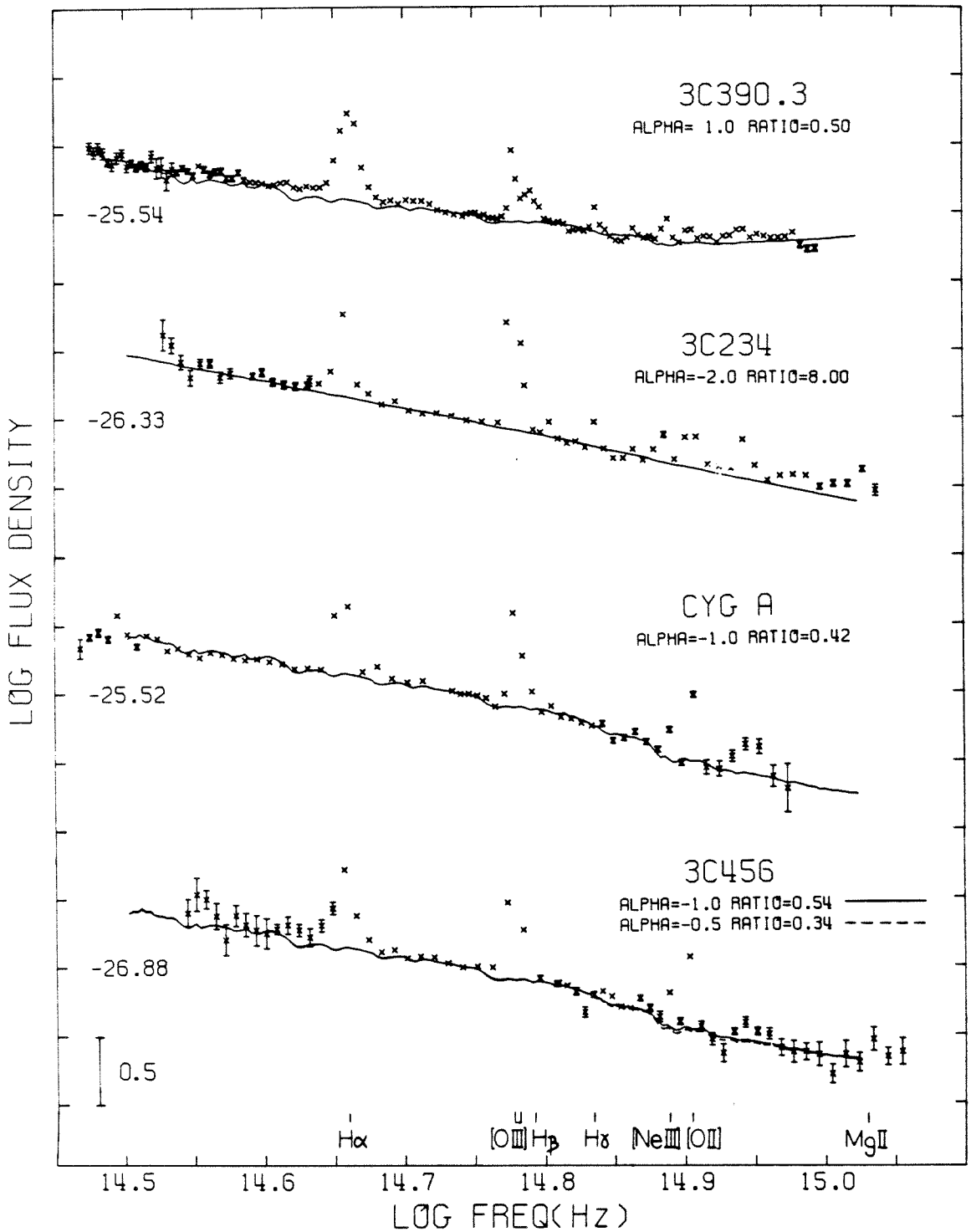

FIG. 1.—Examples of absolute spectral energy distributions of objects with strong emission lines. All plots are shifted to rest frame and corrected for reddening. The ordinate is marked in intervals of 0.5 in log flux density (ergs cm^{-2} s^{-1} Hz^{-1}), with the absolute value for each scan at log ν_0 = 14.740 indicated. Solid lines are plots of two-component models with α and $R(\nu_0)$ indicated.

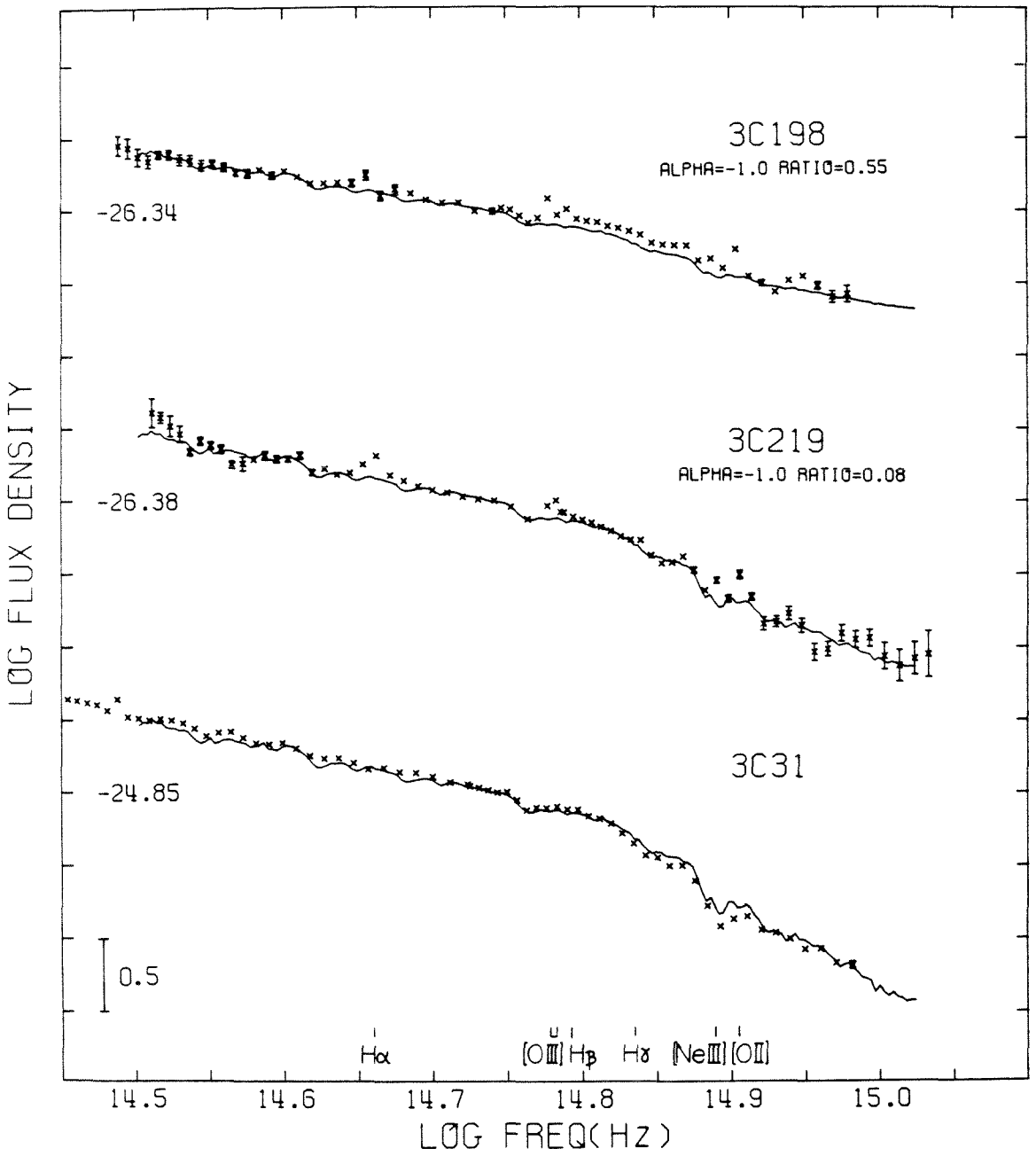

FIG. 2.—Same as Fig. 1; examples of absolute spectral energy distribution of objects with moderately strong (3C 198, 3C 219) or no (3C 31) emission lines.

the strength of the [O III] lines is measured by assuming that Hβ is not wide enough to contaminate the channel containing the [O III] λ5007 line. The ratio [O III] λ4959/λ5007 = 1/3 is applied to the flux of [O III] λ5007 to obtain the strength of [O III] λ4959. The remaining flux of the emission feature is assumed to be due to Hβ. This procedure produces an underestimate of the Hβ strength only if the full width of Hβ is greater than about 200 Å. The spectra of Osterbrock, Koski, and Phillips (1976) and photographic slit spectra taken by Schmidt (1965) of most objects were used to check that the Hβ line was not wide enough to grossly affect the analysis. The slit spectra of 3C 459 show that Hβ extends well beyond the [O III] lines. The multichannel scans of 3C 459 seems to confirm this; both Hα and Hβ exhibit a very broad, low profile

extending over several channels. Apart from Balmer lines, no other allowed transitions except Mg II λ2798 are detected. There is evidence of Mg II λ2798 in all objects whose redshift is large enough for it to come into the observed region.

It is noteworthy that all galaxies in this group have a large excess of continuum flux in the ultraviolet as compared to a normal elliptical galaxy. They are also in general more luminous in the radio continuum emission than the other sources in the sample. The radio luminosity of this group ranges from $10^{42.7}$ to 10^{45} ergs s^{-1}.

ii) *Objects with Moderately Strong or Easily Detected Emission Lines*

The galaxies 3C 33, 3C 219, 3C 277.3, and 3C 293 are classified as D galaxies, while 3C 28, 3C 98, 3C 192, and 3C 198 are E galaxies. Also included is 3C 305, which originally was classified as an E galaxy according to the Palomar 1.2 m sky survey; Sandage (1966) reclassified it as an "abnormal" spiral Sa with faint dust lanes. Most of these objects show rather prominent forbidden lines such as [O II] λ3727 and [O III] λλ5007, 4959, with either very weak or undiscernible Balmer lines. Because of the weakness of the Balmer lines, in most cases the Hα–[N II] complex is probably due mostly to [N II] λλ6548, 6583 and [S II] λλ6717, 6731. These objects show a varying degree of excess in the UV; the excess is large in 3C 198 but absent in 3C 293 and 3C 98. They are in general less bright in the radio spectrum than the first group, with radio luminosities ranging from $10^{42.2}$ to $10^{43.8}$ ergs s^{-1}.

iii) *Objects with Very Weak or Undetected Emission Lines*

Of the remaining six sources, 3C 31, 3C 264, and 3C 296 are classified as E galaxies, while 3C 76.1, 3C 78, and 3C 88 are D galaxies. They have continua with absorption features resembling normal elliptical galaxies. Some show evidence of very weak forbidden emission lines. They are all close-by objects with $z < 0.035$, and are relatively weak in radio emission, ranging from $10^{41.8}$ to $10^{42.2}$ ergs s^{-1}.

b) Continua

One of the advantages of multichannel photometry is the ability to obtain reasonably accurate continuum absolute fluxes. As mentioned in § IV*a*, there is a whole range of UV excess found in the objects, and they seem to be correlated somewhat with the emission line characteristics. In order to get a semiquantitative picture of the excess, the continuum light from the galaxies is decomposed into two components, a standard underlying galactic component, and a power-law spectrum of the form $F_{NT}(\nu) \propto \nu^{\alpha}$, which can be assumed to be nonthermal in origin. This seems to be an appropriate model to use, since the large errors in the infrared and ultraviolet would not allow one to delineate more complex models, and there is a natural physical mechanism in electron synchrotron radiation to explain the nonthermal component.

The underlying galactic component is assumed to be like that of giant elliptical galaxies. While there is no conclusive evidence on the question of whether the underlying galaxy of an N galaxy is elliptical or spiral (Tinsley 1977), the fact that there are no spiral galaxies (with the possible exception of 3C 305) which are strong radio emitters (i.e., $L_R \approx 10^{43}$ ergs s^{-1}) makes the choice of an elliptical galaxy a logical one. To obtain a standard elliptical galaxy, a series of multichannel scans of five normal elliptical galaxies was taken, with a resolution of 40/80 Å. All of these galaxies are first-ranking ellipticals in clusters and have high galactic latitude $|b^{II}| > 40°$, so that only minimal reddening corrections are necessary. They have redshifts between 0.1 and 0.2, which approximate the average z of our sample. The scans are normalized according to each V_I value. The energy distributions are interpolated, in the rest frame of each object, at an interval of $\Delta \log \nu = 0.003$, which corresponds to a resolution of ~70 Å in the infrared and ~23 Å in the ultraviolet. They are then averaged, each one weighted according to the standard deviation. This final standard energy distribution is shown in Figure 2 superposed on the energy distribution of 3C 31. It is also listed in Table 5 in terms of *AB* magnitudes normalized to 0.00 at $\log \nu_0 = 14.740$.

To this standard energy distribution a two-parameter nonthermal component is added. This component, $F_{NT}(\nu)$, takes the form

$$\frac{F_{NT}(\nu)}{F_G(\nu_0)} = R(\nu_0)\left(\frac{\nu}{\nu_0}\right)^{\alpha}, \qquad (1)$$

where α is the spectral index, $\log \nu_0 = 14.740$, and $F_G(\nu_0)$ is the flux of the underlying galactic component at frequency ν_0. Hence $R(\nu_0)$ is the ratio of the nonthermal to the galactic component at ν_0, and

$$\frac{F_{NT}(\nu_0)}{T_{Total}(\nu_0)} = \frac{R(\nu_0)}{1 + R(\nu_0)}. \qquad (2)$$

It should be noted that $R(\nu_0)$ is not the ratio of the two components in the strict sense, but only the ratio within the aperture used in the observation.

The model-fitting was performed by visual means. It was felt that, for example, mathematical least-squares fitting would not improve the accuracy of the value of the model parameters, because there are two parameters in the model and because the error base in both the infrared and ultraviolet is relatively large, making minute discrimination between similar models impossible.

Three galaxies 3C 109, 3C 234, and 3C 445, all of type N, have steep dominating nonthermal components, enabling α to be specified to an accuracy of $\sim \pm 0.1$. The underlying galaxy, however, is largely obscured, and we can only place a lower limit for $R(\nu_0)$ on 3C 109 and 3C 234. This is illustrated by 3C 234 in Figure 1. For 3C 445, because some absorption features are still discernible, both $R(\nu_0)$ and α can be determined. The resulting models are given in Table 6.

Most of the objects with ultraviolet excesses have

TABLE 5

STANDARD GALAXY

Log ν	Relative Magnitude	Log ν	Relative Magnitude	Log ν	Relative Magnitude	Log ν	Relative Magnitude
14.502.....	−1.16	14.634.....	−0.50	14.766.....	+0.35	14.898.....	+1.89
14.505.....	−1.22	14.637.....	−0.51	14.769.....	+0.33	14.901.....	+1.90
14.508.....	−1.20	14.640.....	−0.50	14.772.....	+0.30	14.904.....	+2.00
14.511.....	−1.27	14.643.....	−0.46	14.775.....	+0.32	14.907.....	+1.98
14.514.....	−1.21	14.646.....	−0.40	14.778.....	+0.34	14.910.....	+1.94
14.517.....	−1.22	14.649.....	−0.37	14.781.....	+0.32	14.913.....	+2.00
14.520.....	−1.14	14.652.....	−0.40	14.784.....	+0.31	14.916.....	+2.13
14.523.....	−1.11	14.655.....	−0.43	14.787.....	+0.35	14.919.....	+2.21
14.526.....	−1.11	14.658.....	−0.44	14.790.....	+0.39	14.922.....	+2.36
14.529.....	−1.07	14.661.....	−0.41	14.793.....	+0.36	14.925.....	+2.42
14.532.....	−1.08	14.664.....	−0.40	14.796.....	+0.36	14.928.....	+2.40
14.535.....	−1.05	14.667.....	−0.38	14.799.....	+0.38	14.931.....	+2.42
14.538.....	−0.96	14.670.....	−0.35	14.802.....	+0.40	14.934.....	+2.45
14.541.....	−0.89	14.673.....	−0.33	14.805.....	+0.44	14.937.....	+2.57
14.544.....	−0.85	14.676.....	−0.30	14.808.....	+0.48	14.940.....	+2.50
14.547.....	−0.89	14.679.....	−0.22	14.811.....	+0.47	14.943.....	+2.44
14.550.....	−0.95	14.682.....	−0.18	14.814.....	+0.44	14.946.....	+2.54
14.553.....	−0.85	14.685.....	−0.19	14.817.....	+0.52	14.949.....	+2.55
14.556.....	−0.88	14.688.....	−0.21	14.820.....	+0.54	14.952.....	+2.59
14.559.....	−0.91	14.691.....	−0.22	14.823.....	+0.58	14.955.....	+2.65
14.562.....	−0.92	14.694.....	−0.24	14.826.....	+0.63	14.958.....	+2.64
14.565.....	−0.91	14.697.....	−0.23	14.829.....	+0.68	14.961.....	+2.67
14.568.....	−0.89	14.700.....	−0.20	14.832.....	+0.71	14.964.....	+2.76
14.571.....	−0.87	14.703.....	−0.15	14.835.....	+0.81	14.967.....	+2.82
14.574.....	−0.95	14.706.....	−0.11	14.838.....	+0.82	14.970.....	+2.89
14.577.....	−0.79	14.709.....	−0.15	14.841.....	+0.93	14.973.....	+3.01
14.580.....	−0.80	14.712.....	−0.17	14.844.....	+1.00	14.976.....	+2.96
14.583.....	−0.82	14.715.....	−0.16	14.847.....	+1.06	14.979.....	+2.93
14.586.....	−0.86	14.718.....	−0.13	14.850.....	+1.03	14.982.....	+3.02
14.589.....	−0.75	14.721.....	−0.10	14.853.....	+1.04	14.985.....	+3.08
14.592.....	−0.74	14.724.....	−0.09	14.856.....	+1.10	14.988.....	+3.18
14.595.....	−0.73	14.727.....	−0.07	14.859.....	+1.12	14.991.....	+3.20
14.598.....	−0.78	14.730.....	−0.06	14.862.....	+1.13	14.994.....	+3.24
14.601.....	−0.81	14.733.....	−0.05	14.865.....	+1.14	14.997.....	+4.43
14.604.....	−0.80	14.736.....	−0.01	14.868.....	+1.20	15.000.....	+3.32
14.607.....	−0.77	14.739.....	+0.01	14.871.....	+1.22	15.003.....	+3.44
14.610.....	−0.72	14.742.....	+0.01	14.874.....	+1.29	15.009.....	+3.43
14.613.....	−0.67	14.745.....	+0.02	14.877.....	+1.47	15.012.....	+3.52
14.616.....	−0.60	14.748.....	+0.03	14.880.....	+1.70	15.015.....	+3.54
14.619.....	−0.50	14.751.....	+0.07	14.883.....	+1.89	15.018.....	+3.59
14.622.....	−0.43	14.754.....	+0.13	14.886.....	+1.82	15.021.....	+3.57
14.625.....	−0.43	14.575.....	+0.21	14.889.....	+1.97	15.024.....	+3.57
14.628.....	−0.47	14.760.....	+0.29	14.892.....	+2.10		
14.631.....	−0.50	14.763.....	+0.33	14.895.....	+2.07		

comparable nonthermal and galactic components. They are 3C 17, 3C 79, 3C 171, 3C 198, 3C 382, 3C 390.3, 3C 405, 3C 456, and 3C 459; all the remaining N galaxies are in this group. Of all these, 3C 382 and 3C 390.3 (see Fig. 1) show a definite upturn in the ultraviolet, indicating that the nonthermal component has $\alpha > 0$. Because of this well-defined section in the continuum, the slope of the nonthermal component can be determined to within $\sim \pm 0.5$. These two objects are also the *only* two in this group of galaxies where there is no evidence for stellar absorption features. What we have described as galaxy components could equally well be described as nonthermal power laws with values of α near -2. For the other objects in this group, the ranges in the models are larger. Often α is uncertain by as much as $\sim \pm 1.0$. All cases can be fitted with α between 0.0 and -2.0, with the appropriate $R(\nu_0)$. Models with different α's within the range are essentially indistinguishable. This is shown by 3C 456 in Figure 1, where models with $\alpha = -1.0$ and -0.5 are plotted. Also plotted from this group are Cyg A in Figure 1 and 3C 198 in Figure 2. Representative models are listed in Table 6.

The third group consists of 3C 28, 3C 33, 3C 219, 3C 277.3, and 3C 305. These contain small ultraviolet excesses and $R(\nu_0) \lesssim 0.10$. Because the galactic component dominates, the range of models is very large. Typically, any α between -3 and $+2$ can be used for the nonthermal component. In these cases, we have limited our models to values of α between -0.5 and -1.5, since most sources in the previous group can be fitted by this range of α. The fit for 3C 192 is show in Figure 2. The range of models considered is given in Table 6.

The remaining nine objects have energy distributions like the standard elliptical galaxy. An example is 3C 31 in Figure 2.

It is interesting to compare our decomposition of

TABLE 6

NONTHERMAL COMPONENT MODELS

OBJECT	APERTURE CORRECTION (mag)	MODEL I				MODEL II				STEADY-STATE IONIZATION MODEL	
		α	$R(\nu_0)$	log L_{NT}	M_V (galaxy)	α	$R(\nu_0)$	log L_{NT}	M_V (galaxy)	α	$R(\nu_0)$
3C 17	−0.03	−0.5	0.14	43.46	−22.02	−1.0	0.22	43.62	−21.82	−0.9 ± 0.3	0.21 ± 0.05
3C 28	−0.07	−0.5	0.05	43.06	−22.18	−1.5	0.09	43.28	−22.00	...	...
3C 33	−0.85	−0.5	0.06	42.77	−21.84	−1.5	0.10	42.95	−21.80	−1.1 ± 0.3	0.09 ± 0.01
3C 79	+0.03	−0.5	0.20	43.69	−22.11	−1.5	0.45	43.94	−21.90	−0.9 ± 0.2	0.27 ± 0.09
3C 109	+0.09	−3.0	>3.0	44.99	>−22.24	...	...	...	...	...	...
3C 171	−0.18	−0.5	0.24	43.43	−21.49	−1.5	0.55	43.68	−21.25	−0.9 ± 0.1	0.31 ± 0.04
3C 198	−0.56	−0.5	0.35	43.25	−21.14	−1.5	0.85	43.47	−20.79	−1.6 ± 0.2	0.90 ± 0.10
3C 219	−0.12	−0.5	0.05	43.23	−22.69	−1.5	0.09	43.45	−22.41	∼−1.1	∼0.08
3C 234	−0.09	−2.0	>4.0	44.46	>−21.19	...	...	...	...	...	...
3C 277.3	−0.28	−0.5	0.03	42.76	−22.26	−1.5	0.06	43.01	−22.05	∼−1.2	∼0.06
3C 305	−0.77	−0.5	0.05	42.91	−22.67	−1.5	0.09	43.13	−22.63	∼−1.4	∼0.09
3C 382	−0.81	+0.5	0.70	44.09	−22.86	+1.5	0.35	43.99	−22.61	...	...
3C 390.3	−0.54	+0.5	0.75	44.05	−22.36	+1.0	0.53	44.01	−22.08	...	...
3C 405	−0.54	−0.5	0.26	43.65	−22.49	−1.5	0.55	43.87	−22.26	−1.1 ± 0.2	0.40 ± 0.10
3C 445	−0.54	−2.4	1.50	43.62	−20.54	−2.5	2.00	43.68	−20.34	...	...
3C 456	−0.10	−0.5	0.34	43.62	−21.39	−1.5	0.80	43.83	−21.07	−0.94 ± 0.07	0.50 ± 0.03
3C 459	−0.31	−0.5	0.50	44.15	−22.35	−1.5	1.30	44.36	−21.88	−1.2 ± 0.2	0.93 ± 0.3

the N galaxies with those made by Sandage (1973*a*). Sandage used the color-versus-aperture effect to decompose 3CR N galaxies into a V_Q and a V_G component, that is, a central "quasar-like" nucleus and an underlying galaxy which is assumed to be an elliptical. Seven of those are common to our sample. By comparing the V_Q value with the equivalent visual magnitude of our nonthermal component, we find that they are comparable, within ~ 0.4 mag, with the exception of 3C 109 and 3C 234. In these two, the nonthermal radiation dominates, and our result, for both cases, is ~ 1.4 mag brighter than Sandage's. This discrepancy can easily be understood. Both 3C 109 and 3C 234 have rather steep straight spectra, with $\alpha \approx 3$ and 2, respectively. These approximately mimic the gross slope of a normal elliptical galaxy, but there are no absorption features. Thus, in a broad-band analysis, the color would approximate an ordinary galaxy, causing the conclusion that the nonthermal component is very small in comparison with the underlying galaxy.

V. DISCUSSION

a) Ionization

We have noted that a continuum excess in the ultraviolet is accompanied by emission lines in all cases. This was also concluded by Markarian (1977), when he examined galaxies with a UV continuum, and Osterbrock (1977), who noted that there is a very weak correlation between Balmer emission and $U - B$ in his sample of Seyfert 1 galaxies.

To put this correlation on a more quantitative level, we define L_{NT} as the integrated luminosity due to the nonthermal component between $\log \nu = 14.52$ and $\log \nu = 15.00$ in the rest frame, again using $q_0 = 0$, $H_0 = 55$. Despite the large range of possible models for some objects, $\log L_{NT}$ is uncertain by at most 0.3. In Figure 3*a* we have plotted $\log J_{H\beta}$, where $J_{H\beta}$ is the emitted luminosity of Hβ, versus $\log L_{NT}$. The correlation is good with increased nonthermal radiation accompanied by stronger Hβ emission; the correlation coefficient is 0.92. The horizontal bars on the plot represent the range in the models that are used for each object. We have also included upper limits of $\log J_{H\beta}$ for 3C 28, which has an observable excess but undetectable Hβ. In addition, for 3C 192, which has as observable Hβ but no measurable excess, we place an upper limit on the nonthermal component by assuming the detectability of a nonthermal component to be approximately $R(\nu_0) = 0.01$ at $\alpha = -0.5$. These data are plotted using dotted lines with arrows indicating the direction of uncertainty. These upper-limit points also follow the general trend of the plot.

The strong correlation between nonthermal luminosity and Hβ luminosity shows that the two are intimately connected. However, this connection could be either direct or indirect. The most obvious direct physical explanation would be that the emission lines arise from photoionization of hydrogen by the nonthermal radiation in the nucleus of the galaxy. Of course, the defined nonthermal luminosity in the optical regime does not take part in the ionization process, but it is not difficult to envision that there is a close relationship between the optical radiation and the radiation beyond the Lyman limit which causes ionization. On the other hand, it is possible that the mechanism or physical conditions giving rise to the nonthermal radiation are responsible only indirectly for ionization of hydrogen. If this is the case, the correlation merely points out that the Hβ luminosity has approximately the same dependence on existing physical conditions as the nonthermal radiation flux. However, the strong correlation tends to favor the point of view that the nonthermal radiation is directly affecting Hβ emission.

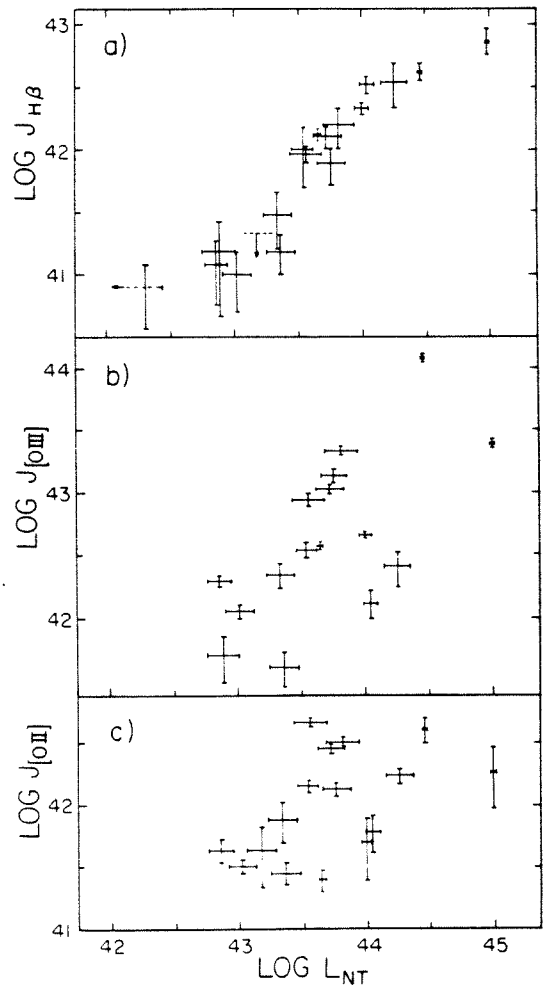

FIG. 3.—Correlations of emission line luminosity and optical nonthermal luminosity. Coordinates are in units of ergs s^{-1}.

To investigate further the direct photoionization hypothesis, we use the following calculation to check whether there is sufficient radiation within the ranges of our model for ionization to produce the observed Hβ luminosity. Following Osterbrock and Miller (1975), we can relate the equivalent width of the Hβ line with the power-law nonthermal component by assuming that it extends beyond the Lyman limit.

Assuming steady state, using the ionization equation and the equation for Hβ emission luminosity along with a power-law ionizing source $L_\nu \propto \nu^\alpha$ (see Osterbrock and Miller 1975), we have

$$W_{\rm NT}({\rm H}\beta) = -\frac{\lambda_{{\rm H}\beta}}{\alpha}\frac{\alpha_{{\rm H}\beta}}{\alpha_B}\left(\frac{\nu_{\rm Ly}}{\nu_{{\rm H}\beta}}\right)^\alpha , \quad (3)$$

where $W_{\rm NT}({\rm H}\beta)$ is the rest-frame equivalent width of Hβ with respect to the nonthermal component only, α_B the effective recombination coefficient, $\alpha_{{\rm H}\beta}$ the emission coefficient of Hβ, $\nu_{\rm Ly}$ and $\nu_{{\rm H}\beta}$ the Lyman limit and Hβ line frequency, respectively, and α the spectral index.

The equivalent width is related to the actual observed equivalent width W_T, i.e., with respect to the total observed continuum, by

$$\frac{W_T}{W_{\rm NT}} = \frac{(1+z)F_{\rm NT}}{F_G + F_{\rm NT}} , \quad (4)$$

where $F_{\rm NT}$ and F_G are the nonthermal flux and the galactic component flux at Hβ, respectively, and the $(1+z)$ term accounts for the redshift transformation of the equivalent width. Hence, using the definition of nonthermal component of equation (1), we have

$$W_T({\rm H}\beta) = -\frac{(1+z)\lambda_{{\rm H}\beta}}{\alpha}\frac{\alpha_{{\rm H}\beta}}{\alpha_B}\left(\frac{\nu_{\rm Ly}}{\nu_{{\rm H}\beta}}\right)^\alpha \times \left[1 + \frac{F_G(\nu_{{\rm H}\beta})}{F_G(\nu_0)}\left(\frac{\nu_0}{\nu_{{\rm H}\beta}}\right)^\alpha \frac{1}{R(\nu_0)}\right]^{-1} . \quad (5)$$

Thus from the Hβ equivalent width and the continuum we can derive a unique model which fits the continuum and also has just enough ionizing photons to produce the observed Hβ luminosity. It should be remembered that this model assumes that no other UV or X-ray component exists, that the optical power law extrapolates to $\nu = \infty$, and that all Lyman continuum radiation is absorbed. Note that this calculation is not strictly valid for $\alpha \geq -1$, since the total luminosity would not converge unless there is a cutoff. However, the ionization equation involves the number of photons; hence, for $0 > \alpha \geq -1$, whether or not there is a cutoff at large energy would have only a vanishingly small effect on the calculation.

The resultant models using $T = 10^4$ K are listed in Table 6. The results are not sensitive to temperature, since α_B and $\alpha_{{\rm H}\beta}$ have approximately the same dependence on temperature. Most of the sources with measurable Hβ have an α and $R(\nu_0)$ that fit both the continuum models already derived above and the Hβ emission constraint. The α's obtained by the Hβ emission constraint represent the *steepest possible* spectral index *if* photoionization is the sole agent. It represents the model with just sufficient UV photons to produce the Hβ line. Hence α must be flatter if some Lyman continuum radiation escapes.

A unique model is not always possible. For 3C 28 we have only an upper limit on $W_{{\rm H}\beta}$; there is an ionization model which is consistent with the upper limits. The galaxies 3C 390.3 and 3C 382 show a definite upturn in the spectrum. This should present no problem in regard to having sufficient ionizing photons, but a simple model with $\alpha > 0$ must have a cutoff at some frequency or allow most Lyman continuum photons, particularly those at high frequencies, to escape. There are three sources that do not have enough UV photons for ionization. They are 3C 109, 3C 234, and 3C 445. Here the galactic component is completely obscured by the power-law component. With the given α dictated by the data, their UV radiation falls short by factors of 8 to 40 of being able to account for the strong Hβ lines in these objects. There are three possible explanations: (1) Other ionization agents are present and dominate. (2) There is strong internal reddening so that the true spectrum is bluer than the observed one. (3) There is a third component of radiation, such as that proposed by Neugebauer *et al.* (1976), causing an upturn in the UV region. Such a component is very possible in all three objects and may very well exist, particularly in 3C 234 and 3C 445, where there is a definite flattening above $\nu = 10^{14.95}$.

Overall, the photoionization picture is consistent with the data. While it is unlikely that this is the only process responsible for the Balmer emission lines, it is probably the dominant one.

Plots of the [O III] λλ4959 + 5007 and the [O II] λλ3727 + 3729 lines versus nonthermal radiation are shown in Figure 3*b* and 3*c*. The [O III] line strength correlates reasonably well with $\log L_{\rm NT}$, which is expected since H^+ and O^{++} are probably in the same regions of space. At electron densities of 10^8 cm^{-3} or higher the [O III] lines are suppressed relative to the Balmer lines due to collisional de-excitation (Souffrin 1969). Since densities of this order appear to exist in Seyferts (Souffrin 1969; Shields, Oke, and Sargent 1972), the [O III] versus $\log L_{\rm NT}$ correlation might be expected to be poorer than that for Hβ versus $\log L_{\rm NT}$.

The correlation of [O II] intensity versus $\log L_{\rm NT}$ is at best suggestive. This is not surprising, since the [O II] lines are not formed in the same region of space as the Balmer lines but must be formed by some other mechanism, such as time-dependent ionization or shadowing effects (Shields and Oke 1975).

b) Luminosities of the Underlying Galaxies

With a decomposition of the continuous spectrum into galaxy and nonthermal parts it is possible to compare the underlying galaxies with normal galaxies. For this purpose it is necessary to correct the underlying galaxy magnitude for aperture effects. This has been done, using Sandage's (1972*a*) empirical growth curve for first-rank cluster galaxies. The magnitudes are corrected to the Gunn-Oke (1975) standard metric diameter of 32 kpc. Because the observations were initially made to study primarily the nuclei, the aperture corrections are in some cases very large; they are given in Tables 6 and 7 along with the calculated values of M_V. Furthermore, the decomposition of the galaxy spectra into two components is itself uncertain. For the 17 objects with blue excesses, the average galactic

TABLE 7

APERTURE CORRECTIONS AND ABSOLUTE MAGNITUDES OF GALAXIES WITH NO UV EXCESS

Object	Aperture Correction (mag)	M_V
3C 31	−1.3	−22.60
3C 76.1	−0.82	−21.48
3C 78	−1.1	−23.01
3C 88	−1.4	−21.76
3C 98	−1.0	−21.93
3C 192	−0.26	−21.87
3C 264	−1.4	−22.35
3C 293	−0.71	−21.91
3C 296	−1.3	−22.96

absolute magnitude $\langle M_V \rangle$ is between -22.0 ± 0.6 mag and -21.7 ± 0.6 mag, depending on the nonthermal component models used. If all 26 galaxies are included, $\langle M_V \rangle$ is between -22.1 and -21.9 mag, depending on models, giving a mean $\langle M_V \rangle = -22.0 \pm 0.6$ mag. After standardizing values of H_0, q_0, and metric diameter, this average value is 0.7 mag fainter than that obtained by Sandage (1972*b*) and 0.8 mag fainter than that obtained by Wilkinson and Oke (1978) for first-rank cluster members. The difference is probably significant and suggests that radio galaxies are not confined to galaxies with absolute magnitudes of first-rank clusters. It should be noted that there is no correlation between M_V of the underlying galaxy and the luminosity of the nonthermal component.

Overall, the optical data stress the continuity of properties in these galaxies. While some appear to be normal galaxies and others have very bright nuclei, and while some have very strong and broad emission lines and others have only barely detectable lines, there does not seem to be any sharp division. This is especially well illustrated by the plots of the emission line strength versus nonthermal luminosity. The plots are continuous and show no prominent breaks. This continuity of properties adds confidence to the notion that the objects are similar and differ only in the matter of degree—i.e., some are more violently active than others.

c) A Comparison of Optical and Radio Properties

It is widely held that the nuclear region of the optical galaxy is responsible for the creation and maintenance of the radio emission. It is not clear how this would be manifested in the two kinds of data. For example, some objects have a nuclear radio component, while others, despite the existence of an optical nonthermal nucleus, only have radio lobes outside of the galaxy. Based on our rather limited sample, a few general, albeit rather loose, inferences can be drawn.

If the amount of nonthermal optical radiation is indicative of the degree of activity in the nucleus, and if the radio emission is a result of such activity, one would expect a correlation to exist. We do indeed find a weak correlation between total radio emission and optical nonthermal luminosity (Fig. 4*a*). The dotted line shows upper limits of objects with no observable nonthermal component. A number of the sources (open dots on Fig. 4*a*), mostly triples, have a radio component coinciding with the optical nucleus. Using the 5 GHz maps from the Cambridge 5 km interferometer (Riley and Pooley 1975; Hargrave and McEllin 1975; Pooley and Henbest 1974; Hargrave and Ryle 1974; Riley and Branson 1973), we can derive approximately the fraction of radio luminosity from such a component alone. Note that in many cases we can obtain only a rough estimate, since the nuclear compact component often tends to be much flatter in spectral index than the overall source. However, the error should be less than ~ 0.3 in $\log L_R$. From nine such sources we find (Fig. 4*b*) that the correlation of the optical nonthermal radiation with the central radio component is much better than that with the overall radio emission. This suggests that the optical nonthermal radiation is probably an extension of, or at least related to, the flat-spectrum compact radio component. It must be cautioned, however, that this better correlation could be due to the smallness of the available sample.

While there is no direct correlation between radio luminosity and emission line strength, it is generally the case that the objects which have prominent lines are intrinsically bright in the radio region. This would follow naturally from the facts that there is a weak correlation between radio and optical nonthermal radiation, and that nonthermal radiation is always accompanied by emission lines. We also noted that Sargent (1977) observed seven other 3CR radio galaxies with strong emission lines, and all seven have a bright radio luminosity of $L_R \gtrsim 10^{43}$ ergs s^{-1}. We conclude that strong radio galaxies ($L_R \gtrsim 10^{42.5}$ ergs s^{-1}) *tend* to be emission line objects, though there are exceptions such as 3C 218 (Hydra A) (Burbidge 1970). This is consistent with the general result that very few identified 4C radio galaxies are strong emission line objects (Sargent 1977); this is presumably a consequence of the fact that 4C sources within the range of z where they are identifiable as galaxies are weaker intrinsic radio emitters than the 3CR radio galaxies.

VI. SUMMARY

In our sample of 26 3CR radio galaxies, we found a continuous range of emission line characteristics and nonthermal UV excess. A strong correlation exists between the nonthermal component luminosity and hydrogen emission, favoring the hypothesis that direct photoionization by the nuclear radiation is responsible for the emission lines observed. Calculations show that, in almost all cases, the power-law component model provides sufficient UV photons to produce the observed Hβ line. While correlations of optical and radio properties are not as conclusive, there are indications that the optical nuclear component is related in some complex fashion to the radio emission. It seems clear

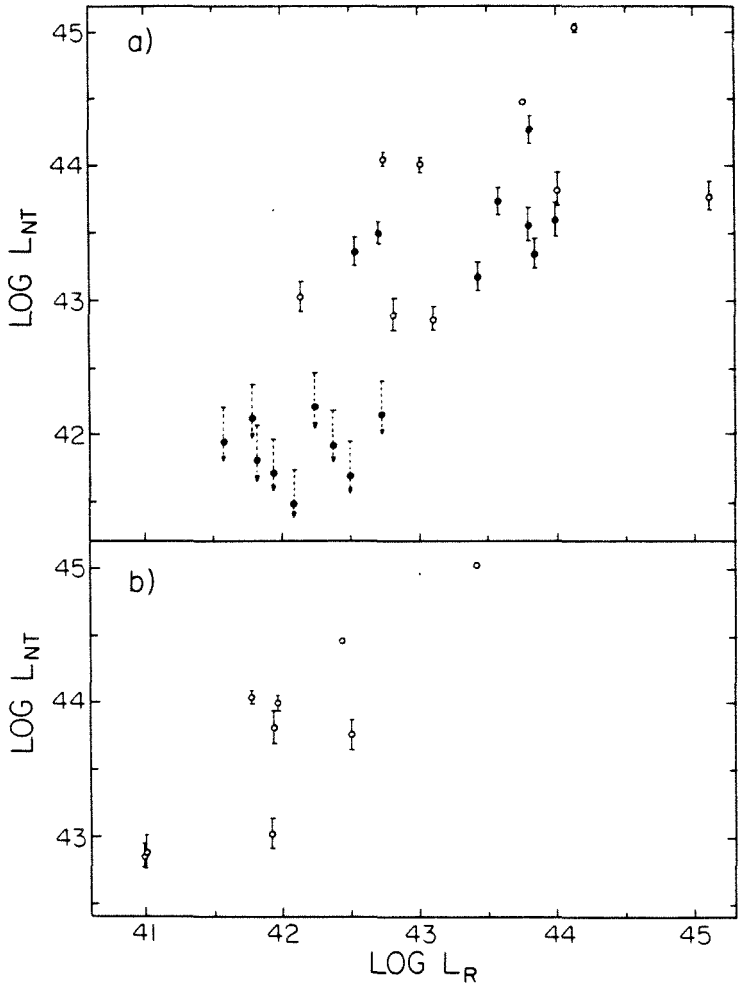

FIG. 4.—(*a*) Correlation of optical nonthermal luminosity (ergs s^{-1}) and integrated radio luminosity (ergs s^{-1}). Opened dots represent sources with triple radio structure. (*b*) Correlation of optical nonthermal luminosity and radio luminosity of the central components of sources with triple structure.

that there is a tendency for strong radio galaxies to be accompanied by UV excess and emission lines.

In order to reach more definitive conclusions, a larger sample of objects should be studied. In addition, high-resolution spectra are required to (*a*) resolve the various emission lines, (*b*) study the emission line profiles, and (*c*) detect or put good limits on the strength of the magnesium *b*-band and H and K lines of Ca II. Finally, more high-resolution multifrequency radio maps are required.

We wish to thank Mr. Gary Tuton and Mr. Juan Carrasco for assistance in making the observations. We also thank Dr. A. Wilkinson for providing the program for the averaging of the empirical standard galaxy and for many helpful discussions. H. Y. is supported in part by an Imperial Oil Graduate Research Fellowship. This work was supported by the National Aeronautics and Space Administration through grant NGL 05-002-134.

REFERENCES

Baade, W., and Minkowski, R. 1954, *Ap. J.*, **119**, 206.
Burbidge, E. M. 1967, *Ap. J. (Letters)*, **149**, L51.
Burbidge, G. R. 1970, *Ann. Rev. Astr. Ap.*, **8**, 369.
Elsmore, B., and Mackay, C. D. 1969, *M.N.R.A.S.*, **146**, 361.
Fomalont, E. B. 1971, *A.J.*, **76**, 513.
Grandi, S. A., and Osterbrock, D. E. 1978, *Ap. J.*, **220**, 783.
Gunn, J. E., and Oke, J. B. 1975, *Ap. J.*, **195**, 255.
Hargrave, P. J., and McEllin, M. 1975, *M.N.R.A.S.*, **173**, 37.
Hargrave, P. J., and Ryle, M. 1974, *M.N.R.A.S.*, **166**, 305.
Kellermann, K. I., Pauliny-Toth, I. I. K., and Williams, P. J. S. 1969, *Ap. J.*, **157**, 1.
Macdonald, G. H., Kenderdine, S., and Neville, A. C. 1968, *M.N.R.A.S.*, **138**, 259.
Mackay, C. D. 1969, *M.N.R.A.S.*, **145**, 31.
Markarian, B. E. 1977, *Astr. Ap.*, **58**, 139.
Neugebauer, G., Becklin, E. E., Oke, J. B., and Searle, L. 1976, *Ap. J.*, **205**, 29.
Oke, J. B., and Schild, R. E. 1970, *Ap. J.*, **161**, 1015.
Osterbrock, D. E. 1977, *Ap. J.*, **215**, 733.
Osterbrock, D. E., Koski, A. T., and Phillips, M. M. 1976, *Ap. J.*, **206**, 898.
Osterbrock, D. E., and Miller, J. S. 1975, *Ap. J.*, **197**, 535.

Pooley, G. G., and Henbest, S. N. 1974, *M.N.R.A.S.*, **169**, 477.
Riley, J. M., and Branson, N. J. B. A. 1973, *M.N.R.A.S.*, **164**, 271.
Riley, J. M., and Pooley, G. G. 1975, *Mem. R.A.S.*, **80**, 105.
Sandage, A. 1966, *Ap. J.*, **145**, 1.
———. 1967, *Ap. J. (Letters)*, **150**, L145.
———. 1972*a*, *Ap. J.*, **173**, 485.
———. 1972*b*, *Ap. J.*, **178**, 25.
———. 1973*a*, *Ap. J.*, **180**, 687.
———. 1973*b*, *Ap. J.*, **183**, 711.
Sargent, W. L. W. 1977, *Ap. J. (Letters)*, **212**, L105.
Schmidt, M. 1965, *Ap. J.*, **141**, 1.
Shields, G. A., and Oke, J. B. 1975, *Ap. J.*, **197**, 5.
Shields, G. A., Oke, J. B., and Sargent, W. L. W. 1972, *Ap. J.*, **176**, 75.
Souffrin, S. 1969, *Astr. Ap.*, **1**, 305.
Tinsley, B. M. 1977, *Pub. A.S.P.*, **89**, 245.
van den Bergh, S. 1976, *Ap. J. (Letters)*, **210**, L63.
Whitford, A. E. 1958, *A.J.*, **63**, 201.
Wilkinson, A., and Oke, J. B. 1978, *Ap. J.*, **220**, 376.
Wyndham, J. D. 1966, *Ap. J.*, **144**, 459.

J. B. OKE and HOWARD YEE: California Institute of Technology, Pasadena, CA 91125

CHAPTER 2

OPTICAL CONTINUUM AND EMISSION LINE LUMINOSITY OF ACTIVE GALACTIC NUCLEI AND QUASARS

I. INTRODUCTION

The notion that quasars are extreme examples of the phenomena occurring in what are generally described as active galactic nuclei (AGN), such as N galaxies and Seyfert galaxies, has been stated by various authors (e.g., Sandage 1971, Lynden-Bell 1971). There are striking similarities in the optical emission line spectra of broadline AGN's and low redshift quasars; and there is essentially no difference between the radio morphology of the two classes of objects (Miley 1971, Schmidt 1975). Establishment of the continuity between quasi-stellar objects and active galactic nuclei would not only provide a strong confirmation of the cosmological interpretation of redshifts of quasars, but also help us in the attempt to understand these objects. Some efforts along this line have been made, for example; by showing that quasars are associated with galaxies of similar redshift (e.g., Gunn 1971, Stockton 1978); by showing that there is continuity in the luminosities of the two classes (Weedman 1976); and by attempts to show that quasars are actually seated within galaxies (Kristian 1973).

A large body of data from both AGN's and quasars is now available in the literature, notably the sizable set of rather homogeneous spectrophotometry data collected over the past 10 years with the multichannel spectrophotometer (MCSP,

Oke 1969), using the Hale 5-meter telescope. In this paper we shall show that there is a strong correlation between non-thermal and Hβ emission for all classes of objects, suggesting that physical parameters such as the overall spectral index and the covering factor are very similar, and that there is a strong continuity of observed spectral properties between broad line active galactic nuclei and quasars.

II. DATA AND REDUCTION

The quasar sample is selected from the objects in Neugebauer et al. (1979). Since objects with Hβ and [OIII] λλ 5007+4959 in the range of spectral coverage are required for comparison with AGN's, this restricts the sample to 27 objects with $z \leqslant 1$. In addition, 3C249.1 (Richstone and Oke 1977) and 3C286 (Oke et al. 1970) are also included. Of these 29 quasars, 9 are radio quiet. For AGN data, both Seyfert and radio galaxies are used. The emission line 3CR radio galaxies from Yee and Oke (1978), plus a few new additions (Yee and Oke 1980b), are used. This subset contains 20 objects. Data for Seyfert galaxies are obtained from Neugebauer et al. (1976), and De Bruyn and Sargent (1978), with Markarian 231 and NGC 1275 discarded on account of their peculiar nature. Markarian 372 was also not used because it neither has a measurable Hβ nor a nonstellar continuum. This gives us 57 Seyfert galaxies and one additional radio galaxy. In total, the sample consists of 29 quasars and 76 active

nuclei, of which 48 are broad-line galaxies. The objects, along with their classification, redshift, and references are tabulated in Table 1. T he classification, which is defined in the usual manner (see e.g., Khachikian and Weedman 1974), is divided into Seyfert I (SyI), Seyfert II (SyII), broad-line radio galaxy (BLRG), narrow-line radio galaxy (NLRG), optically selected quasars (QSO), and radio-selected quasars (QSS). Seyfert I's, BLRG's and quasars will be collectively referred to as broad-line objects in this paper. The classification for a few radio galaxies with no high resolution spectra published is uncertain. In these cases, the classification is inferred from the general nature of the low resolution scans. The primary criterion is that the [OIII] $\lambda\lambda$ 5007+4959/Hβ ratio for broad-line objects tends to be around 1, whereas it is about 10 for narrow-line objects (Neugebauer et al. 1976). Also, [OII] λ3727 and other forbidden lines are in general more prominent in narrow-line objects. Classification based on these criteria is noted with a question mark in Table 1.

For each object, also listed in Table 1 are the non-thermal optical luminosity (L_{NT}) and line luminosities of Hβ, [OIII] $\lambda\lambda$ 5007+4959, and [OII] λ3727. All luminosities are calculated using $q_o = 0$, and $H_o = 55$ km s^{-1} M_{pc}^{-1}. L_{NT} is defined as the luminosity of the nonstellar component of the

continuum, which is assumed to be nonthermal and associated with the central source. It is derived by the following methods: For quasars, it is assumed that the observed continuum is overwhelmingly nonstellar; i.e., the underlying galactic component, if such should exist, only contributes a minimal amount to the continuum. The nonthermal optical luminosity is obtained by a simple integration of fluxes as provided in Neugebauer et al. (1979), from 3000 Å to 9500 Å in the rest frame. This is the same bandwidth used in Yee and Oke (1978), and was chosen because MCSP scans cover this range in the rest frame completely for most Seyfert and radio galaxies. Because it is not necessary to decompose the continua, L_{NT} can be determined rather accurately with typical uncertainties of about 0.05 in log L_{NT}. For the galaxies, in many cases, a significant amount of background galactic component exists, as most of the scans were obtained with a 10" aperture, and many show absorption features. A crude method of decomposition, model fitting by adding a standard galaxy to a power law component, as described in Yee and Oke (1978), is used to derive an approximate nonthermal optical luminosity. Very often a unique model is not possible. This procedure, however, is adequate to produce a luminosity with uncertainty in log L_{NT} from $\sim$0.05 for the strongly nonthermal objects to $\sim$.3 for the weaker ones. For the broad-line galaxies there is a tendency to underestimate L_{NT}, since there is often a

prominent upturn in the spectrum at short wavelengths, which is not taken adequately into account when a single power-law model is fitted. For objects with nonthermal radiation accounting for only a small fraction of the light, L_{NT} is extremely uncertain, as any small variation of the intrinsic color of the underlying galaxy can produce a false fit. It should be pointed out that the standard used is the elliptical standard in Yee and Oke (1978). For the Markarian Seyferts, which are mostly spirals (Adams 1977), this may not apply. However, for nearby objects this should not present a problem, as bulges of spirals are similar to ellipticals (Oke and Sandage 1968).

Most of the 105 objects used are broad-line objects. The blending of Hβ and [OIII] λλ 5007+4959 produces a significant uncertainty in determining line fluxes. The line luminosities used are those tabulated in the references with minor revisions when a higher resolution MCSP has subsequently become available. There are no line measurements published for the De Bruyn and Sargent data. For these objects we have derived from the published data the luminosities of the lines used. These data, which all have a resolution of 20-40 Å, allow reasonably accurate deblending of the [OIII]-Hβ complex, since the three to one ratio between [OIII] λ5007 and [OIII] λ4959 can be utilized. The uncertainties for both [OIII] λλ 5007+4959 and Hβ are estimated to be ∿15% for most of

these objects. The other data used are generally of lower resolution ($\sim$80 Å), and typical uncertainties for [OIII] and Hβ are $\sim$15 to 25% for bright objects with moderately strong lines, and $\geq$ 50% for the very weak lines in some radio galaxies. [OII] λ3727 usually has an uncertainty of $\geq$20% for narrow-line objects, and almost always $\geq$50% for the broad-line objects. While these estimates of uncertainties are large, they do not affect analysis significantly, as there is a large range of luminosities in the objects. We can compare the line flux data with other existing data. Many of the objects observed by De Bruyn and Sargent were also studied by Osterbrock (1977) and Koski (1978) using 10 Å resolution spectra. For almost all narrow-line objects, the line ratio [OIII] λλ 5007+4959/Hβ agrees within about 30% with those obtained by Koski. The ratio for most of the broad-line galaxies also agrees within 30% with those of Osterbrock, except that our ratio is almost always the larger one, and the ratios for galaxies belonging to the first Markarian list are systematically larger by a factor of 1.5 compared to the values obtained by Osterbrock. The differences in the line ratio could be caused by systematic effects in determining continuum levels and deblending, and by the difference in the size and shape of aperture used in the observations. The radically discrepant ratios of a few objects can possibly be attributed either to human error or real changes in the lines themselves.

In comparing the Hβ fluxes of objects which are in common with the list in Weedman (1976), it is found that the log $J_{H\beta}$ values for quasars and BLRG's from MCSP are larger by ∿0.1 to 0.2, whereas values for Seyfert I's are comparable. This could be due to the fact that a 10^4 km s^{-1} cutoff for the wing of the Balmer lines was used in Weedman's data.

III. RESULTS

Several authors have noticed a correlation between Balmer emission and the continuum. This has been expressed indirectly as similar equivalent width in Hβ for quasars and Seyfert I's (Searle and Sargent 1968), or quantitatively as in Weedman (1976) for Seyfert I's and in Yee and Oke (1978) for radio galaxies. In Figure 1, Hβ luminosities are plotted against the nonthermal luminosity; this should be a much better measure of the ionizing flux than simply the total visual flux. As in the case for radio galaxies, there is a strong correlation between Hβ and L_{NT} with a slope of one. Similarly in Figure 2, we plot the line luminosities of [OIII] λλ5007+4959 and [OII] λ3727 versus L_{NT}. The scatter is much larger than that of the Hβ plot. Also, the slope no longer equals one.

Before we go on to discuss the significance of the correlations, let us examine the problem of selection effects. The quasar sample of Neugebauer et al. (1979) is based on all

quasars in the Burbidge, Crown, and Smith (1977) catalogue brighter than magnitude 17. The Seyfert sample of De Bruyn and Sargent (1978) is based on all Seyfert galaxies in the first five Markarian lists. The radio galaxies come from an observation program of all 3CR radio galaxies with $z < 0.09$, plus some additional larger redshift ones. Hence, while incomplete, the set of objects used is a representative sample. One might argue that, by assuming the redshift to be cosmological, luminosities are consequently a strong function of redshift, which by itself would produce a correlation between emission line and continuum luminosities. We can avoid this problem by plotting the observed fluxes instead of luminosities, as in Figure 3 for Hβ, hence discarding the dependence on redshift. This produces a smaller range in the data, and thus relatively more scatter, but a strong correlation still exists. For the forbidden lines, because the slope is not unity, plotting apparent fluxes will produce a meaningless scatter diagram. Also, the choice of q_o will have a small effect on the correlation. It might also be argued that the correlations are based only on whether a line is visible above the continuum. A strong argument against this possibility is the fact that the three emission lines behave differently. The correlations have different amounts of scatter and different slopes. Also, a selection effect due

to line visibility would only select against objects with weak lines, i.e., points in the lower right half of the luminosity plots, not the upper left, as in the case for [OII]; yet, for the Hβ plot we observe a sharp cutoff in the upper left. In addition, the decomposition of the continuum places radio and Seyfert galaxies on the correlation line. Without such decomposition, some objects would have luminosities larger by an order of magnitude, producing a random scatter diagram on the lower end of the luminosity range. There is direct evidence that the Balmer lines are correlated with the nonthermal luminosity within objects that are variable. It has been found that Hβ emission varies with nonthermal radiation in 3C382 and 3C390.3 (Yee and Oke 1980a) and in 3C120 (Oke, Readhead and Sargent 1980). The above points demonstrate convincingly that the Hβ-L_{NT} correlation is not an artifact of some selection effect.

IV. DISCUSSION

a) Hβ Versus Nonthermal Luminosity

The correlation of $J_{H\beta}$ and L_{NT} is very good over five orders of magnitude, and it is still very good over three orders of magnitude when apparent luminosities are used. Apart from the broader scatter of points for the narrow-line objects, which could just be due to the larger uncertainty of L_{NT} for the generally weaker continuum, there are basically

no differences among narrow-line galaxies, broad-line galaxies, and quasars. Using least square regression, the slope for the quasars is 1.05 ± 0.15, where the uncertainty is the 95% confidence level for the slope. For the broad- and narrow-line galaxies, the slopes are 1.00 ± 0.09 and 0.99 ± 0.20 respectively. If all objects are considered together, a slope of 0.97 ± 0.04 is obtained. This flatter slope is caused by slight systematic displacement of points belonging to the different classes of objects.

Considering that the data have a typical error of 0.05 to 0.2 in the log, the difference is not significant, and we shall consider that the relation has a slope of 1. With this we can define a quantity $\Delta_{H\beta}$, which is the log of the ratio of nonthermal luminosity to Hβ luminosity:

$$\Delta_{H\beta} = \log L_{NT} - \log J_{H\beta} \ . \qquad (1)$$

In Figure 4 a histogram of the distribution of $\Delta_{H\beta}$ is plotted. The distribution, with a slight skewness toward the higher end, is centered at 1.77 with a standard deviation of 0.24. The average value of $\Delta_{H\beta}$ for quasars, 1.89 ± 0.24 (standard deviation), is slightly larger than that of the broad-line galaxies, 1.67 ± 0.21, and narrow-line galaxies 1.81 ± 0.33. The shifting of $\langle\Delta_{H\beta}\rangle$ of one standard deviation between quasars and broad-line galaxies is probably due to some systematic difference in determining the broad H_β flux by

different authors. Taking into account that the average uncertainty of $\Delta_{H\beta}$ is of the order of the half-width of the distribution, the difference of $\langle\Delta_{H\beta}\rangle$ is not significant. We can compare our relation with that found for a sample of Seyfert I's by Weedman (1976). Weedman found the relation between Hβ luminosity and a bolometric luminosity with a bandwidth of 350μ to 230 Å to be: $\log L_{bol} = L_{H\beta} + 3.2$. When this is adjusted to the optical bandwidth described here by assuming a typical spectral index of -0.7, it corresponds to an average $\Delta_{H\beta}$ of 1.9, which is only slightly larger than the value found here. The larger value is again due to the fact that Weedman's bolometric luminosities are upper bounds, as no decomposition was performed.

The simplest physical interpretation of the very strong correlation between L_{NT} and $J_{H\beta}$ is that the Balmer lines arise from recombination after ionization by the nonthermal continuum, as previously suggested by numerous authors (e.g., Greenstein and Schmidt 1964, Oke and Sargent 1968). We can derive the relation between Hβ luminosity and nonthermal optical luminosity by assuming the ionizing radiation to be in the form of a power law: ν^{α}, with spectral index α. By assuming steady state and combining the equation for Hβ luminosity with the integrated continuum luminosity, we obtain:

$$J_{H\beta} = CL_{NT} \frac{\nu_{Ly}^{\alpha} \nu_{H\beta} \alpha_{H\beta}}{\alpha_B} \frac{(\alpha+1)(n^{\alpha}-1)}{\alpha} \left| \nu_2^{\alpha+1} - \nu_1^{\alpha+1} \right|^{-1} \qquad (2)$$

where $\alpha \neq 0$ or -1. Here α_B is the effective recombination coefficient, $\alpha_{H\beta}$ the emission coefficient of Hβ, ν_{Ly} and $\nu_{H\beta}$ the Lyman limit and Hβ line frequency respectively, n a multiplicative constant which sets the cutoff in Rydberg in the ionizing continuum, ν_1 and ν_2 the limits for the definition of optical luminosity as defined earlier, and C, the covering factor, which would allow a different amount of ionizing radiation to escape without taking part in producing the line spectrum.

Hence:

$$\Delta_{H\beta}(\alpha) = \log \frac{\alpha}{\alpha+1} \frac{\nu_2^{\alpha+1} - \nu_1^{\alpha+1}}{n^{\alpha}-1} - \alpha \log \nu_{Ly} + \log \frac{\alpha_B}{\alpha_{H\beta} \nu_{H\beta}} - \log C \qquad (3)$$

Thus, we expect a correlation of L_{NT} and $J_{H\beta}$ with a slope of one if all continua have approximately the same spectral index. Hence, by assuming a simple recombination model, we can map the distribution of $\Delta_{H\beta}$'s into a distribution of equivalent overall spectral indices.

Using values for α_B and $\alpha_{H\beta}$ at 10^4, $\nu_1 = 10^{14.52}$ hz, and $\nu_2 = 10^{15.0}$ hz, and assuming a covering factor of unity, the $\Delta_{H\beta}$ distribution corresponds to an approximately Gaussian spectral index distribution of -1.0 ± 0.2 (hwhm) for no cutoff in the ionizing continuum and $\sim -0.9 \pm 0.2$ if a four

Rydberg (n = 4) cutoff, where He ionization becomes important, is used. If a covering factor of less than 1.0 is used, a further flattening of α is needed to compensate. We now compare this equivalent distribution of spectral indices with observed distributions obtained by Neugebauer et al. (1979) and Richstone and Schmidt (1980). For a complete sample of radio-loud quasars, Richstone and Schmidt obtained a spectral index distribution centered at $\sim$-0.6 and a broader spread of $\sim$1.0 (fwhm) with a tail toward steeper α's, and a cutoff at +0.3. The smaller sample of mixed radio- loud and quiet quasars of Neugebauer et al. (1979) gives essentially the same distribution. If a covering factor of $\sim$0.3 is used, we would obtain an equivalent distribution of α for both quasars and active galactic nuclei with the same peak value and skewness as the observed ones except that ours is narrower. This covering factor is in agreement with the fraction of quasars showing a Lyman edge by Osmer (1979) – 2 out of 8; and Oke (private communication) – 3 out of 10. The broadness of the observed spectral index distribution can be attributed to the fact that a local spectral index is very often greatly different from the overall spectral index.

There are several ways that a local spectral index can be altered drastically without too much effect on $\Delta_{H\beta}$. One is the existence of the feature at $\sim$3200 Å in the spectra of most quasars (Richstone and Schmidt 1980), and some Seyfert

I's (Neugebauer et al. 1976). This causes a large flattening of the optical spectral index accompanied by only a small increase in $\Delta_{H\beta}$. Another mechanism that can be used to alter the optical spectral index is reddening, which has been invoked often to account for the Balmer decrement observation, especially for the narrow-line objects. To determine how reddening affects the function $\Delta(\alpha)_{H\beta}$, for simplicity, we approximate the reddening law by using:

$$D(\nu) = 10^{+\xi\left(\frac{\nu}{\nu_o}\right)^{\gamma}} \tag{4}$$

where ξ and γ are functions of the extinction, and $D(\nu)$ is defined as the multiplicative factor needed to bring the intrinsic flux to the observed flux, i.e.,

$$F(\nu)_{\text{observed}} = F(\nu)_{\text{intrinsic}} \times D(\nu) \ , \tag{5}$$

so that the effect on L_{NT} is:

$$\Delta \log L_{NT} = \xi + \log\left\{\frac{\alpha+1}{\alpha+\gamma+1}\left[\frac{\nu_1}{\nu_0}\right]^{\gamma}\left[\frac{1-\left(\frac{\nu_2}{\nu_1}\right)^{\alpha+\gamma+1}}{1-\left(\frac{\nu_2}{\nu_1}\right)^{\alpha+1}}\right]\right\} \tag{6}$$

We can approximate the Whitford (1958) type reddening with extinction E_{B-V} by using $\xi \sim -1.25\ E_{B-V}$ and $\gamma \sim 4.3\ E_{B-V}$. The effect of reddening on Hβ flux is simply:

$$\Delta \log J_{H\beta} = \frac{A(\nu_{H\beta})}{-2.5} = -1.45\ E_{B-V} \qquad (7)$$

where $A(\nu_{H\beta})$ is the absorption coefficient at 4861 Å. Thus, for a continuum with an intrinsic α of -0.9, an extinction E_{B-V} of 0.5 causes a change of the observed α by $\sim$-2.0, but produces an increase in $\Delta_{H\beta}$ by only 0.16. It is interesting to note that the skewness toward large $\Delta_{H\beta}$ mainly comes from narrow-line objects, which is consistent with the idea that there is a large amount of reddening in Seyfert II galaxies. If we assume the distribution of $\Delta_{H\beta}$ to be intrinsically symmetric, then some narrow line objects would require a reddening of E_{B-V} up to $\sim$1.2 to account for their large $\Delta_{H\beta}$ value.

The tightness of the distribution of $\Delta_{H\beta}$, in which 70% of the objects are within a narrow band of $\sim$0.4, suggests that the physical parameters in these objects are very similar. For the simplest picture, the main factors that can affect $\Delta_{H\beta}$ for an individual object are: a) spectral index; b) the covering factor; and, c) to a small extent, reddening. It seems very unlikely that all these effects conspire to produce such a tight correlation. Hence, if we hold the covering factor constant at 0.3, then 70% of the objects would have an overall spectral index between 0.4 and 0.8. And similarly, if we hold the spectral index constant, we can only vary the covering factor in 70% of the objects by no more than a factor of 3.

The similarity between narrow- and broad-line objects in the correlation between $J_{H\beta}$ and L_{NT} offers some insight into the problem of the observed Lα/Hβ ratios. In both quasars and Seyfert I's, all observations have indicated that Lα/Hβ is of the order 3 to 5, almost an order of magnitude smaller than the ratio predicted by simple recombination theory (e.g. Baldwin 1977, Davidsen et al. 1977). The various approaches to resolve this discrepancy involve either the enhancement of Hβ or the destrubtion of Lα (e.g., Baldwin 1977, Ferland et al. 1979, Zirin 1978, Krolik and McKee 1978, and London 1979), by using more detailed and complex models. While there are few or no data on Lα/Hβ ratios for the narrow-line galaxies, the Balmer decrement in these objects seems to be accountable by using standard reddening (e.g. Koski 1978, Neugebauer et al. 1980), hence enhancement of Hβ probably is not required. If the mechanisms for producing the Balmer lines are different between the two classes of objects, i.e. enhancement of Hβ occurs in broad-line objects but not narrow-line objects, one would expect a shift in the correlation plot between the two groups of objects. It seems likely that some other process(es) would exactly cancel out the difference. Thus, the fact that there is no difference in the average $\Delta_{H\beta}$ for the two types of objects suggests that there is at most very slight enhancement of Hβ ($\lesssim$50%) in the broad-line objects, or we must conclude that the same mechanism also applies in the narrow-line objects.

b) Forbidden Lines Versus Nonthermal Luminosity

The division between broad-line and narrow-line objects is clearly seen in the behavior of the forbidden lines with respect to L_{NT}. Unlike Hβ, in the plots of [OIII]λλ5007+4959 and [OII] λ3727 versus L_{NT}, the two classes of objects populate different regions (see Figure 2) with a slight overlap. This is especially pronounced for [OII], which is not detected in most quasars. While the scattering is large in both plots, again, as in the Hβ plot, the similarity and continuity with overlapping luminosities between broad-line galaxies and quasars is evident. There is also an indication that the forbidden line luminosities do not scale exactly with nonthermal luminosity. In a formal regression fit, both broad-line and narrow-line objects produce a slope of $\sim 0.8 \pm 0.2$ for $J_{[OIII]}$ versus L_{NT}, which is only barely consistent with a slope of unity. The same 0.8 ± 0.2 slope is obtained for the narrow-line objects for [OII]. For the broad-line objects, the [OII] diagram is probably random, limited by the detection of the line.

To minimize the effect of z, we form $\Delta_{[OIII]}$ and $\Delta_{[OII]}$, the analogous quantities to $\Delta_{H\beta}$. We found the mean value of the distribution of $\Delta_{[OIII]}$ to be 2.15 ± 0.33, 1.76 ± 0.42, and 0.88 ± 0.46 for quasars, broad-line galaxies, and narrow-line galaxies respectively. The differences are statistically significant. Assuming that they are the same type of object, the difference between quasars and broad-line

galaxies can be explained by a possible luminosity dependence of $\Delta_{[OIII]}$. Using the overlapping luminosity range of $10^{44.4}$ to 10^{45} erg s^{-1}, populated equally by our sample of quasars and broad-line galaxies, we found $<\Delta_{[OIII]}>$ to be identical: 2.20 ± 0.40 and 2.20 ± 0.31, respectively, for 7 objects in each category. (3C 234 is omitted because it is an intermediate type object with a narrow Hβ component only (Grandi and Osterbrock 1978).) However, the difference between narrow- and broad-line galaxies cannot be due to a luminosity dependence of $\Delta_{[OIII]}$. The values, with a difference of two standard deviations, 1.93 ± 0.31 and 1.03 ± 0.43 are obtained for broad- and narrow-line galaxies, respectively, when $<\Delta_{[OIII]}>$ is calculated using objects in the range of L_{NT} between 10^{43} and 10^{44} ergs s^{-1}. A similar difference is obtained for the [OII] line. In the same luminosity range, $<\Delta_{[OII]}>$ is 1.47 ± 0.37 for the narrow-line galaxies and $\geq$ 2.6 (only a lower limit can be determined) for the broad-line galaxies.

The difference of approximately one order of magnitude in the relative strength of forbidden lines between narrow- and broad-line objects has been noted indirectly via the difference in the [OIII]/Hβ ratio (e.g. Neugebauer et al. 1976). This shows that the direct cause for the lower [OIII]/Hβ ratio is a decrease in the forbidden line strengths in the broad-line objects with respect to the narrow-line object, rather than an increase of Hβ strength. This, along

with similarity in the $J_{H\beta}$ versus L_{NT} correlation, is consistent with the current view of these objects. The high electron density of $\sim 10^9$ cm^{-3} of the broad-line region suppresses the forbidden line without much effect on the total flux of Hβ line. The weak forbidden lines of broad-line objects are produced only in the narrow-line region of these objects after most of the ionizing radiation has been absorbed by the high density region.

c) BL Lac Objects

The lack of emission lines put BL Lac objects off the correlation line of $J_{H\beta}$ versus L_{NT} plot. Typical BL Lac objects would have $\Delta_{H\beta} \geq 4$. From the distribution of $\Delta_{H\beta}$, only $\sim$ 0.001% of active objects are expected to have $\Delta_{H\beta} >$ 3.5. As there are at least 3 to 4 BL Lac objects (depending on classification definition) in the 3CR and Markarian survey, BL Lac objects are not the tail end of the distribution. Hence, assuming that all active objects have similar central energy sources, i.e., there is some smooth distribution of spectral index, this paucity of intermediate line strength objects is consistent with the view that the lack of lines in BL Lac objects is due to a lack of gas rather than the lack of ionizing radiation.

V. SUMMARY

From a collection of spectra of quasars and active galactic nuclei, we have studied the relationship between

the non-thermal continuum, which is believed to be the manifestation of the central engine, and the emission lines. It is found that the behavior of emission lines with respect to the optical continuum is indistinguishable between quasars and broad-line galaxies. This firmly supports the hypothesis of continuity between broad-line galaxies and quasars, and hence the cosmological interpretation of quasar redshifts. The strong correlation between Hβ flux and non-thermal radiation suggests that Balmer emission lines arise from recombination after photoionization by the non-thermal continuum, and that physical parameters, such as underlying overall spectral indices and covering factors, are similar from object to object. The difference between broad- and narrow-line objects lies in the relative strength of the forbidden lines to the continuum. This is consistent with the view that forbidden lines are suppressed in the broad-line region of broad-line objects. There is some indication that the forbidden oxygen lines do not scale directly with continuum luminosity, but more data would be needed for a more definite conclusion.

REFERENCES

Adams, T. F. 1977, Ap. J. Suppl., 33, 19.

Baldwin, J. A. 1977, M.N.R.A.S., 178, 67P.

Burbidge, G., Crown, A. H., and Smith, H. E. 1977, Ap. J. Suppl., 33, 113.

Davidsen, A. F., Fastie, W. G., and Hartig, G. F. 1977, Nature, 269, 203.

De Bruyn, A. G., and Sargent, W. L. W. 1978, A. J., 83, 1257.

Ferland, G. F., Rees, M. J., Longair, M. S., and Perryman, M. A. C. 1979, M.N.R.A.S., 187, 65P.

Grandi, S. A., and Osterbrock, D. E. 1978, Ap. J., 220, 783.

Greenstein, J. L., and Schmidt, M. 1964, Ap. J., 140, 1.

Gunn, J. E. 1971, Ap. J. (Letters), 164, L113.

Khachikian, E. Ye., and Weedman, D. W. 1974, Ap. J., 192, 581.

Koski, A. T. 1978, Ap. J., 223, 56.

Kristian, J. 1973, Ap. J. (Letters), 179, L61.

Krolick, J. H., and McKee, C. F. 1978, Ap. J. Suppl., 37, 459.

London, R. 1979, Ap. J., 228, 8.

Lynden-Bell, D. 1971, M.N.R.A.S., 155, 119.

Miley, G. K. 1971, M.N.R.A.S., 152, 477.

Neugebauer, G., Becklin, E. E., Oke, J. B., and Searle, L. 1976, Ap. J., 205, 29.

Neugebauer, G., Oke, J. B., Becklin, E. E., and Matthews, K. 1979, Ap. J., 230, 79.

Neugebauer, G., et al. 1980, Ap. J., 238, 502.

Oke, J. B. 1969, P.A.S.P., 81, 11.

Oke, J. B., Neugebauer, G., and Becklin, E. E. 1970, Ap. J., 159, 34.

Oke, J. B., Readhead, A. C. S., and Sargent, W. L. W. 1980, preprint.

Oke, J. B., and Sandage, A. 1968, Ap. J., 154, 21.

Oke, J. B., and Sargent, W. L. W. 1968, Ap. J., 151, 87.

Osmer, P. S. 1979, Ap. J., 227, 18.

Osterbrock, D. E. 1977, Ap. J., 215, 733.

Richstone, D. O., and Oke, J. B. 1977, Ap. J., 213, 8.

Richstone, D. O., and Schmidt, M. 1980, Ap. J., 235, 361.

Sandage, A. 1971, Nuclei of Galaxies, p. 271, ed. D. J. K. O'Connell (New York: Am. Elsevier).

Schmidt, M. 1975, Stars and Stellar Systems, Vol. IX, p. 283, ed. A. Sandage, M. Sandage, and J. Kristian (Chicago: University of Chicago Press).

Searle, L., and Sargent, W. L. W. 1968, Ap. J., 153, 1003.

Stockton, A. 1978, Ap. J., 223, 744.

Weedman, D. W. 1976, Ap. J., 208, 30.

Whitford, A. E. 1958, A. J., 63, 201.

Yee, H. K. C., and Oke, J. B. 1978, Ap. J., 226, 753.

——. 1980a, preprint.

——. 1980b, in preparation.

Zirin, H. 1978, Ap. J. (Letters), 222, L105.

TABLE 1

LUMINOSITY DATA

Object	Classification	z	log L_{NT}	log $J_{H\beta}$	log $J_{[OIII]}$	log $J_{[OII]}$	ref*
3C 48.....	QSS	0.367	45.63	43.85	43.66	...	1
3C 95.....	QSS	0.614	45.87	43.96	43.85	...	1
3C 94.....	QSS	0.962	46.49	44.85	44.60	...	1
3C249.1.....	QSS	0.311	45.72	43.89	43.64	...	4
3C273.....	QSS	0.158	46.21	44.29	43.42	...	1
3C279.....	QSS	0.538	45.56	43.12	43.22	...	1
3C286.....	QSS	0.846	45.98	43.94	44.38	...	5
3C334.....	QSS	0.555	45.59	44.08	43.91	42.24	1
3C351.....	QSS	0.371	45.91	44.20	43.69	<42.2	1
3C454.3.....	QSS	0.859	46.38	44.36	44.65	...	1
PKS0405-12....	QSS	0.574	46.45	44.69	...	...	1
PKS0837-12....	QSS	0.200	44.85	43.07	42.98	41.92	1
PKS1004+13....	QSS	0.240	45.62	43.45	42.93	...	1
PKS1510-08....	QSS	0.361	45.75	43.53	...	...	1
PKS2251+11....	QSS	0.323	45.63	44.08	43.64	...	1
4C 31.30.....	QSS	0.462	46.06	44.22	44.03	...	1
4C 37.43.....	QSS	0.371	45.60	43.82	43.50	...	1
4C 31.63.....	QSS	0.297	45.75	43.99	43.21	...	1
PG0026+12.....	QSO	0.142	45.16	43.22	42.86	...	1
PG 0906+48....	QSO	0.118	44.98	42.49	42.20	...	1
PG 1001+05....	QSO	0.161	44.85	42.93	42.28	...	1
PG 1351+64....	QSO	0.088	44.98	43.04	42.89	...	1
PG 1358+04....	QSO	0.427	45.73	43.90	43.39	<41.7	1
TON 202.....	QSO	0.366	45.72	43.83	43.63	42.35	1
TON 256.....	QSO	0.131	44.89	43.31	43.29	42.28	1
III ZW2.....	QSO	0.089	44.90	43.12	42.72	...	1
NAB0205+024...	QSO	0.155	45.07	43.20	42.92	42.19	1
B 264.....	QSO	0.095	44.03	42.04	41.99	...	1
MKN 205.....	QSO	0.070	44.52	42.58	42.22	...	1
3C 109.....	BLRG	0.3056	44.99	42.85	43.39	42.26	2
3C 227.....	BLRG	0.0861	43.80	42.33	42.48	41.26	6
3C 234.....	BLRG	0.1848	44.46	42.62	43.60	42.60	2
3C 382.....	BLRG	0.0578	44.43	42.88	42.11	41.78	6
3C 390.3.....	BLRG	0.0569	44.03	42.67	42.66	41.70	2
3C 445.....	BLRG	0.0569	43.65	42.11	42.57	41.41	2
4C 459.....	BLRG?	0.2199	44.25	42.54	42.41	42.23	2
PKS 2349-01...	BLRG	0.1741	44.88	43.19	42.91	41.99	3
3C 17.....	NLRG?	0.2197	43.55	41.99	42.54	42.15	2
3C 33.....	NLRG	0.0595	42.86	41.25	42.29	41.63	2
3C 79.....	NLRG	0.2559	43.81	42.21	43.34	42.50	2
3C 171.....	NLRG	0.2384	43.55	41.97	42.94	42.63	2
3C 198.....	NLRG	0.0815	43.36	41.18	41.60	41.45	2
3C 219.....	NLRG	0.1744	43.34	41.55	42.34	41.08	2
3C 277.3.....	NLRG	0.0857	42.88	≤41.15	41.70	...	2
3C 285.....	NLRG	0.0794	43.08	40.60	41.87	40.92	6
3C 305.....	NLRG	0.0416	43.02	41.01	41.54	41.51	2
3C 405.....	NLRG	0.0570	43.76	41.91	43.13	42.12	2
3C 456.....	NLRG?	0.2330	43.72	42.12	42.41	42.45	2
MKN 9.....	Sy I	0.0402	43.80	42.07	41.90	<40.7	3
MKN 10.....	Sy I	0.0293	43.40	41.86	41.77	41.11	3
MKN 40.....	Sy I	0.021	42.54	41.00	41.19	40.66	3
MKN 42.....	Sy I	0.024	42.92	41.04	40.53	40.80	3
MKN 50.....	Sy I	0.0230	43.10	41.39	40.74	40.24	3

Object	Classification	z	log L_{NT}	log $J_{H\beta}$	log $J_{[OIII]}$	log $J_{[OII]}$	ref*
MKN 69.....	Sy I	0.0763	43.94	42.01	41.96	41.35	3
MKN 79.....	Sy I	0.0219	43.48	42.04	41.94	41.29	3
MKN 106.....	Sy I	0.124	44.26	42.73	42.47	41.61	3
MKN 110.....	Sy I	0.0360	43.56	42.01	42.07	41.45	3
MKN 124.....	Sy I	0.0566	43.92	42.17	42.46	...	7
MKN 141.....	Sy I	0.039	43.55	41.71	41.52	40.71	3
MKN 142.....	Sy I	0.045	43.50	41.71	41.30	41.28	3
MKN 279.....	Sy I	0.0308	43.93	42.19	41.77	41.51	3
MKN 290.....	Sy I	0.0308	43.72	42.06	42.04	40.91	3
MKN 291.....	Sy I	0.035	43.47	41.08	41.22	40.73	3
MKN 304.....	Sy I	0.0665	44.40	42.86	42.19	41.02	3
MKN 335.....	Sy I	0.025	44.07	42.42	41.91	41.19	3
MKN 352.....	Sy I	0.015	42.96	41.32	40.75	<40.0	3
MKN 358.....	Sy I	0.046	43.27	41.48	41.39	40.40	3
MKN 374.....	Sy I	0.044	43.74	41.99	41.76	<40.3	3
MKN 376.....	Sy I	0.056	44.48	42.73	41.96	<41.0	3
MKN 464.....	Sy I	0.051	43.42	42.07	42.31	41.85	3
MKN 474.....	Sy I	0.041	43.26	41.59	41.59	40.40	3
MKN 478.....	Sy I	0.079	44.58	42.89	42.38	<41.6	3
MKN 486.....	Sy I	0.039	43.89	42.18	41.75	<40.4	3
MKN 506.....	Sy I	0.043	43.07	41.60	42.06	41.15	3
MKN 509.....	Sy I	0.0355	44.38	42.86	42.68	41.77	3
MKN 618.....	Sy I	0.034	43.65	41.98	41.88	41.06	3
NGC 3516.....	Sy I	0.0093	43.15	41.26	41.22	39.89	3
NGC 4051.....	Sy I	0.023	41.54	39.64	40.02	39.25	3
NGC 4151.....	Sy I	0.0033	42.74	41.21	41.78	40.91	3
NGC 5548.....	Sy I	0.0166	43.22	41.89	41.86	40.75	3
NGC 6814.....	Sy I	0.0053	41.37	39.65	40.26	39.37	3
NGC 7469.....	Sy I	0.0167	43.67	41.92	41.94	41.19	3
NGC 7603.....	Sy I	0.0294	43.28	41.33	41.30	40.83	3
I Zw 1.....	Sy I	0.061	44.47	42.76	42.62	41.58	3
II Zw 136.....	Sy I	0.0617	44.33	42.83	42.54	<41.2	3
III Zw 77.....	Sy I	0.033	43.24	41.50	41.24	40.58	3
KKH 21.....	Sy I	0.136	44.38	42.92	42.68	41.72	3
MCG 8-11-11...	Sy I	0.020	42.88	41.63	42.14	41.41	3
MKN 1.....	Sy II	0.016	42.47	40.71	41.88	41.01	3
MKN 3.....	Sy II	0.0137	42.48	41.24	42.51	41.84	3
MKN 6.....	Sy II	0.0176	43.01	41.48	42.08	41.53	3
MKN 34.....	Sy II	0.051	43.42	41.76	42.95	42.27	3
MKN 78.....	Sy II	0.036	42.78	41.36	42.61	42.00	3
MKN 176.....	Sy II	0.027	42.61	40.41	41.85	41.22	3
MKN 198.....	Sy II	0.024	42.80	40.56	41.57	41.16	3
MKN 268.....	Sy II	0.041	43.00	40.42	41.86	41.83	3
MKN 270.....	Sy II	0.009	41.42	39.81	41.02	40.81	3
MKN 273.....	Sy II	0.034	43.10	41.11	42.14	41.79	3
MKN 315.....	Sy II	0.0395	43.36	41.56	41.71	41.90	3
MKN 348.....	Sy II	0.0140	42.20	40.45	41.61	41.10	3
MKN 463.....	Sy II	0.0505	43.61	42.00	42.97	42.44	3
NGC 1068.....	Sy II	0.0036	42.49	40.92	42.09	41.22	3
NGC 3227.....	Sy II	0.0033	41.20	39.46	40.47	40.10	3
I Zw 92.....	Sy II	0.039	43.59	41.87	42.96	42.23	3
III Zw 55.....	Sy II	0.0246	42.71	40.34	41.29	41.23	3

*References: 1 Neugebauer et al. (1979), 2 Yee and Oke (1978), 3 De Bruyn and Sargent (1978), 4 Richstone and Oke (1977)
5 Oke et al. (1970), 6 Yee and Oke (1980b), 7 Neugebauer et al. (1976)

FIGURE CAPTIONS

Figure 1 - Correlation of Hβ line luminosity and nonthermal luminosity. Coordinates are in units of ergs s^{-1}.

Figure 2 - Correlations of forbidden line luminosity and nonthermal luminosity. Arrows represent upper limits for 1) broad-line galaxies (•) and 2) quasars (-).

Figure 3 - Correlation of apparent flux of Hβ and apparent nonthermal flux. Coordinates are in units of ergs s^{-1} cm^{-2}.

Figure 4 - Histogram of $\Delta_{H\beta}$, filled boxes represent broad-line galaxies; shaded boxes quasars; and open boxes narrow-line galaxies.

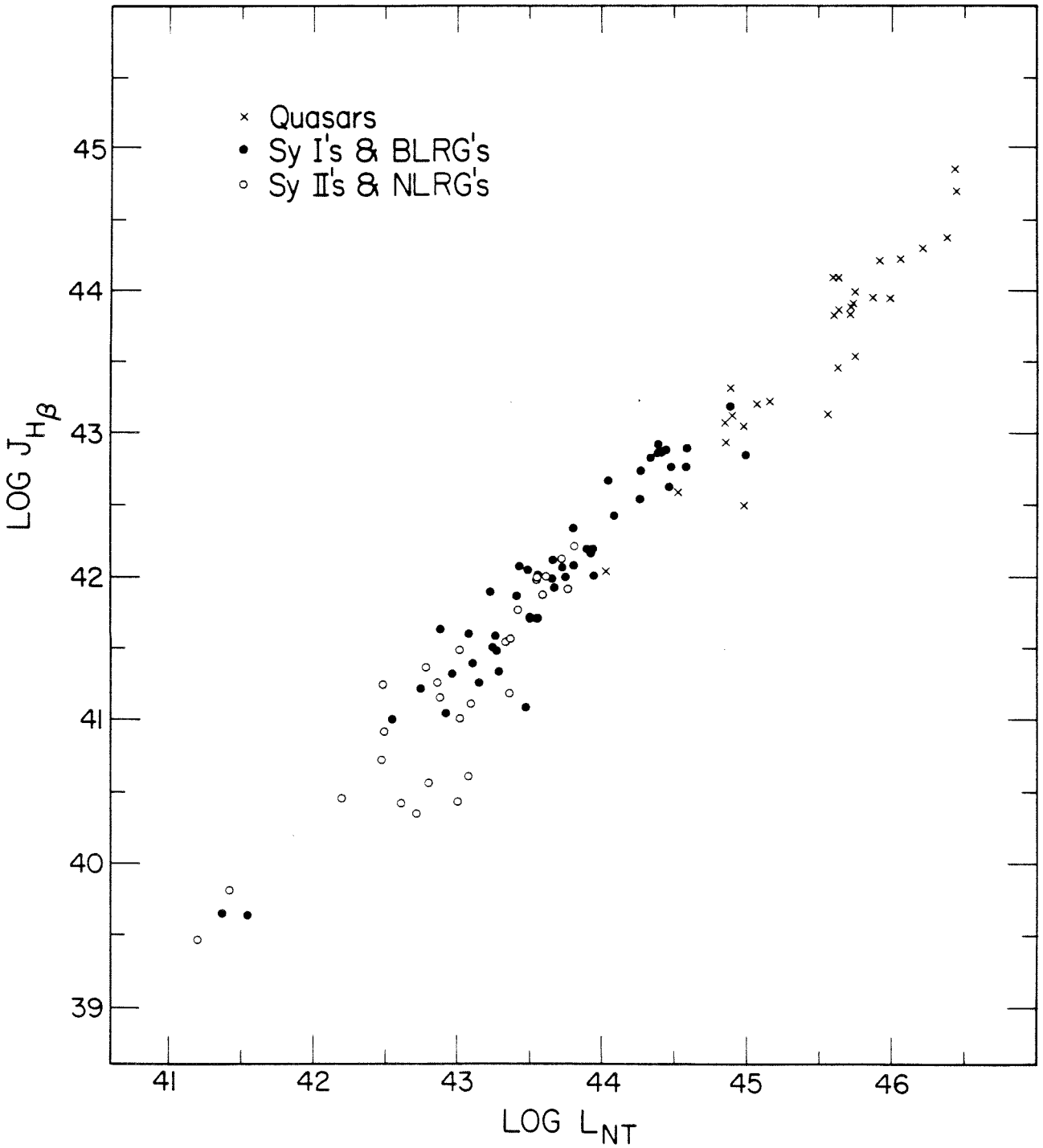
× Quasars
• Sy I's & BLRG's
○ Sy II's & NLRG's
LOG $J_{H\beta}$
LOG L_{NT}
39
40
41
42
43
44
45
41
42
43
44
45
46

Figure 1

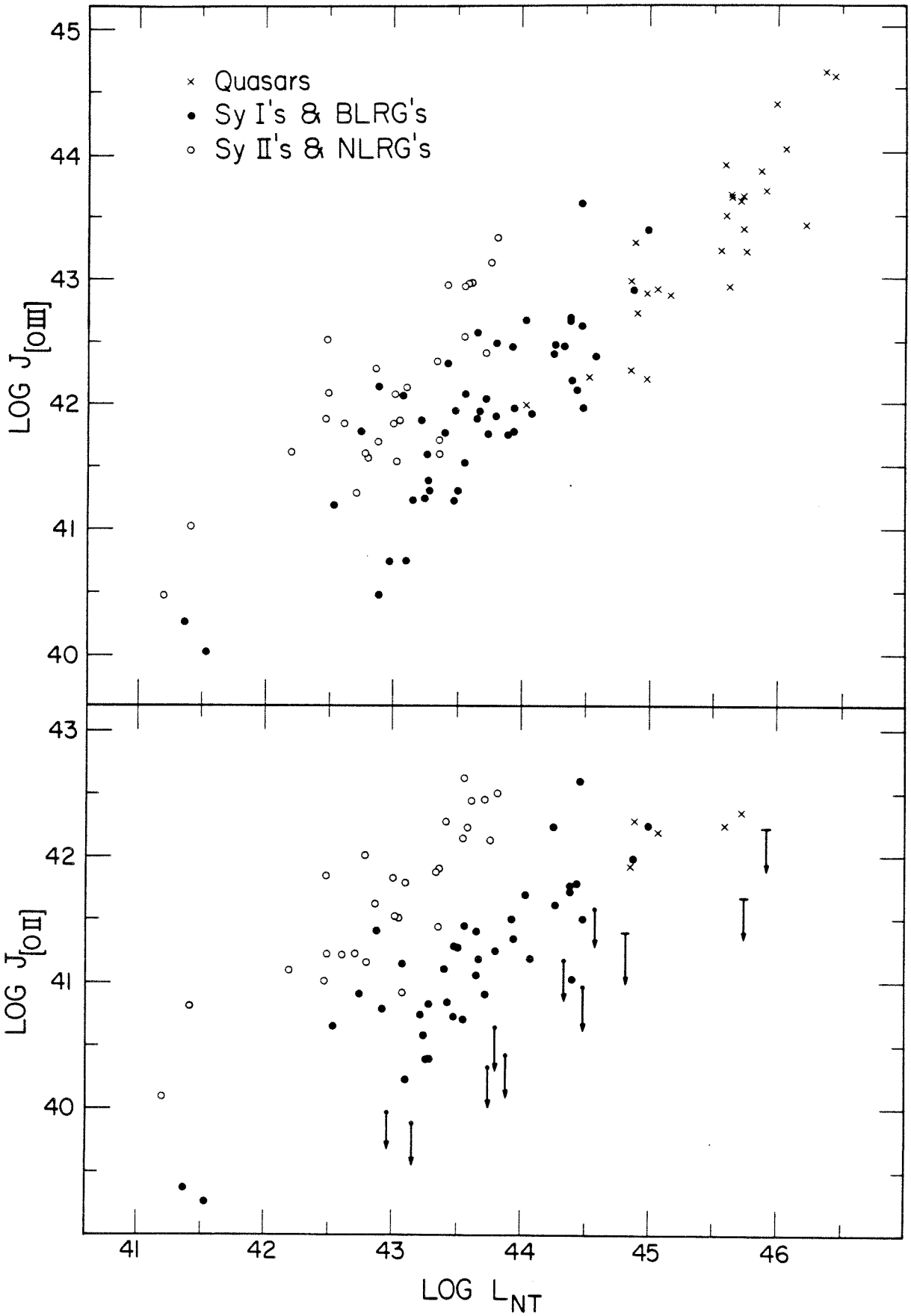
Quasars
Sy I's & BLRG's
Sy II's & NLRG's
LOG J[OIII]
LOG J[OII]
LOG L_NT
45
44
43
42
41
40
46

Figure 2

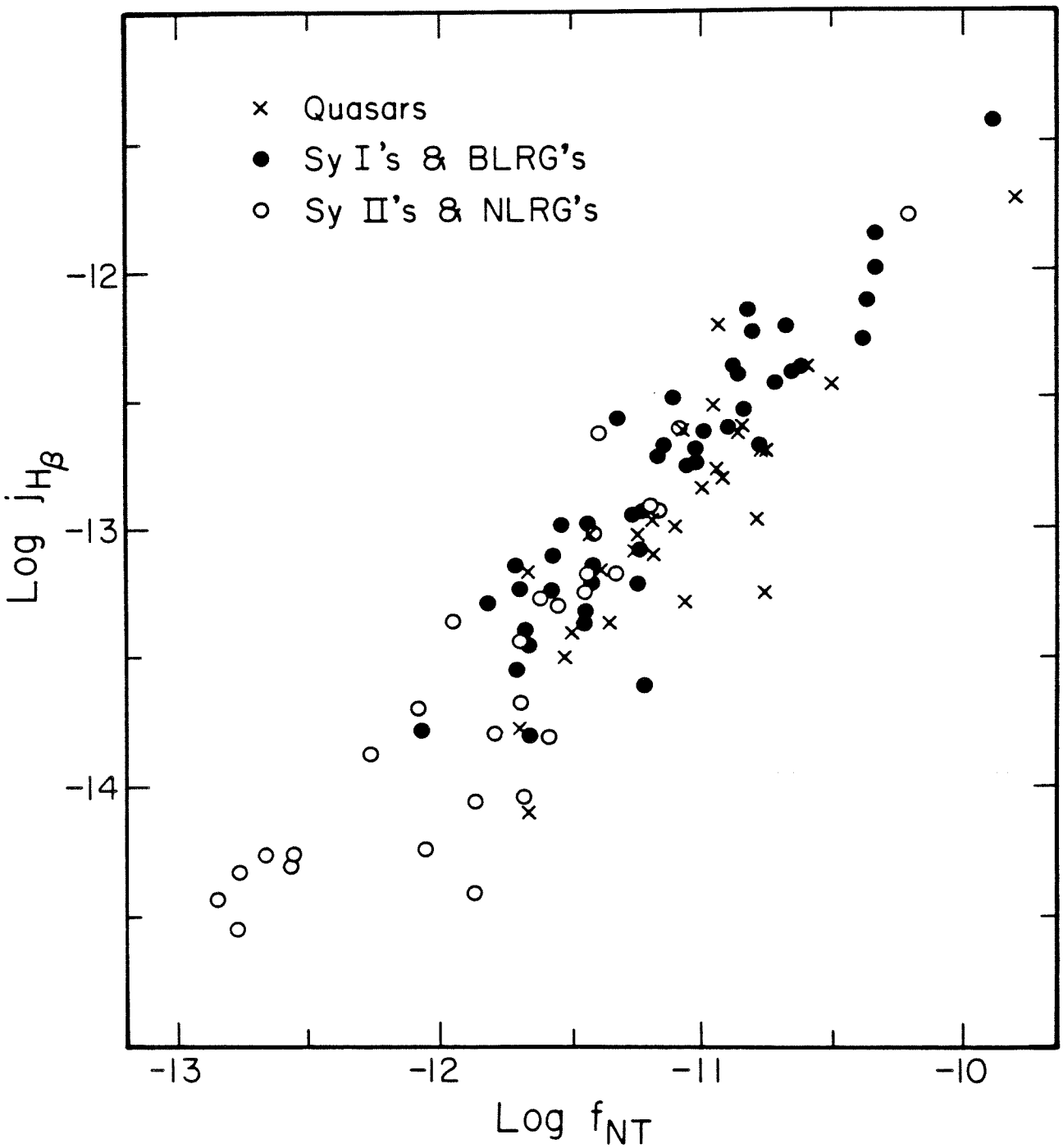
× Quasars
● Sy I's & BLRG's
○ Sy II's & NLRG's
-12
-13
-14
Log $j_{H\beta}$
-13
-12
-11
-10
Log f_{NT}

Figure 3

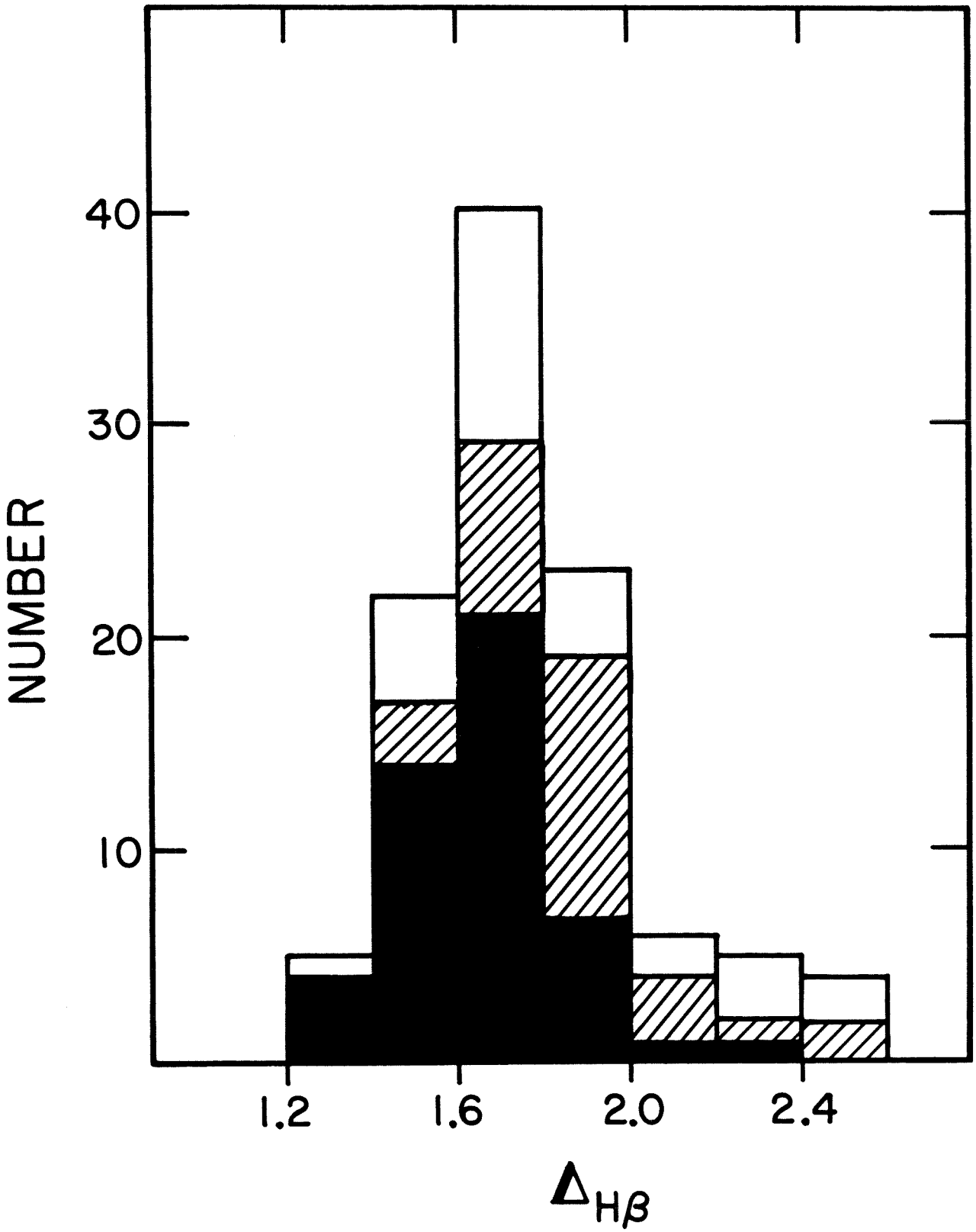

Figure 4

CHAPTER 3

OPTICAL SPECTRAL VARIABILITY OF THE N-GALAXIES 3C 382 AND 3C 390.3

I. Introduction

The study of luminosity variation of Seyfert galaxies, N-galaxies and quasars is of great importance as it is not only the most direct means of placing limits on the size of these objects, but it can also provide other constraints in model construction. There have been many programs of monitoring of luminosity variation of quasars and active galactic nuclei. Most of these are broad-band photographic monitoring programs (e.g., Selmes, Tritton and Wordsworth, 1975, and Scott *et al.* 1976).

One of the first of the active galaxies to be reported as variable is the N-galaxy 3C 390.3. (Sandage, 1967). In this paper, we present a study, using low to moderate resolution multichannel spectrophotometry (MCSP), of recent variations in the absolute optical energy distribution of 3C 390.3, and another N-galaxy, 3C 382 which was first reported to be variable by O'Dell *et al.* (1978). The similarity between 3C 382 and 3C 390.3 is striking. Both are strong radio sources at about the same redshift: 0.0578 and 0.0569 respectively. In the radio regime, they have similar luminosity ($\sim 10^{43.5}$ ergs s^{-1}), and identical radio morphology -- a double with a unresolved compact flat-spectrum central component coinciding with the galaxy (Riley and Branson, 1973; and Hargrave and McEllin, 1975). Optically, both are of approximately equal apparent brightness ($\sim$ 15.5 mag, visual). They have similar optical spectra: they are both broad-line radio galaxies, possessing very broad permitted Balmer lines (Osterbrock, Koski and Phillips, 1976), though 3C 390.3 has relatively stronger forbidden lines. Morphologically, they both can be classified as N-galaxies, with a bright point-like nucleus surrounded by an amorphous body.

There are many advantages in using multichannel spectrophotometry to study the variation of these objects, as we can study both the changes in the continuum

energy distribution and emission line strengths, and the correlation between them. We find that the spectral variations are consistent with the assumption that the energy distribution of these objects consists of a variable central nonstellar continuum of constant spectral shape superimposed on an elliptical galaxy spectrum. Furthermore, the broad permitted lines covary with the central continuum, but not in direct proportionality. We also find evidence of variation of the line profiles of the permitted lines of both galaxies.

II. Observations and Data

The data used consist of absolute energy distributions obtained with the multichannel spectrophotometer (Oke, 1969) attached to the Cassegrain focus of the Hale 5.08-meter telescope. The epochs covered range from 1969 to 1980. Some of the data have been published previously (Penston and Penston, 1973; de Bruyn and Sargent 1978; Yee and Oke, 1978). All absolute fluxes are based on the calibration of α Lyrae by Oke and Schild (1970). Thus, we have a very homogeneous set of data for the study of the variations in the absolute energy distribution of these objects. A journal of the observations is provided in table 1. Listed for each epoch are the date of observation, the aperture used, the resolution and the reference.

Representative spectra of epochs with different luminosity are plotted in figures 1a and 1b, for 3C 382 and 3C 390.3 respectively. The equivalent visual magnitude AB_{5450} (magnitude at $\lambda = 5450$Å, $\log \nu = 14.74$) of each observation is tabulated in table 1. The transformation between magnitude AB and flux F in units of mJy (i.e. 10^{-26} ergs s^{-1} cm^{-2} hz^{-1}) can be obtained by the relation: $AB = -2.5 \log F - 22.60$.

In figures 2a and 2b, we have plotted the approximate B magnitudes derived from the multichannel scans for each epoch for 3C 382 and 3C 390.3. They are

obtained by averaging the fluxes over a band width of ~ 1000Å centered around 4500Å. A correction of +0.21 mag is applied to bring the magnitudes to the B band of the UBV system. Note that the magnitudes plotted have not been corrected for aperture effect. The variations are color dependent, with the visual magnitudes having a smaller range than the blue magnitudes.

For 3C 382, we do not have MCSP data in the interval between 1970 and 1977. The broad-band observation of O'dell *et al.* (1978), also plotted in figure 1a, was made in 1976 and they obtained a B magnitude of 15.47 in an aperture of 18", close to that of the 1977 MCSP scan of de Bruyn and Sargent (1978). Hence, a large part of the increase in the brightness of 3C 382 occurred between 1970 and 1976. There was at least one other episode of brightness increase which occurred between 1964 and 1970. Sandage (1972b) reported a B magnitude of 16.50 in an aperture of 11.2" in 1964, compared with 15.9 from our MCSP observation of 1970. This faint phase in the 1960's probably accounts for the fact that 3C 382 was classified as a D galaxy earlier in the literature (Matthews, Morgan and Schmidt, 1964) instead of as an N-galaxy.

In the radio regime, because of the dominance of the extended outer lobes, there is no program of monitoring of the radio flux of 3C 382. However, an observation of interest is that of Strom, Willis and Wilson (1978), reporting an apparent decrease of ~ 25% in the radio flux of the central component at 6 cm between their observation of 1974 and that of Riley and Branson (1973) in 1972. With the lack of optical data in that period, it is not clear how this is related to the optical activity.

3C 390.3 is a better studied and monitored object. Shen *et al.* (1972), who obtained a historical light curve to as far back as 1895 using the Harvard plate collection, reported a range of brightness of nearly 2.5 mag. Our data sample the whole range, from the near maximum of B ~ 14.5 of 1970 to the low of B ~ 17 mag

in 1979. The object was probably at or near minimum light in 1979, as the B ~ 17 mag is considerably fainter than any of the measurements in Shen *et al.*. In figure 2b, we have also plotted the B magnitudes between 1969 and 1979 from the monitoring programs of Selmes, Tritton and Wordsworth (1975), Scott *et al.* (1976) and Pica *et al.* (1980). The agreement in general is very good. The more recent data from the photographic monitoring from Pica *et al.* (1980) for the period between 1975 to 1979 show an offset of ~ -0.4 mag from our MCSP data, but with the same downward trend. This difference is due to aperture effect as the light from the nucleus decreases and the light from the galaxy itself becomes prominent.

As in the case of 3C 382, variability of 3C 390.3 in the radio regime is not well monitored. The observations of Hine and Scheurer (1980) show a decrease of ~ 45% in the flux of the central core component between 1975 and 1976, coinciding with the drop in optical luminosity. Also, Marshall *et al.* (1978) have noted that both objects are variable in the x-ray.

For the analysis and discussions in the following sections, all data have been corrected for galactic reddening using the model of Sandage (1973) for galactic latitude dependence and the relation of Whitford (1958) for wavelength dependence. With this, extinctions E_{B-V} of 0.07 and 0.04 mag are obtained for 3C 382 and 3C 390.3, respectively.

The fluxes of the more prominent emission lines for each epoch are listed on table 2. Also included are the values from the MCSP observation of Penston and Penston (1973) for 3C 390.3. All line fluxes have been corrected for galactic reddening. The determination of the continuum level, which is often ambiguous for broad-line objects, contributes most of the uncertainties in the line fluxes of the broad Balmer lines. The uncertainties quoted bracket the fluxes obtained by using the highest and lowest possible continuum level for each line. Line blending

presents additional problems. The uncertainty in separating Hβ from [O III]$\lambda\lambda$5007+4959 is also included in the errors quoted for these line fluxes. With our low resolution, it is impossible to separate the Hα - [N II]$\lambda\lambda$6548+6583 and Hγ - [O III]λ4363 complex . To minimize the relative uncertainty of line fluxes of the broad lines between different epochs of the same object, care was taken to use as similar a continuum level as possible for each line. Thus, the uncertainty in the ratio of a particular broad line between different epochs is usually only about half of the formal error. This however does not apply to the narrow line [O II]λ3727 in the blue end of the spectrum where the large variation and uncertainty in the continuum often preclude the possibility of using a well defined and similar continuum level for each epoch.

Despite the low resolution of our spectra, we nevertheless have observed definite changes in the line profiles of the broad Balmer lines of both objects. The most prominent changes have occurred between the pre-1980 and the 1980 scans. The variations in line profiles are illustrated in figure 3 and 4.

III. Decomposition of the Central Continuum

One of the main problems in determining the nature of the continuum spectrum of active galactic nuclei is the fact that they are contaminated by various amounts of stellar light from the host galaxy. To be able to study confidently the variation of these objects, a suitable means of decomposing the continuous spectrum is necessary. There have been attempts to separate the contributions of the two components, e.g., in Yee and Oke (1978) for radio galaxies, and Koski (1978) for type 2 Seyfert galaxies. However, the procedures are not very satisfactory as, *a priori*, one is forced to assume that the central continuum is of a certain form. This is usually a power law for the sake of simplicity. This form does not produce a

proper fit in many cases. This is because the nuclear component often cannot be adequately represented by a single power-law. This is especially true of objects with Seyfert-I-like spectrum, such as 3C 382 and 3C 390.3, which have an upturn near the blue end.

Here, we shall use a new approach in decomposing the continuum, utilizing the variation of the spectrum as an additional constraint. We assume that the spectrum is composed of a standard elliptical component, taken from Yee and Oke (1978), which does not vary, and a nuclear component. The additional assumption is that the nuclear component preserves its spectral distribution despite the variation. Observationally, there is some evidence from the work of Oke, Nuegebauer and Becklin (1970) that the spectral shape of variable quasars remains more or less the same as the continuum level changes. However, there is also definite evidence that the variablity of some quasars is accompanied by a change in the spectral index (Visvanathan, 1973). In any case, this assumption can be checked for internal consistency: that is, the galaxy component should have the same brightness in the decomposition spectrum of epochs of different luminosity. If such solutions are found, then they must be the most likely, if not unique, ones. This can be seen since it is unlikely that the central component can itself be decomposed further into a galaxy-like component plus a component with the same shape as the difference spectrum.

A difference spectrum of 3C 382 is formed by subtracting the 1970 scan from the 1978 scan. Both spectra were obtained with the 7" aperture and calibrated in the same manner. The resolution of the 1978 scan is degraded by a box-car function to that of the 1970 spectrum. For 3C 390.3, various combinations of scans can be used to form the difference spectrum. An identical shape is obtained in all cases. For the purpose of analysis, the difference spectrum between 1975 and 1980 is used. The difference spectra are plotted as points in figures 5a and 5b.

For each scan of the two objects, a spectrum of the nuclear component is obtained by subtracting various amounts of a standard elliptical galaxy component (Yee and Oke, 1978) from the total spectrum until it matches its respective difference spectrum. The parameter used is R_{υ_0} -- the ratio of nuclear to galactic component at the rest visual wavelength 5450Å (Log υ_0 = 14.74), within the aperture of observation. The matching is performed by eye, as the profusion of emission lines complicates any attempts at least-square type fitting.

Some examples of the fitting are presented in figure 5a and 5b. The decomposed spectra are plotted as solid lines on top of the difference spectra. The erorr bars of the decomposed spectra are typically 1/2 to 3/4 of those of the difference spectra. For all cases, five spectra for 3C 382 and eight spectra for 3C 390.3, a nuclear component of the same shape as their respective difference spectrum is obtained.

The results of the decomposition are tabulated in table 1. Included are the ratio R_{υ_0}, the derived visual magnitude V'_G of the underlying galaxy (within the aperture of the observation), and V_{NT} of the nuclear component. The latter two are measured at 5450Å rest frame, and corrected for galactic reddening. Also listed is the quantity log L_{NT}, in ergs s^{-1} — the integrated luminosity of the nuclear component between log υ = 14.52 and 15.00 in the rest frame, as defined in Yee and Oke (1978), using $q_0 = 0$ and H_0 =55 km s^{-1} Mpc^{-1}. In addition, by using the average value of the galactic magnitudes obtained from our four 10" aperture scans, we also derive the nuclear component of the 1971 spectrum of Penston and Penston (1973). The result is also listed in table 1.

From the magnitudes of the galactic component obtained from the different epochs, the internal consistency check for this procedure of decomposition works out extremely well. For 3C 382, from the 7" aperture observations of 1970 and

1978, we obtain an average magnitude of 15.49 ± 0.08 for galactic component, while the 10" aperture scans of 1977, 1979 and 1980 give 15.27 ± 0.09. This difference of 0.22 mag is in good agreement with -0.28 mag obtained with Sandage's (1972a) empirical curve of growth for first first-rank elliptical galaxies. Similarly, all the scans of 3C 390.3 provide very consistent answers within the uncertainties of the fitting. The weighted average magnitude of the galaxy from the four 10" aperture observations is 16.04 ± 0.07 mag, while in the same four scans the nuclear component has varied by a factor of 10. The average of the four 7" scans is 16.25 ± 0.06 mag. Again, comparing with Sandage's aperture correction of -0.29 mag, the difference of -0.21 mag obtained is consistent. We can compare our result of 3C 390.3 with that of Penston and Penston (1973) in which they obtained an apparent magnitude of the galaxy by subtracting a 5" aperture scan from a 10" aperture scan. After standardizing the reddening, their result corresponded to ~ 16.0 mag in a 10" aperture, in good agreement with that obtained here. Comparing the resultant luminosities of the nuclear component with those in previous studies shows that while the power-law model fitting procedure leaves much to be desired, it does provide a reasonable estimate for L_{NT}. For the 1970 (in Yee and Oke, 1978) and the 1978 (in Yee, 1980) scans of 3C 382, the power law model produces a Log L_{NT} of ~ 0.04 smaller than here. The same is true of the 1975 scan of 3C 390.3 (Yee and Oke, 1978).

IV. Emission Lines

There have been various attempts to study the covariation of emission lines and continuum (e.g., Cherepashchuck and Lyuty, 1973; Boksenberg and Netzer, 1977; and Oke, Readhead and Sargent, 1980). However, most do not have the homogeneity and the extensive coverage of the data presented here.

From our data, we find that the observable narrow lines, both forbidden and permitted, have remained unchanged over a period of ~ 10 years despite variations of up to a factor of 10 in the central continuum. This is best illustrated in figures 5a and 5b by the cancellation of the [O III]λλ5007+4959 lines in the difference spectra of both objects. The narrow component of Hβ of 3C 390.3 also cancel out rather well in the difference scans. The tabulation of the line fluxes of [O III]λλ5007+4959 and [O II]λ3727 shows that the strength of each has remained constant within the uncertainty of flux determination.

The constancy of the narrow lines is consistent with the current standard model which postulates the existence of a large (~ 100 pc) narrow line emitting region, and a much smaller broad line region.

The broad permitted lines behave much differently from the narrow lines. They are variable in a time scale of less than one to two years. This variability, however, is not directly proportional to the continuum. This can be seen visually by comparing the contrast of the Balmer lines against the continuum between the diffference scans and the decomposed scans (figures 5a and 5b) . To study the covariation of the broad lines and the continuum, in figures 6 and 7, we plotted the line luminosities of Hα and Hβ versus L_{NT} for each object. The line luminosities have been roughly corrected for the weak narrow-line component so that they represent only the broad component. The corrections are not large, ranging from a maximum of ~ 15% applied to the 1980 Hα flux of 3C 390.3 to < 2% for the Hβ flux of 3C 382. Hence, qualitatively at least, they do not exert a significant effect on the analysis. The corrections which are listed in table 2, are obtained by the following methods. To correct for the narrow component of Hβ, for 3C 382, a line ratio of broad to narrow component of ~ 80 is obtained from a digital spectrum taken with the cooled-SIT-vidicon spectrograph on the Hale 5.08-meter telescope in 1978. The absolute flux which is subtracted from the flux of Hβ of all epochs of 3C 382, is

derived by applying this ratio to our 1978 MCSP scan. For 3C 390.3, fluxes of the narrow component of Hβ are obtained from both our 1978 scan when it was prominent, and the higher resolution (20Å) MSCP scan obtained in 1974 by de Bruyn and Sargent (1978). The average of the two is used for the correction. To estimate the flux of the narrow Hα component and the forbidden lines [O I]$\lambda\lambda$6300+6363, [N II]$\lambda\lambda$6548+6583 and [S II]$\lambda\lambda$6717+6731 in the Hα complex, we rely on the line ratios obtained in 1974 by Osterbrock, Koski and Phillips (1976). Since the strength of the Hα blend of 3C 382 has remained more or less constant from 1970 to 1979, we apply the 1974 ratio of Osterbrock, Koski and Phillips (1976) to our scan of 1978 to obtain an estimate for all the narrow lines in the blend. Similarly, we combined the ratios in Osterbrock, Koski and Phillips and our 1974 scan to obtain a correction to Hα for 3C 390.3.

From the plots, the permitted line flux departs significantly from a direct proportional dependence on the continuum luminosity of the nuclear component. For 3C 390.3, where data sampling the whole range of variability are available, a power law of the form -- $L_{LINE} \propto L_{NT}^{\Gamma}$ can be used to describe the dependence. There are basically only two epochs of significantly different L_{NT} for 3C 382, but the characteristic is essentially the same. For the power-law fitting, we have excluded the 1980 data for both objects because there are compelling reasons to believe that, for both objects, the 1980 scans show a different behavior from those of earlier epochs. First, as mentioned before, both objects show marked change in the Balmer line profiles. Second, between 1979 and 1980 the Balmer line fluxes of each have changed significantly without an accompanying change in the continuum luminosity. And the change is consistent with the trend of the change in the continuum in the previous few years. We shall discuss the possible significance of the 1980 scans of both objects in the next section. Ignoring the points from the 1980 epoch of both objects, we have the following results from least square fitting. For

3C 382, we have $\Gamma = 0.23$ for Hβ and 0.0 for Hα ; and for 3C 390.3, $\Gamma = 0.47$ for Hβ, and 0.41 for Hα. With the continuum staying the same shape throughout the variation, the equivalent width of the lines varies as $L_{NT}^{1-\Gamma}$. Also with the different Γ for the Hα and Hβ versus L_{NT} correlation, it is clear that the Balmer decrement has changed in 3C 382. The ratio Hα/Hβ has gone from 3.4 in 1970 to 2.7 in 1977.

VI. Discussions

a) The Correlation of Emission-line and Continuum Luminosities

The non-proportional relationship between emission line luminosities and the variable continuum luminosity derived in the last section for both 3C 382 and 3C 390.3 is also found in 3C 120 by Oke, Readhead and Sargent (1980). It has also been hinted at by other earlier observations. Notably from the optical-violent-variables (OVV) quasars, 3C 446 and 3C 279 in which the emission lines do not vary with the continuum (Oke, 1967). Cherepashchuk and Lyuty (1973), by using narrow band photometry, studied the correlation between Hα and U band magnitudes of variable type I Seyferts. The correlations that they obtained after applying a time delay of 15 to 30 days between the line flux and continuum flux, suggest a similar relation with $\Gamma < 1$.

The nonlinear correlation obtained here is very different from the finding in Yee (1980) that L_{LINE} and L_{NT}, statistically in a large sample of quasars and active galactic nuclei, are directly proportional to each another over a large range of luminosity. However, as we shall show, these seemingly contradictory results are not irreconcilable.

There are several possible interpretations of the $\Gamma < 1$ correlation. The simplest, though somewhat *ad hoc*, is that the ionizing radiation beyond the Lyman-limit does not vary as the optical continuum. This can only be verified through

simultaneous optical, uv, and x-ray monitoring. An alternative possibility is that the non-linear behavior is due to a time-lag effect. A simple time-lag cannot explain the data completely since it would seem likely that a simple time-lag would produce a much more scattered diagram in the L_{LINE} versus L_{NT} plot for 3C 390.3 for which we have data covering both an outburst (between 1969 and 1970) and the subsequent decline (between 1971 and 1973).

A slightly more complicated scenario, where we assume that there are two components of broad-line gas: a short-time-scale (STS) component and a long-time-scale (LTS) component, can adequately explain the correlations. In this picture, in the time interval of ~ 1 year, only the short-time-scale component would vary directly with the continuum. From the photographic monitoring data of 3C 390.3, the shortest time-scale for variation of the nuclear source is approximately a few months. Using typical parameters, the time-scale for variation of the broad-lines of the broad-line gas clouds can be made to be as small as one to two months (e.g., see Tohline and Osterbrock, 1976). Thus , the covariation of the short-time-scale component and the continuum can be easily achieved over the period of a year. The long-time-scale component, on the other hand, should have a time-scale for change considerably larger than that of the continuum, so that as the continuum fluctuates, it will only respond to the long-term averge of the central source.

By assuming that over the period of our observations, only a fraction of the broad-line gas covaries proportionately with the nuclear continuum, the L_{LINE} versus L_{NT} relation, over a small range of luminosity, mimics a power-law with index < 1. In figure 7, for 3C 390.3, we have plotted the curve obtained from fitting with the two-component assumption. As before, we have ignored the data points from the 1980 epoch. It fits the data adequately. A larger range of variation is required to distinguish between a power-law fit and the two-component assumption fit.

The most convenient parameter for the two-component fit is the luminosity of the long-time-scale (hence constant) component. The results obtained, along with the Hα/Hβ line ratio of each component are listed in table 3. The uncertainty of the fit is rather large due to the small range and the scatter of the data. The uncertainty in the line ratio is at least 25% for 3C 390.3, and $\sim$ 50% for 3C 382. The ratio of 3C 382 suggests that the long-time-scale component has a steeper Balmer decrement. Thus, as the luminosity changes, there would be a different mix of the two component, creating a change in the total Balmer decrement. The one interesting problem with this picture is the very low Hα/Hβ ratio of < 1.3 of the short-time-scale component. While most recent detailed calculations of hydrogen line spectrum focus on the steep Balmer decrement generally observed in these objects, nevertheless, very low Hα/Hβ ratio can also arise from some of these models. An example is the calculation by Canfield and Puetter (1980): with a very high density of 10^{12} cm s^{-1} and moderately large optical depth at the Lyman limit (> 10), a Hα/Hβ ratio of as low as ~ 1.3 can be achieved. Thus, the physical conditions of the two broad-line components of 3C 382 can be very different: one may have the cannonical density of $\sim 10^9$ cm s^{-1}, and the other a thousand times higher.

With the two-component time-lag hypothesis, the contradiction between the non-proportional relation between line flux and continuum flux obtained here for an individual object and the directly proportional correlation obtained in Yee (1980) for a whole class of these objects can be resolved. The non-proportionality of line and nuclear fluxes in a variable object would only contribute to the scatter of the correlation of Yee (1980). On the average, objects would be observed with the long-time-scale component in equilibrium with the ionization source producing the $\Gamma=1$ correlation statistically for a large number of objects. The $\Gamma< 1$ correlation is only a transient phenomenon occurring in the rapidly variable objects.

The simplest physical explanation for the two-component assumption utilizes the geometry of the broad-line gas clouds. This would require two physically distinct components -- for example, a small component coinciding with the central continuum source; probably having a size of < 0.1 pc, and a shell or ring of gas with radius larger than 1 pc. A core-halo sort of structure with the appropriate dimensions is also possible. Another possibility is that the long-time-scale component is produced by process(es) other than photo-ionization from the central continuum. An example of this is shock excitation which would have a time-scale of change of up to hundreds of years (Collin-Souffrin, Alloin and Andrillat, 1973)

The changes in the luminosity and profile of the Balmer lines observed in both objects in 1980 can also be explained in the context of the two time-scale assumption, i.e., in the 1980 scans, we are beginning to see the response of the long-time-scale component to the changing continuum. This a reasonable hypothesis, since there does not seem to be any rapid large scale fluctuation in the continuum in neither object since about 1976. 3C 382 has remained more or less constant from 1976 to 1980, though a detailed monitoring program does not exist. The photographic monitoring of 3C 390.3 by Scott *et al.* (1976) and Pica *et al.* (1980) shows a rather steady decline, with no convincing evidence for large amplitude short term variations which existed earlier. With this and the geometric interpretation, we can estimate the long-time-scale component to be ~ 5 ly in size. We shall discuss the geometry in more details in the next section concerning line profile changes.

It is also possible that the $\Gamma < 1$ relation is intrinsic to the radiative process(es) in the gas clouds, although this could make interpreting the $L_{H\beta} \propto L_{NT}$ result in Yee (1980) difficult. For this, time-dependent calculations of the recent more complex models (such as those of Netzer, 1976; Krolic and McKee, 1978; and Canfield and Puetter, 1980) would be required. An example of this possibility is the self-absorption model of Netzer (1977) in which a change of Balmer decrement is

predicted to accompany a change in the ionizing flux. This is due to the change in the depth of the H II region in each individual cloud as the continuum varies, and hence causing a change in the optical depth in the lines. In more realistic models, because of the extreme physical conditions generally believed to exist in these objects, a combination of detailed radiative process calculations along with a two-component geometry is probably required. In their study of the variation in the Seyfert galaxy NGC3516, Boksenberg and Netzer (1977) applied a combination of the self-absorption model and a core-halo geometry to the broad-line gas cloud to explain the observations. Their dimensions of the core and halo are $\sim 10^{17}$ and 10^{18} cm, respectively, with the core containing $\sim 30\%$ of the gas. These numbers are similar to our estimates. They cited a numerical example with this set-up in which a change of a factor of four in continuum produces a change of only 30% in Hβ flux and 8% in Hα flux.

b) Emission-Line Profile

There is little doubt concerning the validity of the changes in the broad-line profiles of both objects, since, as illustrated in figures 3 and 4, different Balmer lines show the same changes. Relative to the red side, a large drop in flux blue-ward of the narrow component in both Hβ and Hγ is obseved in 3C 390.3. For Hα, a similar drop, though not extending as far to the blue as the others, is also seen. This is at least partly due to the contamination of the broad Hα complex by the constant forbidden-lines. We have also obtained higher resolution spectra of 3C 390.3 from the Hale 5.08-meter telescope using the cooled-SIT-vidicon spectro-graph in 1978 and 1979, and the PFUEI (Prime Focus Universal Extragalactic Instrument) in 1980. These show that the dipping of the blue-wing of Hβ began in the 1979 spectrum and continued in 1980. In addition, an IUE spectrum of 3C 390.3 obtained by Oke, Osterbrock and Wu (private communication) in 1980 shows the same dropping of the blue side of the line CIVλ1550 when compared with the

spectrum obtained in 1979 (Oke and Goodrich, 1980). Smaller changes in the line profiles of 3C 390.3 between 1973 and 1975 have been reported by Osterbrock (1978), and Osterbrock, Koski and Phillips (1976).

Between 1979 and 1980, 3C 382 exhibits the profile change mostly in the region to the red of the narrow component. Our resolution is too low to determine exactly how far the increase extends. From Hβ, we can place a limit on the blue side of at most to $\sim$-2500 km s^{-1}. In the red wing, the change occurs up to at least +4500 km s^{-1}; beyond this point the [OIII] lines begin to affect the Hβ profile. However, the red side of Hα profile suggests that significant changes only happens up to $\sim$+4500 km s^{-1}. In the blue side of Hα , changes in the profile are seen out to somewhere between $\sim$-2500 to -6000 km s^{-1}. There is also strong evidence that there are changes in the Balmer line profiles between the 1970 scan and the post-1977 scans. Refering to figure 3, the 1970 profile of Hβ shows a definite non-symmetry in the sense that to blue of the line center (from $\sim$-5000 km s^{-1} on) there is a prominent drop of line flux. The profile of Hβ in 1979, however, shows a rather smooth drop-off to the blue side of the line center. The resolution around Hα of the 1970 scan is very poor, but there is also a suggestion of assymmetry in the line which does not exist in the 1979 scan.

Changes in line profiles of Seyfert galaxies have often been interpreted as an appearance or disappearance of absorbing or line-emitting clouds (e.g. Cromwell and Weyman, 1970; Osterbrock, 1978). In our case, however, it is very tempting to associate the changes with the variable ionizing flux. This is because the change occurs over a wide velocity range -- the complete blue half of the lines in 3C 390.3, and at least for an interval of 4500 km s^{-1} in the red wing of the lines of 3C 382. Furthermore, for each object, the sense of change is the same as that of its continuum.

If the profile variability is in fact the response to the change in the continuum, co-monitoring of both would be a powerful probe of the geometry and motions of the gas clouds in the nucleus of these objects. With our limited spectral and temporal resolution, we can only offer some general comments.

The non-symmetry of the profile change in both objects seems to rule out the possibility that the broadness of the lines comes from rotation, unless one also invokes some non-symmetrical absorption effect. Also, if one is to interpret the long-time-scale component geometrically: i.e., the broad-line gas clouds of the component are at a distant > 1 pc, a rotational model would require a rather large central mass of $\sim 10^{11} M_{\odot}$.

The data, however, strongly suggest that the line profile variations are the responses of an expanding shell or ring of gas clouds to a change in the central ionizing continuum, with the width of the lines produced by the mass-motion of the expanding gas clouds. Thus, a simplistic model for 3C 390.3, in keeping with the geometrical assumptions of the last section, is to have an expanding shell or ring with radius of a few light years as the long-time-scale component. This would naturally explain the dimming of the blue wing first after a decrease in the continuum flux.

Similarly, we can interpret the line profile change in 3C 382 between 1970 and 1978 as the initial response of the emission-line clouds in the blue wing to the increase of the central continuum; and the subsequent change observed between 1979 and 1980 as the continuation of this increase in line flux spreading toward the red side. This is exactly the response to a change in the ionizing continuum expected from an expanding shell or ring of gas clouds. Using such a geometry and the line profiles of the 1979 and 1980 scans, we can obtain an estimate of the radius of the shell or ring structure. Assuming a velocity of expansion of ~ 15,000

km s^{-1} estimated from the Balmer lines, a radius between ~2.5 to 5.0 light years for the shell or ring is obtained. The large uncertainty is due to the inability to determine the exact velocity interval in the profile in which changes have occurred. For a ring structure, there is the added uncertainty of projection effect.

Thus, both the $\Gamma < 1.0$ relation between nuclear and Balmer line luminosities and the changes in the Balmer line profiles in the two objects can be adequately explained by the geometrical model derived from the two-time-scale component hypothesis. If the continuum source of both objects stays quiescent for the next few years, perhaps more revealing data, tracing the further response of the line profiles to the continuum change, can be collected for a more detailed study.

c) Continuum

As demonstrated by the decomposition, the color dependent variation of the two N-galaxies can be explained entirely by the mixed nature of their spectrum. From the consistency of the results of the decomposition and the agreement of the aperture dependence with the growth curve of elliptical galaxies, the nebulosity surrounding both objects can be attributed to an underlying elliptical galaxy. Also absorption features associated with elliptical galaxies are appearing in scans of the fainter phases of 3C 390.3. Using Sandage's (1972a) curve of growth, correcting to the metric diameter of 32 Mpc of Gunn and Oke (1977), we obtained an absolute magnitude of -22.47 and -21.87 for 3C 382 and 3C 390.3 respectively. Thus, both galaxies are fainter than the average magnitude of -22.8 for first-rank elliptical obtained by Wilkinson and Oke (1978). This is not surprising as neither is situated in a sizeable cluster. Burns and Owens (1977) have classified 3C 390.3 as a field galaxy and 3C 382 as a possible member of a Zwicky cluster.

The nuclear component is very similar for both objects, and each can be

represented by two power-laws. For 3C 382, the continuum follows a ν^{α} law with $\alpha \sim +1.2$ and -0.7 for blue-ward and red-ward of Hβ, respectively. For 3C 390.3, the two spectral indices are $\sim +0.9$ and -1.0 for blue-ward and red-ward of Hβ, respectively. This shape of the continuum is remarkably similar to that of 3C 273 and other quasars (Neugebauer *et al.*, 1979). The upturn at the blue end can be identified with the 3000Å bump in Seyfert I's reported by Neugebauer *et al.* (1976) and in quasars by Richstone and Schmidt (1980). An important result from the decomposition is that the shape of the nuclear component can not have varied by a significant amount despite the change by a factor of up to 10 in the luminosity of the component. By comparing the difference scans obtained by using the various epochs of 3C 390.3, the spectral index of the central continuum cannot have changed by more than $\sim \pm 0.15$ over the period of observation. Also a change of ~ 0.15 magnitude in the flux of the 3000Å feature relative to other parts of the continuum would have been easily detected by our method of decomposition.

The physical reason behind the existence of the 3000Å bump is not well understood. Several explanations have been put forward. (see Richstone and Schmidt, 1980). The constancy of this feature offers a new constraint in modelling it. The co-variation of the feature with the continuum eliminates any possibilities that it is associated with hot stars or other component related to the underlying galaxy. In fact, the 3000Å feature must originate from a region $< 10^{18}$ cm in size, since it varies with the continuum in a time-scale of less than one year.

The explanation that the feature is Balmer continuum emission (Baldwin, 1975) cannot be ruled out completely in spite of the fact that Hβ line does not vary directly with the continuum. For example, it is possible that only the short-time scale component of the Balmer emission line region is responsible for most of the Balmer continuum emission. Similarly, any explanation that attributes the feature to some unidentified and unresolved lines would require that these lines arise from

a region comparable in size to the short-time-scale emission line region.

Another possibility is that it is the radiation from a blackbody at a temperature of $\sim$ 12,000° K. The co-variation of the feature with the continuum requires the temperature to stay constant as the continuum luminosity changes, and the emitting region to be less than a light-year in size. Since the luminosity of a black body of constant temperature is proportional to the emitting area, the size of the emitting region of, for example, a disc-like structure, has to change as the square-root of the continuum luminosity. Thus, the emitting region probably needs to be considerably small than a light year in size. This does not impose a serious restriction, since a blackbody of a few light-days in size can produce the required luminosity of $\sim 10^{43}$ ergs s^{-1} emitted by the 3000Å feature.

VI. Summary

From the study of the variation of absolute energy distributions and emission lines, we have obtained new results that should be taken into consideration in attempts to model the nuclear regions of broad-line active galaxies. We find that:

1. The data are consistent with the hypothesis that the variation of the continuum is due to a variable nuclear component superimposed on an elliptical galaxy component, and that the variable nuclear component retains its spectral shape independent of its luminosity.

2. The nuclear component for both objects has an energy distribution very similar to that observed in many quasars, including a prominent 3000Å feature.

3. The 3000Å feature varies directly with the continuum; hence must be closely related to it.

4. The forbidden lines and the narrow Balmer lines do not vary with the contin-

uum, but he broad Balmer lines covary with the continuum, approximating a power-law relation with the optical luminosity with index < 0.5. There is also a definite change of Balmer decrement in 3C 382. An assumption that can explain the relationship between continuum and line luminosities is to have two components of broad-line gas clouds, one having a time-scale for change of ~ months and the other, years. The simplest model based on this assumption is a geometrical one that includes a component of < 0.1pc and a much larger one of ~ 1pc in size. Other models based on radiative mechanisms may also be possible.

5. Variability of broad Balmer line profiles occurs in both objects, This can be explained as the time-lag response of an expanding shell or ring, with a radius of a few light years, of line-emitting gas clouds to a varying central continuum. This also imply that the width of the broad emission-lines arises from mass-motion of the gas cloud.

Further monitoring of these objects, including both spectrophotometry for studying the absolute energy distribution and higher resolution spectral observation for line profile variations, may enable one to unravel the structure and motion of the broad-line gas clouds which could be extremely useful in detailed modelling of the nuclear region of active galaxies and quasars.

REFERENCES

Boksenberg, A. and Netzer, H. 1977, Ap. J., 212, 37.

Baldwin, J, A., 1975, Ap. J., 201, 26.

Burns, J. O., and Owen, F. N. 1977, Ap. J., 217, 34.

Canfield, R. C., and Puetter, R. C. 1980, preprint.

Cherepashchuk, A. M. and Lyuty, V. M. 1973, Ap. Lett., 13, 165.

Collin-Souffrin, S., Alloin, D., and Andrillat, Y. 1973, Astro. and Astrophys., 22, 343.

Cromwell, R. and Weyman, R. 1970, Ap. J., 159, L147.

de Bruyn, A. G., and Sargent, W. L. W. 1978, A. J., 83, 1257.

Gunn, J. E., and Oke, J. B. 1975, Ap. J., 195, 255.

Hargrave, P. J. and McEllin, M. 1975, M.N.R.A.S., 173, 37.

Hine, R. G. and Scheurer, P. A. G. 1980, M. N. R. A. S., 193, 285.

Koski, A. T. 1978, Ap. J.,223, 56.

Krolic, J. H. and McKee, C. F. 1978, Ap. J. Suppl. 37, 459.

Marshall, F. E.,, Mushotzky, R. F., Boldt, E. A., Holt, S. S., Rothschild, R. E. and Serlemitsos, P. J. 1978, Nature, 275, 624.

Matthews, T. A., Morgan, W. W., and Schmidt, M. 1964, Ap. J., 140, 35.

Netzer, H. 1977, M.N.R.A.S., 178 ,489.

Netzer, H. 1975, M.N.R.A.S., 171, 395.

Neugebauer, G., Becklin, E. E., Oke, J. B., and Searle, L. 1976, Ap. J., 205, 29.

Neugebauer, G., Oke, J. B., Becklin, E. E., and Matthews, K. 1979, Ap. J., 230, 79.

O'Dell, S. L., Puschell, J. J., Stein, W. A., Warner, J. W., and Ulrich M.-H., 1978, Ap. J., 219, 818.

Oke, J. B. 1967, Ap. J., 147, 901.

-------- 1969, P.A.S.P., 81, 11.

Oke, J. B., and Goodrich, D. 1980, preprint.

Oke, J. B., Neugebauer, G., and Becklin, E. E. 1970, Ap. J., 159, 341.

Oke, J. B., Readhead, A. C. S., and Sargent, W. L. W. 1980, preprint.

Oke, J. B. and Schild, R. E. 1970, Ap. J., 161, 1015.

Osterbrock, D. E. 1978, Physica Scripta, 17, 285.

Osterbrock, D. E., Koski, A. T., and Phillips, M. M. 1976, Ap. J., 206, 898.

Penston, M. V. and Penston, M. J. 1973, M.N.R.A.S., 162, 109.

Pica, A.J., Pollock, J. T., Smith, A. G., Leacock, R.J., Edward, P. L. and Scott, R. L. 1980, A. J., in press (Nov).

Richstone, D. O. and Schmidt, M. 1980, Ap. J., 235, 377.

Riley, J. M. and Branson, N. J. B. A. 1973, M.N.R.A.S., 164, 271.

Sandage, A. 1967, Ap. J., 150, L9.

-------- 1972a, Ap. J., 173, 485.

-------- 1972b, Ap. J., 178, 25.

-------- 1973, Ap. J., 183, 711.

Selmes, R. A., Tritton, K. P., and Wordsworth, R. W. 1975, M.N.R.A.S., 170, 15.

Scott, R. L., Leacock, R. J., McGimsey, B. Q., Smith, A. G., Edwards, P. L., Hackney, K. R., Hackney, R. L. 1976, A. J., 81, 7.

Shen, B. S. P., Usher, P. D., and Barrett, J. W. 1972, Ap. J., 171, 457.

Strom, R. G., Willis, A. G., and Wilson, A. S. 1978, Astro. and Astrophys., 68, 367.

Tohline, J. E. and Osterbrock, D. E. 1976, Ap. J., 210, L117.

Visvanathan, N. 1973, Ap. J., 197, 1.

Whitford, A. E. 1958, A. J., 63, 201.

Wilkinson, A. and Oke, J. B. 1978, Ap. J., 220, 376.

Yee, H. K. C. 1980, Ap. J., 241, in press (Nov).

Yee, H. K. C. and Oke, J. B. 1978, Ap. J., 226, 753.

TABLE 1

OBSERVATIONS AND RESULTS

Object	Date	Aperture (arc sec)	Resolution[a]	AB_{5450}	R_{v_o}	V'_G	V_{NT}	Log L_{NT}	Ref.[b]
3C 382	6 Jul 1970	7	80 -160	15.36	0.55 ± 0.10	15.50 ± 0.10	16.15 ± 0.20	44.10	3
	21 Jul 1977	10	20 - 40	14.86	1.05 ± 0.15	15.37 ± 0.12	15.33 ± 0.10	44.43	4
	9 May 1978	7	40 - 80	14.82	1.35 ± 0.15	15.48 ± 0.10	15.15 ± 0.09	44.50	2
	30 May 1979	10	40 - 80	14.78	0.90 ± 0.10	15.20 ± 0.10	15.30 ± 0.12	44.46	1
	17 Jul 1980	10	40 - 80	14.72	1.10 ± 0.15	15.25 ± 0.12	15.15 ± 0.11	44.50	1
3C 390.3	11 Jul 1969	7	40 - 80	15.60	1.03 ± 0.12	16.23 ± 0.09	16.30 ± 0.09	44.04	1
	6 Jul 1970	10	80 -160	14.70	3.3 ± 0.5	16.13 ± 0.16	14.84 ± 0.06	44.58	1
	-- Jul 1971	10	40 - 80	15.00	1.65[c] --	---	15.51 --	44.31	5
	2 Jul 1973	7	40 - 80	15.72	0.98 ± 0.10	16.28 ± 0.08	16.30 ± 0.08	44.0	1
	25 Jul 1974	7	80 -160	15.66	1.08 ± 0.10	16.32 ± 0.11	16.24 ± 0.10	44.02	1
	13 Jul 1975	10	40 - 80	15.43	0.88 ± 0.12	15.96 ± 0.11	16.10 ± 0.12	44.08	3
	2 Nov 1978	10	40 - 80	15.87	0.43 ± 0.05	16.05 ± 0.08	16.97 ± 0.10	43.73	1
	26 Oct 1979	7	40 - 80	16.06	0.35 ± 0.05	16.18 ± 0.10	17.32 ± 0.20	43.59	1
	17 Jul 1980	10	40 - 80	16.00	0.30 ± 0.05	16.05 ± 0.08	17.35 ± 0.19	43.58	1

Notes: a) Resolution in Angstroms: blueward of ~5600 Å - redward of ~5600 Å .
b) References: 1. present paper, 2. Yee (1980), 3. Yee and Oke (1978), 4. de Bruyn and Sargent (1978), 5. Penston and Penston (1973).
c) Estimate only, see text.

TABLE 2

LINE STRENGTHS (in units of 10^{-13} ergs s^{-1} cm^{-2})

Object	Epoch	LINES						
		Hα 6562 +[OI]6300,6363 +[NII]6548,6583 +[SII]6717,6731	Hα narrow comp. +[OI]6300,6363 +[NII]6548,6583 +[SII]6717,6731	[OIII] 5007,4959	Hβ 4861	Hβ 4861 narrow component	Hγ 4340 + [OIII] 4363	[OII] 3727
3C 382	1970	17.5 ± 0.8	—	0.95 ± 0.25	5.2 ± 0.80	—	---	0.45 ± 0.10
	1977	17.2 ± 1.0	—	1.00 ± 0.10	6.17 ± 0.80	—	---	0.32 ± 0.07
	1978	18.2 ± 1.0	~0.9	1.03 ± 0.12	6.07 ± 0.80	~0.07	---	0.46 ± 0.11
	1979	17.1 ± 0.8	—	1.01 ± 0.14	6.65 ± 0.95	—	---	0.38 ± 0.09
	1980	20.4 ± 0.6	—	0.98 ± 0.25	7.56 ± 0.95	—	---	0.42 ± 0.10
3C 390.3	1969	15.2 ± 0.8	—	2.81 ± 0.20	3.10 ± 0.50	—	1.13 ± 0.19	0.17 ± 0.07
	1970	22.4 ± 0.8	—	2.45 ± 0.45	6.50 ± 0.70	—	1.70 ± 0.50	0.4
	1971	20.6 —	—	---	4.6 —	—	---	---
	1973	16.6 ± 0.5	—	2.76 ± 0.20	3.46 ± 0.60	—	1.28 ± 0.19	0.41 ± 0.17
	1974	13.8 ± 0.6	~1.5	2.57 ± 0.30	3.43 ± 0.60	~0.2	1.01 ± 0.20	0.29 ± 0.10
	1975	15.8 ± 0.4	—	2.85 ± 0.25	3.42 ± 0.60	—	1.38 ± 0.20	0.41 ± 0.17
	1978	11.0 ± 0.3	—	2.78 ± 0.20	2.58 ± 0.50	~0.2	0.88 ± 0.13	0.23 ± 0.10
	1979	10.1 ± 0.4	—	2.67 ± 0.25	2.50 ± 0.45	—	0.87 ± 0.14	0.30 ± 0.10
	1980	9.3 ± 0.3	—	2.57 ± 0.17	1.84 ± 0.50	—	0.58 ± 0.12	0.26 ± 0.14

TABLE 3

PARAMETERS OF TWO-COMPONENT FIT

Object	LTS Component			STS Component
	log $L_{H\alpha}$ *	log $L_{H\beta}$	$H\alpha/H\beta$	$H\alpha/H\beta$
3C 382	>43.27	42.72	3.5	<1.3
3C 390.3	42.98	42.33	4.1	4.0

Note: * luminosity in ergs s^{-1} .

FIGURE CAPTIONS

Figure 1a - Light curve of 3C 382 in B magnitude. Crosses (X) are points from multichannel observations; open circle (o), from O'Dell et al. (1976); and solid circle (●), from Sandage (1972b).

Figure 1b - Light curve of 3C 390.3 in B magnitude. Crosses (X) are points from multichannel observations; and dots (•) are photographic monitoring data from Selmes, Tritton and Wordsworth (1975), Scott et al. (1976) and Pica et al. (1980).

Figure 2a - Examples of observed absolute energy distributions of 3C 382. The ordinate is marked in intervals of 0.5 in log flux density (in ergs s^{-1} cm^{-2} Hz^{-1}), with the absolute value for each scan at log ν = 14.74 indicated.

Figure 2b - Same as figure 2a, for 3C 390.3.

Figure 3 - Variability in the Balmer line profiles of 3C 382. Positions of narrow forbidden lines are marked.

Figure 4 - Same as figure 3, but for 3C 390.3.

Figure 5a - Difference spectrum for 3C 382 and examples of the fit of decomposed spectra. Crosses (x) represent the difference spectrum obtained by subtracting the 1970 scan from the 1978 scan; solid line represent the best-fitting decomposed spectrum of the epoch indicated. The plot is in the rest-frame of 3C 382 and corrected for galactic reddening.

Figure 5b - Same as figure 5a for 3C 390.3. The difference scan is obtained by subtracting the 1980 spectrum from that of 1975.

FIGURE CAPTIONS (Continued)

Figure 6 - Luminosity of nuclear component (L_{NT}) versus luminosities of Balmer lines (L_{LINE}) for 3C382. Luminosities are in units of ergs s^{-1}.

Figure 7 - Same as figure 6 but for 3C 390.3. Dashed lines indicate best-fitting two-component assumption fit.

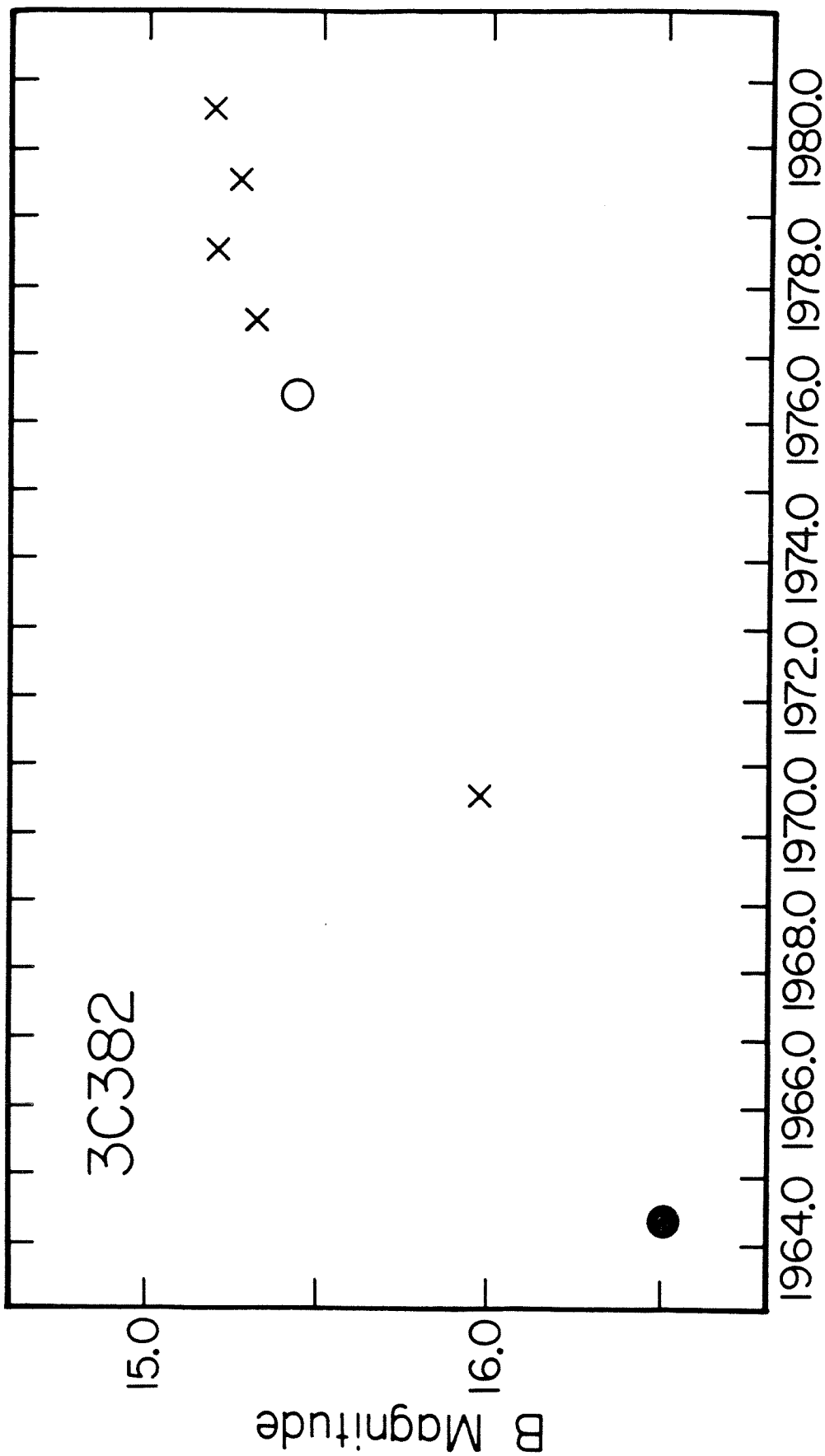
3C382
B Magnitude
15.0
16.0
1964.0
1966.0
1968.0
1970.0
1972.0
1974.0
1976.0
1978.0
1980.0
Epoch

Figure 1a

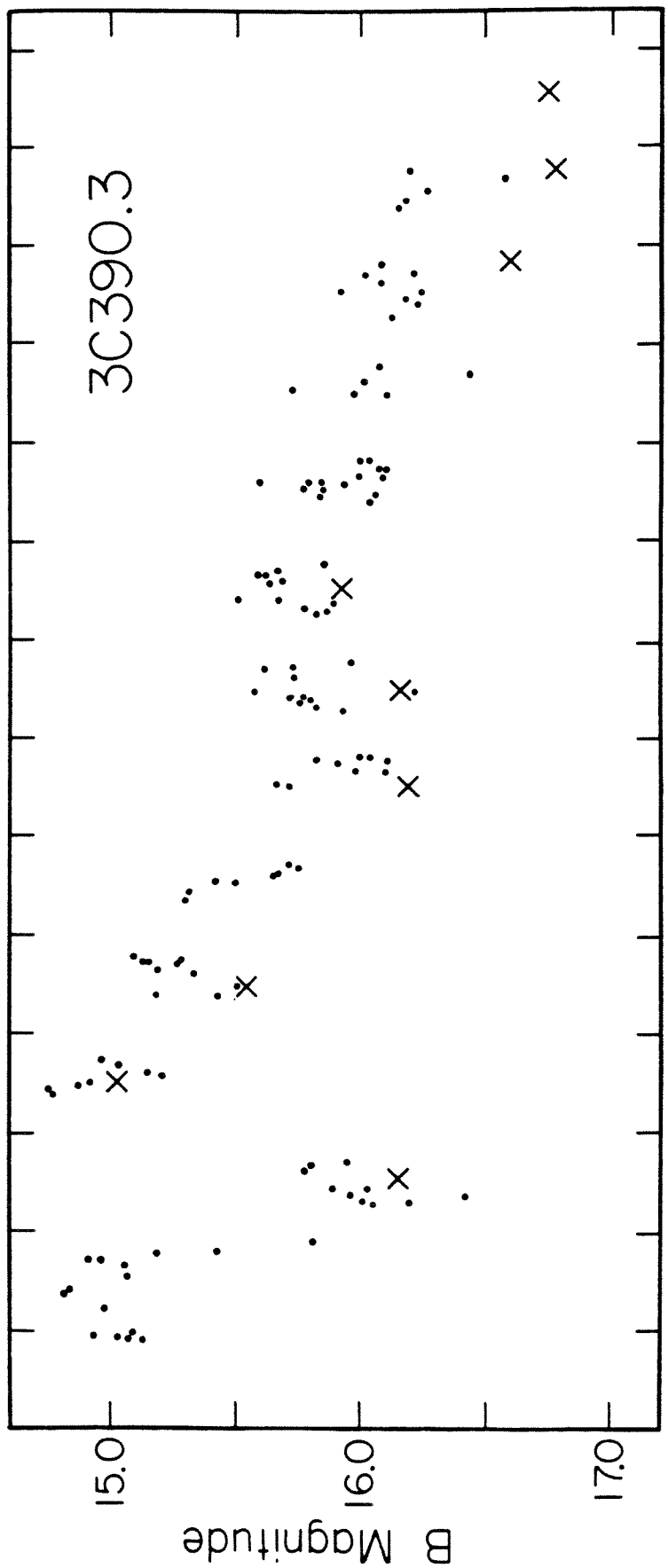
3C390.3
B Magnitude
15.0
16.0
17.0
1968.0
1970.0
1972.0
1974.0
1976.0
1978.0
1980.0
Epoch

Figure 1b

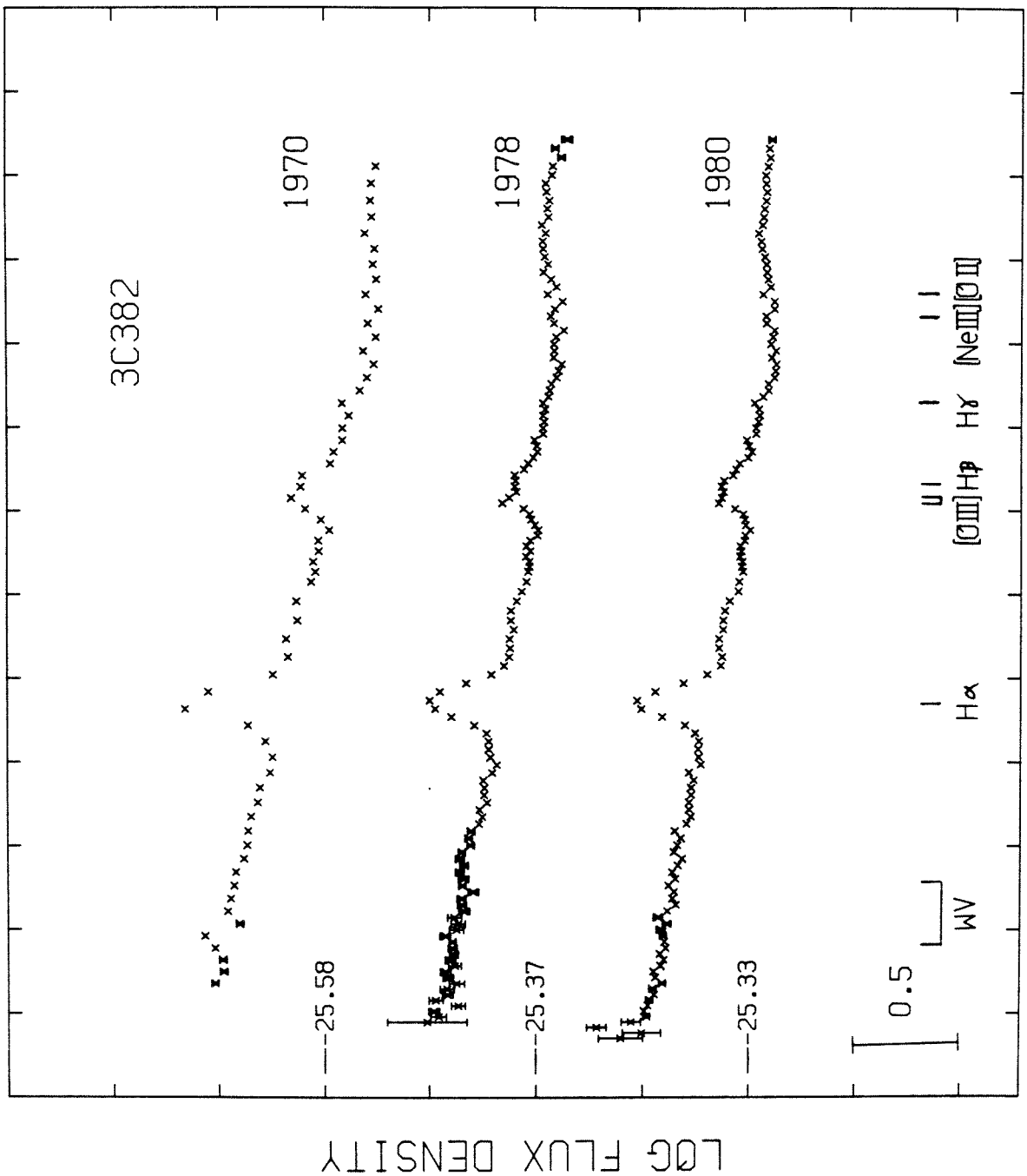
3C382
1970
1978
1980
-25.58
-25.37
-25.33
0.5
1V
Hα
[OIII]Hβ
Hγ
[NeIII][OII]
14.5
14.6
14.7
14.8
14.9
15.0
LOG FREQ(Hz)
LOG FLUX DENSITY

Figure 2a

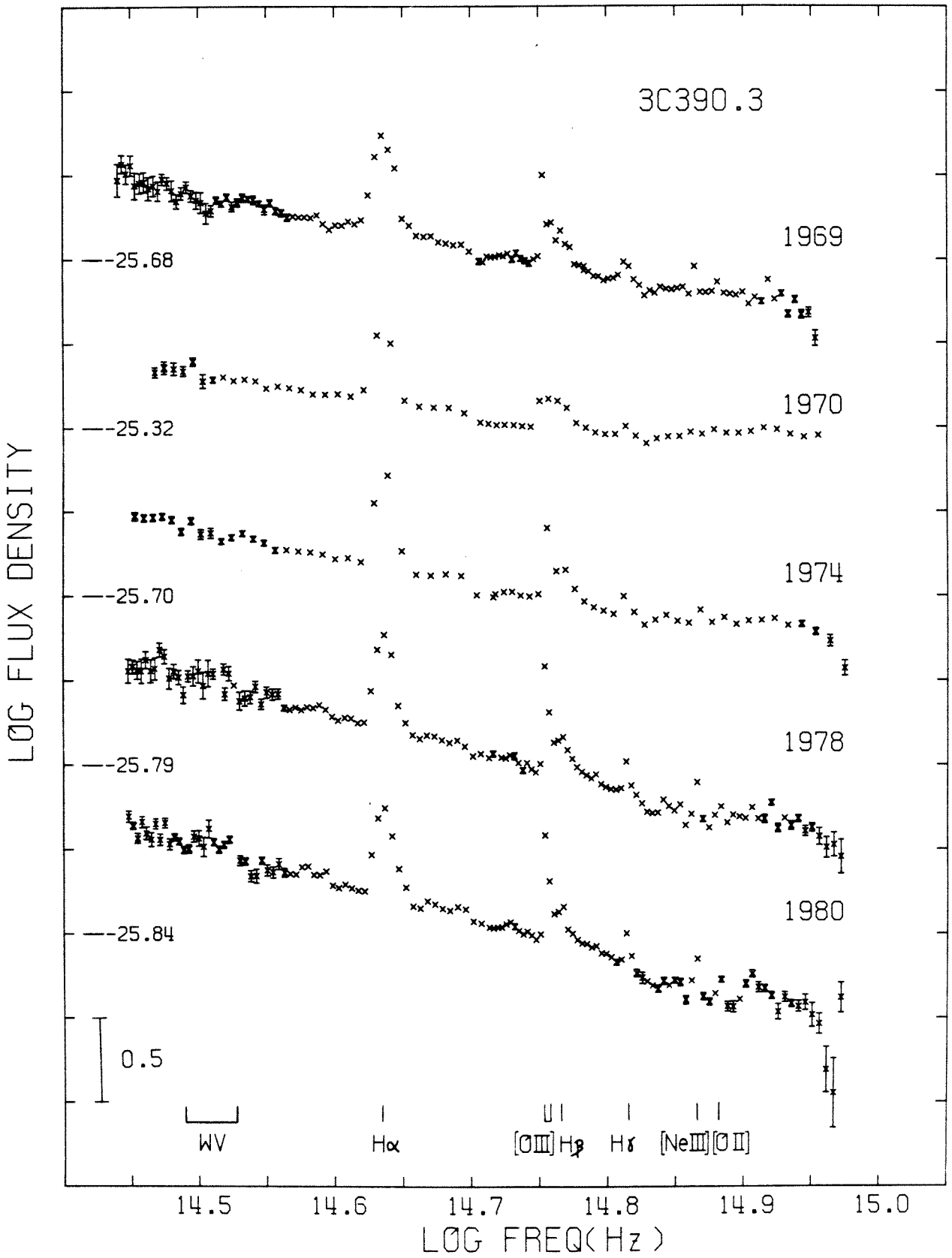
3C390.3
1969
1970
1974
1978
1980
-25.68
-25.32
-25.70
-25.79
-25.84
0.5
WV
Hα
[OIII]Hβ
Hγ
[NeIII][OII]
14.5
14.6
14.7
14.8
14.9
15.0
LOG FREQ(Hz)
LOG FLUX DENSITY

Figure 2b

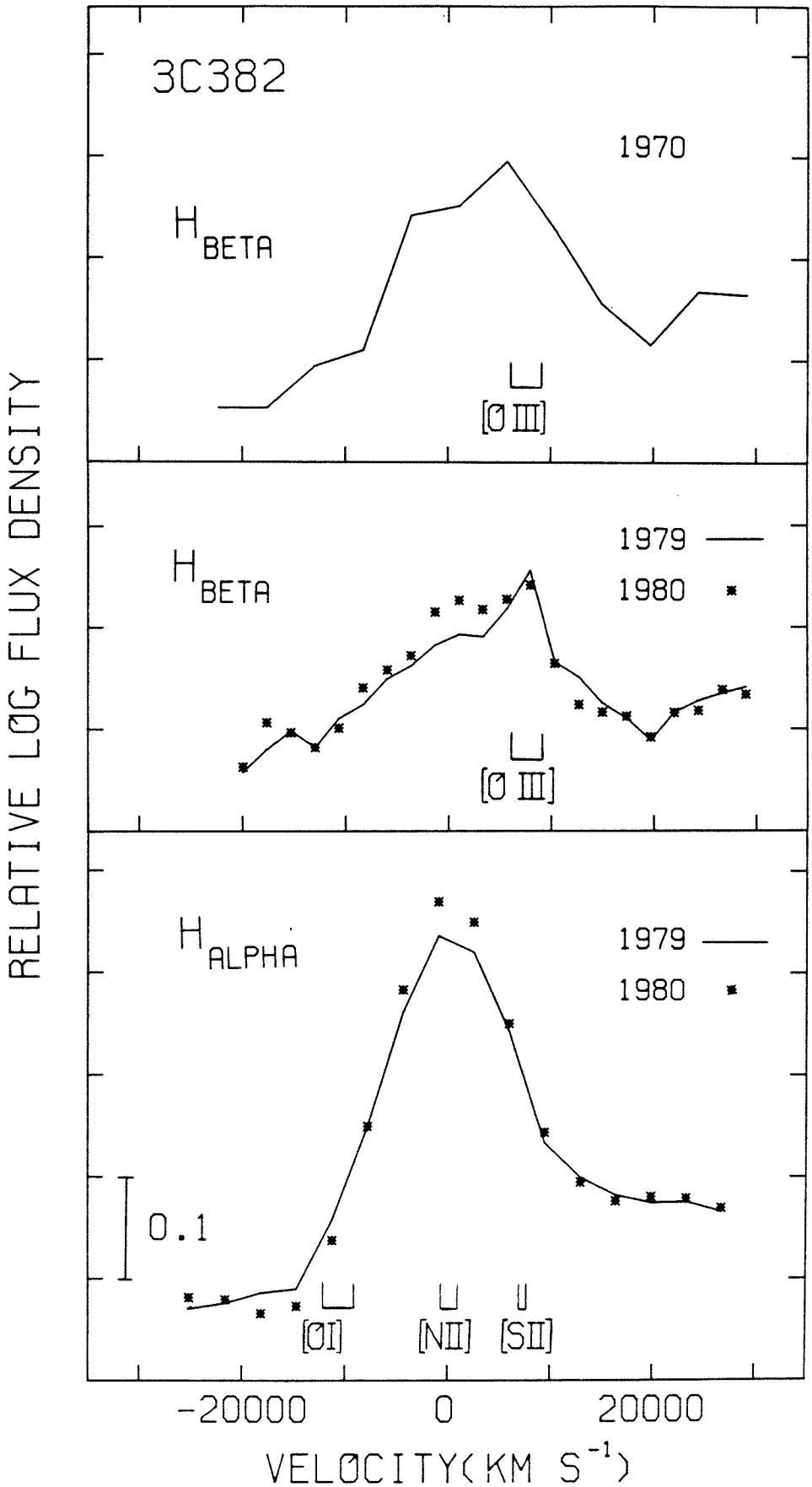
3C382
1970
H BETA
[O III]
1979
1980
H BETA
[O III]
H ALPHA
1979
1980
0.1
[OI]
[NII]
[SII]
-20000
0
20000
VELOCITY(KM S^{-1})
RELATIVE LOG FLUX DENSITY

Figure 3

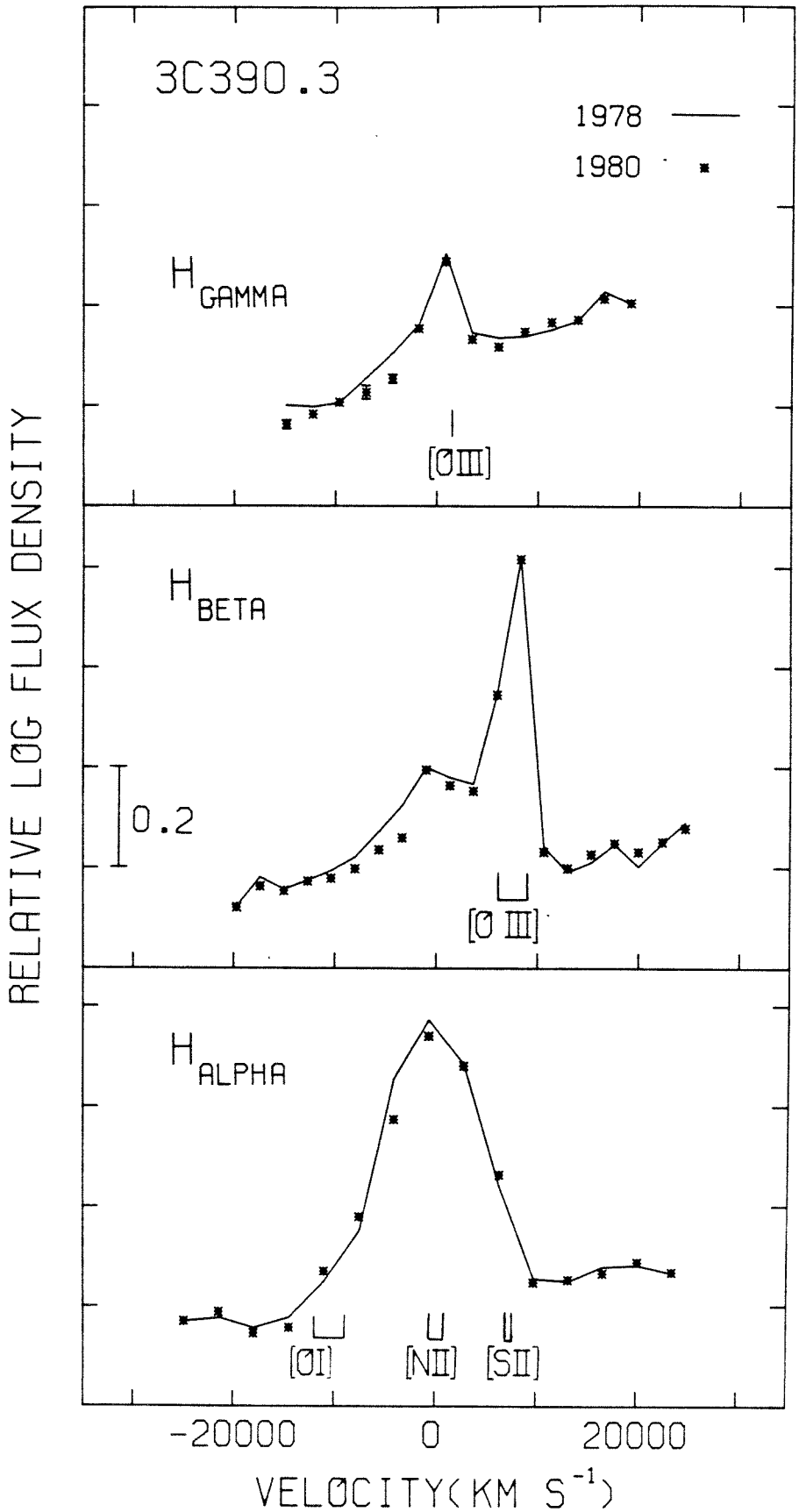
3C390.3
1978
1980
H GAMMA
[OIII]
H BETA
0.2
[O III]
H ALPHA
[OI]
[NII]
[SII]
RELATIVE LOG FLUX DENSITY
-20000
0
20000
VELOCITY(KM S-1)

Figure 4

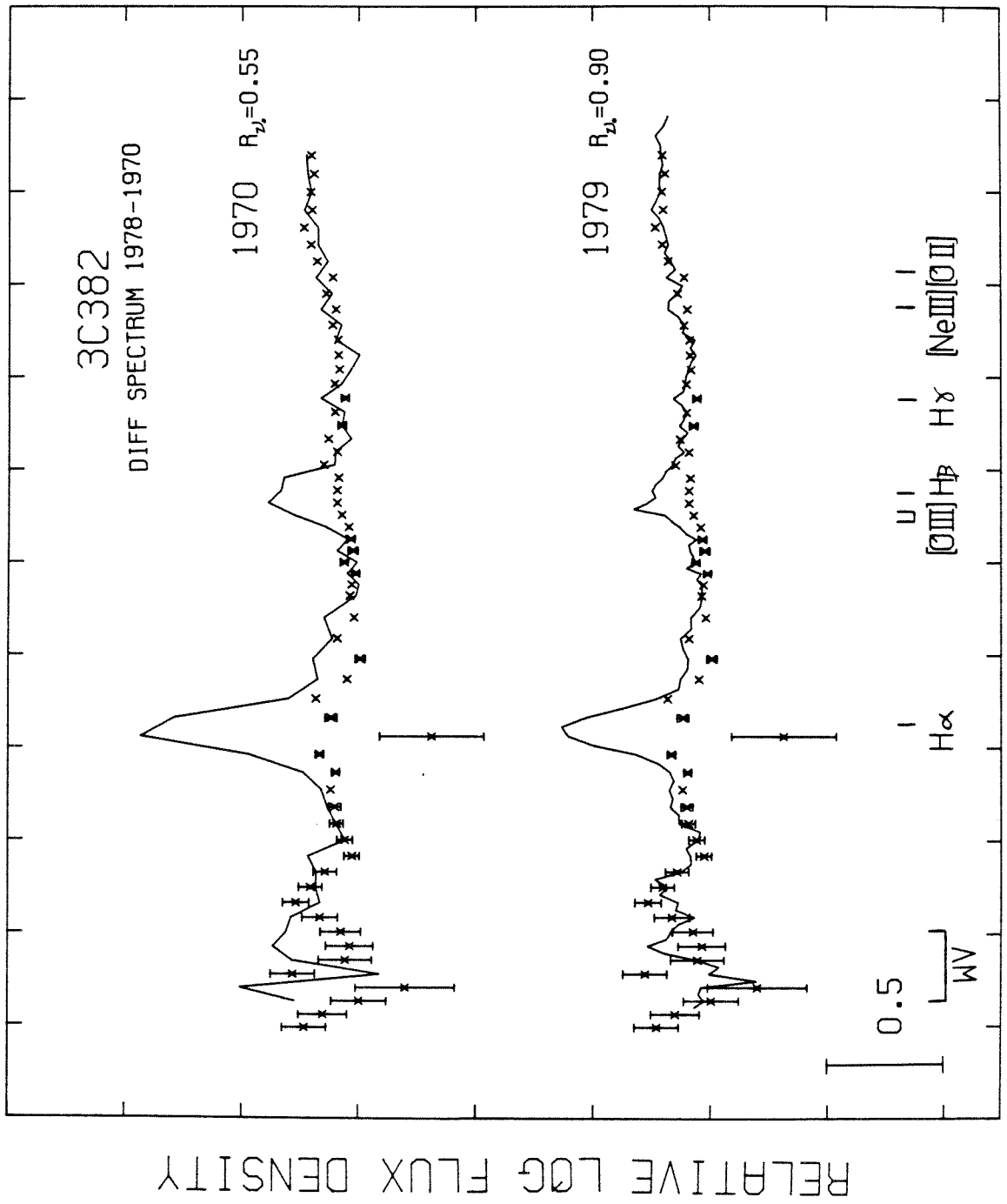
3C382
DIFF SPECTRUM 1978-1970
1970 $R_{2.}$=0.55
1979 $R_{2.}$=0.90
Hα
[OIII]Hβ
Hγ
[NeIII][OII]
0.5
1V
14.5
14.6
14.7
14.8
14.9
15.0
LOG FREQ(Hz)
RELATIVE LOG FLUX DENSITY

Figure 5a

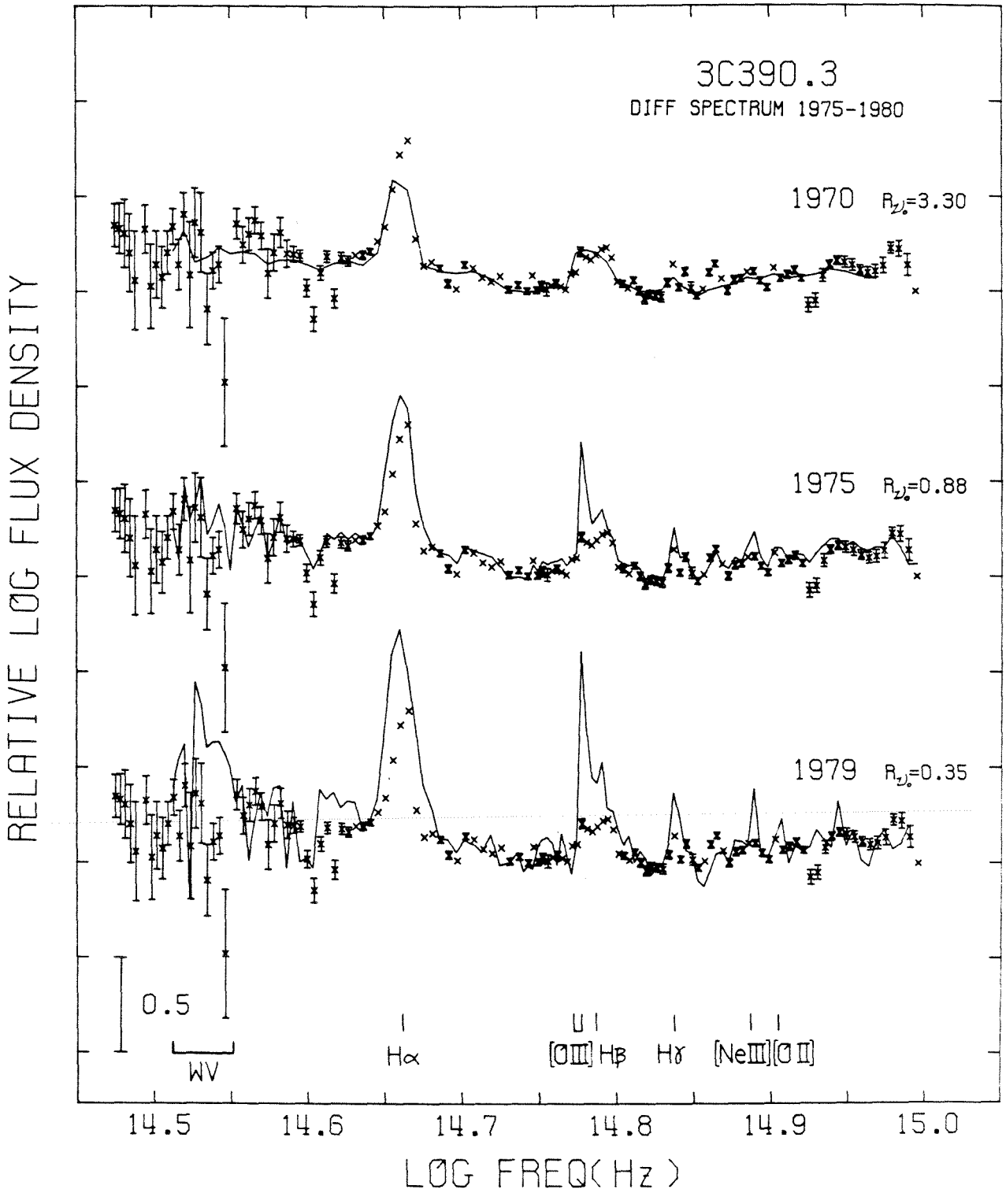
3C390.3
DIFF SPECTRUM 1975-1980
1970 R$_{2,1}$=3.30
1975 R$_{2,1}$=0.88
1979 R$_{2,1}$=0.35
RELATIVE LOG FLUX DENSITY
0.5
WV
Hα
[OIII] Hβ
Hγ
[NeIII][OII]
14.5
14.6
14.7
14.8
14.9
15.0
LOG FREQ(Hz)

Figure 5b

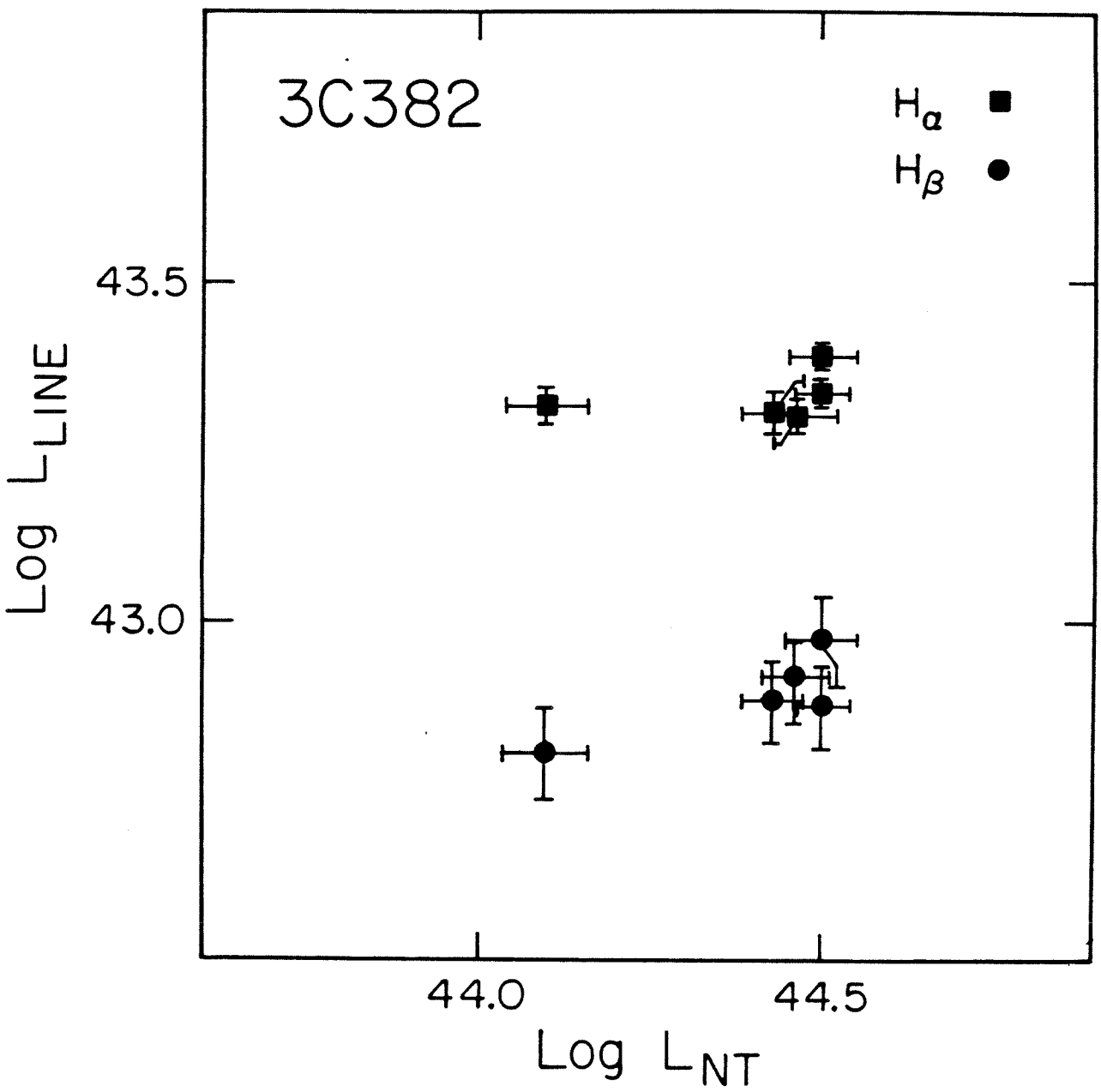

Figure 6

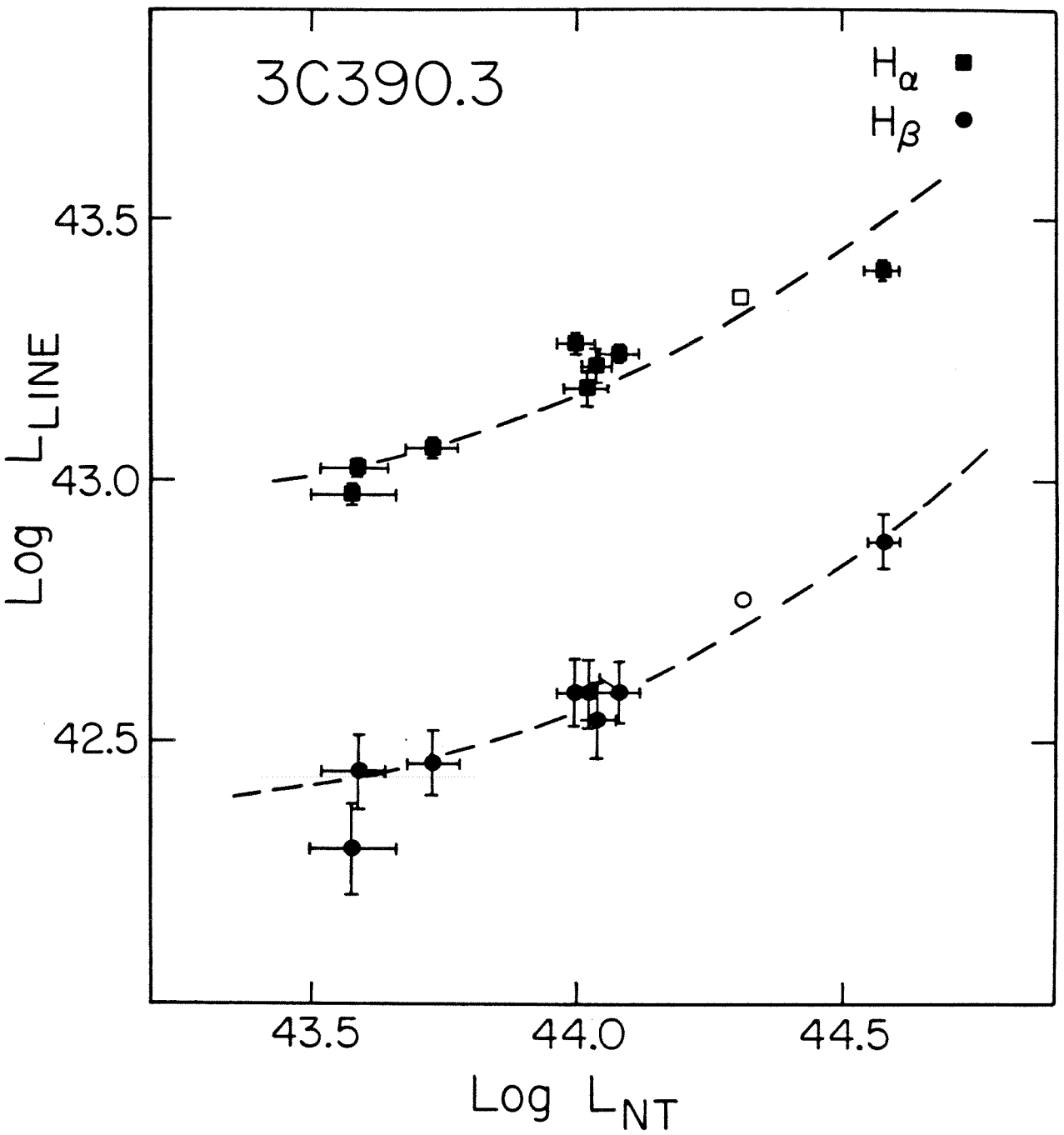

Figure 7

CHAPTER 4

SURFACE PHOTOMETRY OF MARKARIAN SEYFERT GALAXIES

I. Introduction

Currently, the study of active galactic nuclei focuses mostly on the spectrophotometric properties of the nucleus of these objects. The host-galaxy has received only limited attention. Adams (1977) has studied the morphology of an extensive number of Seyfert galaxies using large scale image-tube pictures, but little or no quantitative work has been done.

One important problem that can be addressed by studying the underlying galaxies of Seyfert and N-galaxies is how they compare with normal galaxies. Other properties such as the color and the magnitude of the galaxy component can be obtained to provide constraints in decomposing the spectrum of the nuclear region. Proper decomposition of the optical spectrum is important since along with spectrophotometry data in the uv and x-ray one can then obtain a more complete spectrum of the nucleus for the modelling of the central energy source of these objects.

In this chapter, some preliminary results from a study of surface photometry of Seyfert galaxies using data from 10 Markarian galaxies, are presented. These objects were chosen arbitrarily from the list in Adams (1977), and are part of an intended larger study that will include most of the galaxies in the list. It is found, within this small sample, that properties such as color, scale length, total brightness, surface brightness of the underlying galaxies do not depart systematically from those of the normal luminous spiral galaxies. There is a moderate range of color in the host-galaxies. This non-uniformity in color of the underlying galaxies does not affect the decomposition of the spectrum of type 1 Seyferts with a strong nuclear continuum very much; however, it may severely affect that of type 2 Seyferts.

II. Observation and Data

The data were acquired using the cooled Direct SIT-vidicon Area Photometer (DSAP) (Kent, 1979) attached to the Cassegrain focus of the 1.5-meter telescope at Palomar Observatory during the nights of October 30, 31 and November 1, 1979. The r, g and v filters (red, green and violet) of the system described in Thuan and Gunn (1976) were used. (The filter system will be referred to as the Gunn system in the remainder of the paper). For each object, three frames of each color were obtained. Since the original intention was to use the photometry to separate spatially the contribution of the nuclear and galaxy component, only short exposure frames were taken, so that the nucleus would not saturate the images. The silicon target is 256x256 pixels with a scale of 0.55" per pixel, giving a total field of view of 141"x141".

Listed in table 1 are the name of the objects in the program, the classification, the redshift, the galactic latitude and the night of the observation. The observing conditions for all 3 nights were similar -- clear sky but with poor seeing. Estimating from stellar images, seeing on the first two nights was around 3 to 4 arc seconds (fwhm), and on the third night about 2 to 3 seconds of arc.

The data were reduced by standard techniques (see Kent, 1979; and Hoessel, 1980) to the standard star table listed in Thuan and Gunn (1976). Each night, 5 to 8 standard stars were observed in each color throughout the night. The frames were stacked to obtain better signal to noise ratio in the surrounding nebulosity. Because most of the objects are small in angular extent, local sky subtraction using a ring around the object could be performed.

Surface profiles for each object are obtained in the following manner. Due to the low surface brightness of the nebulosity relative to the nucleus, it is necessary to obtain the profile by integrating the brightness in concentric circles to minimize

the noise. A surface profile is then found by differentiating the integrated magnitudes obtained within circular apertures of various sizes. Examples of the profiles are shown on figure 1. Color gradients are also formed using the profiles. Examples are plotted in figure 2. Note that near the nucleus, the seeing disk affects the color gradient enormously, because from comparing star profiles, the v color images have a considerably larger seeing disk than that of the r and g images.

Also listed in table 1 for each object are integrated magnitudes for each color within a 10" aperture. The integrated photometry is estimated to be accurate to about 5%. This is estimated from the r.m.s. deviation of the standard stars observed. Internally, from comparing the photometry of the two objects (Mkn 1 and Mkn 79) that were observed on more than one night, we see that they agree to within 2% in all three colors, well within the estimated uncertainty.

Since one of the objectives is to apply the surface photometry to decompose the spectral energy distributions of the nucleus of these galaxies as obtained with the Multi-channel-spectrophotometer (MCSP) on the Hale 5.08-meter telescope of Palomar Observatory by others (Neugebauer *et al.*, 1976; de Bruyn and Sargent, 1978), transformations between the MCSP photometry and the Gunn system are desirable. Due to a lack of the necessary data, only approximate transformations between the two can be obtained. Integrated magnitudes in the MCSP system of stars from the standard table of Thuan and Gunn (1976) are obtained by applying the transfer functions for the Gunn filters as published in Thuan and Gunn to MCSP scans of the stars. These transfer functions are for the filters plus one reflection off aluminum and an S-20 photocathode, and can only be regarded as approximations for the Direct-SIT Area Photometer. Using five standards (BD+17°4708, HD19445, Fiege 34, BD+28°4211, and Ross 451) having g-r color ranging from -0.86 to +1.18 , the following transformations are obtained:

$$r_M - r_G = -0.15 + 0.06\,(g-r)_G \qquad (1)$$

$$g_M - g_G = 0.05 + 0.07\,(g-r)_G \qquad (2)$$

$$v_M - v_G = 0.51 + 0.06\,(v-g)_G \qquad (3)$$

where the subscript G and M stand for the magnitude in the Gunn system and the integrated magnitude from MCSP scans, respectively. The following notations will also be used: for a color band designated with two subscripts, the first one refers to the system in which it was measured, and the second one refers to the system to which it has been transformed. Thus, r_{GM} represents an r magnitude obtained in the Gunn system (with the Direct-SIT Area Photometer) and transformed to the MCSP system.

For comparison of the photometry, listed in table 1 for each object and color, are the direct-SIT magnitudes transformed to the MCSP system and the integrated MCSP magnitudes obtained from 10" scans from Neugebauer *et al.* (1976), de Bruyn and Sargent (1978), and Oke and Goodrich (1980) and Oke (private communication). The accuracy of the transformations is about 0.05 to 0.1 magnitude. For spectra with strong emission lines, as in the case of Seyfert galaxies, there are additional uncertainties, since only approximate transfer functions for the filters and instrument are used. Hence, when comparing these magnitudes, an uncertainty of at least 0.1 magnitude can be expected. For the majority of the objects, the photometry obtained from the SIT-camera and the MCSP scans agrees to within the expected uncertainty. For at least two objects, Mkn 79 and Mkn 358, and possibly a third, Mkn 376, the discrepancies in photometry between the two systems can probably be attributed to brightness variations in these objects. This is supported also by the fact that the discrepancies in all three objects are color dependent, in the sense that the disagreement in the blue is always larger than that in the red. This is the same pattern that one would expect from a variable active galaxy that is

composed of a variable blue nuclear component and a constant galaxy component, e.g., as observed in 3C 390.3 and 3C 382 (Yee and Oke, 1980).

III. Morphorlogy

A detailed study of the morphology of Seyfert galaxies has been undertaken by Adams (1977). All objects studied in this paper are described there. Only a brief summary will be offered here.

Adams (1977) concluded that most Seyfert galaxies (~ 90%) are spiral galaxies, or at least do not appear to be elliptical galaxies. From the descriptions of Adams, of the objects here, Mkn 79, Mkn 348, Mkn 358 have well defined spiral arms; Mkn 9, Mkn 372 and Mkn 376 have some observable structure; and Mkn 352 is surrounded by an amorphous body, which may contain both a bulge and a disk component. There is no deep plate of Mkn 335, which appears stellar in the Palomar Optical Sky Survey (POSS) print. The short exposure frames obtained with the SIT camera show only slight suggestion of nebulosity surrounding the object. Mkn 374 has a double nucleus, and the SIT photometry show that the off-center nucleus is considerably redder than the central nucleus.

IV. Properties of the Underlying Galaxies

There are fundamental difficulties in studying the host-galaxies of Seyfert galaxies. These arise from the combination of the dominance of the nonthermal radiation from the nucleus and the large cosmological distance of most of these objects. Thus, for the majority of the known Seyfert galaxies, the nucleus significantly contaminates the inner region, such as the bulge, of the galaxy. These difficulties were compounded by the poor seeing condition under which the data

were taken. While these conditions make decomposition of the nuclear and galaxy component directly from the surface profiles very difficult, if not impossible, nevertheless, other properties of the galaxies can be obtained. Here, a study utilizing mostly the outer region (5 to 20 seconds of arc from the nucleus) is presented.

a) Surface Profile

Surface profile of spiral and S0 galaxies can be fitted by using two components – a bulge and an exponential disk of the form $I(r) = I_0\, e^{-\frac{r}{r_0}}$ (e. g., see Kormendy 1977). Because of the bright nucleus, the bulge is mostly obscured in our sample of galaxies, and only the disk component can be obtained. The outer part of the g band profile of each galaxy which is not influenced by either the nucleus or the bulge is fitted to an exponential law. An area is considered to be freed of contamination from the nucleus if the color gradient becomes rather flat and smooth, and it is considered to be outside the bulge if the profile in fact fits an exponential law. The scale length r_0 in kpc, (assuming a cosmological distance for the galaxy inferred from the redshift using $H_0 = 55$ km s^{-1} Mpc^{-1}), and the central brightness $B_0(c)$, (expressed in the B magnitude of the UBV system in magnitude per square arc second), are listed in table 2. $B_0(c)$ is obtained from the g band results by using the transformation between the Gunn System and the UBV system in Thuan and Gunn (1976). Due to the short exposure time and the contamination of the nucleus, usually only a small part of a profile (between 5 to 15" in radius) can be used for the fit. Thus, the uncertainties in the parameters are typically large (~ 20 to 30%), especically for those galaxies with small scale length.

For 28 out of a sample of 36 spiral and S0 galaxies, Freeman (1970) found $B_0(c)$ to be 21.65 ± 0.30. There are questions as to what is responsible for this uniform brightness scale in all observed spiral galaxies (Kormendy, 1977) which we will

not address here. The sample in this study gives an average $B_0(c)$ of 21.5± 0.4, whichis in agreement with that obtained for normal spirals. Also, the typical scale length derived by Freeman (1970) is 1 to 5 kpc. Again, the scale lengths of the sample of Seyfert galaxies fall within the range of the normal spirals, even though, on the average, they tend to be on the large end. This is probably at least in part due to a selection effect, since a host-galaxy with a small scale-length can be easily overwhelmed by its nucleus and hence may not be recognized as a galaxy. Using the fit to the disk component, a crude estimate of the total brightness of the underlying galaxy can be obtained. For each galaxy, an integrated disk magnitude in the g band is obtained by integrating the exponential disk fit within the Gunn and Oke (1976) standard metric diameter of 32 kpc. Since the bulge components are obscured, some estimate of their contribution is needed. Yoshizawa and Wakamutsu (1975) found that there is a large spread of bulge to disk ratio which ranges from 0.007 to 0.8 in a sample of 24 spiral galaxies. By assuming a bulge to disk ratio of ~ 0.3, an estimate within 30 to 40% (~ 0.4 mag) of the true total brightness can be obtained. The g band magnitudes obtained this way are corrected to V magnitudes of the UBV system using the transformations in Thuan and Gunn (1976). They are listed as M_V in table 1 after converted to absolute magnitudes using $H_0 = 55$ km s^{-1} Mpc^{-1}. An upper brightness limit for M_V is obtained for Mkn 335 which appears stellar in POSS print, by using the rather noisy profile beyond the nucleus. These magnitudes are similar to those of the luminous spiral galaxies, which range from -18 to -23 mag. Comparing them with the elliptical galaxy component of the radio galaxies obtained in Yee and Oke (1978), the Markarian Seyfert galaxies have a larger range of absolute magnitude, but the average M_V of $\sim$-20.7 for the sample is considerably fainter than -22.0 obtained for the radio galaxies.

In figure 3, the absolute magnitudes of the Seyfert galaxies are plotted against the quantity L_{NT}, the integrated luminosity of the nuclear component between $\log \nu = 14.52$ to 15.00 obtained by Yee (1980) by a crude power-law model fitting procedure. For comparison, the same quantities obtained for the radio galaxies in Yee and Oke (1978) are also plotted. For the Markarian Seyferts, there is no correlation between the total brightness of the underlying galaxy and the luminosity of the nuclear component. The same result was also obtained by Yee and Oke (1978) for radi galaxies. The points, however, do appear to fall below an upper limit formed by a 45° line as drawn approximately in figure 3. This can be attributed to the selection-effect from the definitions for active galactic nuclei and quasars. In an object with luminosity such that it falls in the region above the 45° line, the nucleus is probably bright enough so that, at moderately large cosmological distance, the object would appear point-like and hence be classified by its appeareance as a quasar. The three points above the 45° line in figure 3 belong to 3C 109, 3C 234 and Mkn 335 for which only upper limits of the brightness of the galaxy can be obtained. These three objects in fact are described in Wyndham (1964) (for 3C 109), Matthews Morgan and Schmidt (1964) (for 3C234) and Adams (1977) (for Mkn 335), as stellar-like with little or no fuzziness around them in POSS prints.

b) Color of the Underlying Galaxy

The color of the underlying galaxy is of primary interest when one wants to decompose the spectrum of an active galactic nuclei. In some previous works, (e.g., Yee and Oke, 1978; and Yee 1980), it was assumed that the underlying-galaxy has the same spectral energy distribution as that of an elliptical galaxy defined by averaging a number of first-ranking cluster elliptical galaxies (Yee and Oke, 1978). This clearly can present a problem in decomposing the energy distributions of the

Markarian Seyfert galaxies which are mostly non-ellipticals.

Surface photometry can provide a reasonable estimate of the color of the underlying galaxy. Since the data were acquired with rather short exposure time, to get a more reliable measure of the color of the galaxies, integrated magnitudes around rings of various sizes are used. For each object, the color gradient plot is examined to pick out the region closest to the center but is not contaminated by the nucleus. Thus, factors such as seeing and relative brightness of the nucleus affect the choices. Because of the poor seeing, the area used to determine the color of the host-galaxy is usually between 4 to 10" in radius from the center. The resultant g-r and v-r colors, transformed to the MCSP system are listed in table 2. The color has also been corrected for galactic reddening from our galaxy, but not for inclination of the underlying galaxy. For extinction correction for our galaxy, the absorption-free polar-cap model of Sandage (1973) is used for galactic latitude dependence, and Whitford's (1958) relation for color dependence. Two objects are not included: Mkn 335 does not have a convincing nebulous component, and Mkn 374 is confused by another object in the amorphous body of the host-galaxy. The accuracy of the color is estimated to be $\sim +0.1$ mag. Also listed in table 1, for comparison purpose, is the integrated MCSP color expected from the standard elliptical galaxy of Yee and Oke (1978) at the redshift of the respective object. For g-r, with the exception of Mkn 1 and Mkn 358, all have color comparable to the standard galaxy, although on the average they are slightly bluer (by < 0.1 mag). For v-r, however, with the exception of Mkn 372, all are signifigantly bluer than the standard galaxy by an amount ranging from 0.3 to 1.0 mag. The 8 galaxies have an average equivalent B-V color of $\sim +0.6$ mag, similar to that of intermediate- to late-type spiral galaxies (de Vaucouleurs, 1961).

In decomposing the continuum of Seyfert galaxies as done in Yee (1980), excess in the blue over the standard elliptical galaxy will have a large effect for at

least some objects. The color of the galaxies obtained from surface photometry does not necessarily represent the true integrated color of the underlying galaxies within, say, a 10" aperture -- the usual aperture used in MCSP observations. There are observations that the energy distribution of the bulge of spiral galaxies is similar to that of elliptical galaxies (Oke and Schwartzchild, 1975). The data of de Vaucouleurs (1961) on spiral galaxies show that the color of normal spiral galaxies becomes much redder near the central region. Thus, while the surface photometry shows that at a radius of ~ 5" (the size of aperture for the MCSP data), most of the galaxies observed in this program already have a color substantially bluer than that of a standard elliptical, the true integrated color of the underlying-galaxy is probably redder than the color obtained here. By using the color listed in table 2, we can estimate the maximum effect of the color of the galaxy on the method of decomposition of Yee (1980).

First, a pseudo-standard galaxy can be formed by adding a power-law: υ^{α} with spectral index α, to the elliptical standard so that the observed galaxy color is achieved. The parameter for this is R'_G, defined in the same way as R_{υ_0} in Yee and Oke (1978), the ratio of the power-law to standard galaxy component at the rest visual wavelength (λ=5450, $\log \upsilon_0 = 14.74$). If one then proceeds to fit the spectrum of the Seyfert galaxy using a power-law of spectral index α and the standard elliptical galaxy, R'_G is simply the over-estimate of R_{υ_0} committed by using an incorrect spectrum for the underlying galaxy. This is done for five galaxies. Of these, Mkn 1 and Mkn 348 are type 2 Seyferts with small excess in the blue (in the total spectrum). The other 3 are type 1 Seyferts, showing different amounts of excess in the blue from their MCSP scans. The results are listed in table 3. The uncertainties in R_{υ_0} for a fixed α is ~ 10%.

As expected, in type 1 Seyferts, where the nucleus is usually very bright, and

also much bluer than the galaxy, using the incorrect spectrum in the decomposition produces only a small error. For Mkn 376 and Mkn 352, where the nuclear radiation is very strong, an underestimate of even 1 mag in the color of the galaxy produces only a small effect of 10 to 20% in the fitting, which is within the uncertainty of determining R_{v_0} for a fixed α. For Mkn 358, a much weaker source, the effect is significant, but comparable to the uncertainty of the fit (which comes mainly from the inability to distinguish fits using different α's). The more interesting cases are the type 2 Seyferts. For both of these, R'_G is about the same as R_{v_0} , i. e., if we assume the integrated color within a 10" diameter to be the same as that of a ring at ~ 5" radius, there is no significant change of color in the continuum caused by the nuclear component. The large color change in the color gradients of these objects near the nucleus probably comes mostly from the strong emission lines which presumably only originate from the nucleus.

From these examples, it can be concluded that for type 1 Seyferts, where the central continuum is most likely very blue, using a galaxy with incorrect color in the blue for decomposing the energy distributions does not produce a pronounced effect in the result, unless the nuclear component is weak relative to the galaxy component. However, for type 2 Seyferts, which normally have a relatively weak nuclear nonthermal continuum, it may lead to meaningless results.

V. Summary

From a small sample of Markarian Seyfert galaxies, some preliminary results concerning the host-galaxies of these active nuclei are obtained. The underlying galaxies appear to have the same properties as those of the more luminous normal galaxies. Parameters such as scale length and central brightness of the disk, absolute magnitude, and color are similar to normal galaxies. As in the case for radio

galaxies, there does not seem to be a correlation between the brightness of the nulear component and the absolute magnitude of the underlying galaxy. The color of the host-galaxy outside the nuclear region is in general considerably bluer (by 0.3 to 1.0 in v-r) than an elliptical galaxy, which may produce erroneous results in decomposing MCSP scans of these objects if an incorrect spectrum of the underlying galaxy is used. Finally, it should be stressed that these results are based on a very small random sample; further study, using a larger sample, especially of type 2 Seyferts, and deeper images for the galaxy nebulosity is needed to verify some of these findings.

REFERENCES

Adams, T. F. 1977, Ap. J. Suppl., 33, 19.

Bruyn, A .G. de, and Sargent, W. L. W. 1978, A. J., 83, 1257.

Freeman, K. C. 1970 Ap. J., 160, 811.

Gunn, J. E., and Oke, J. B. 1975, Ap. J., 195, 255.

Hoessel, J. G. 1980, Ph. D. Thesis, California Institute of Technology.

Kent, S. M. 1979, P. A. S. P., 91, 394.

Kormendy, J. 1977, Ap. J., 217, 406.

Matthews, T. A., Morgan, W. W., and Schmidt, M. 1964, Ap. J., 140, 35.

Neugebauer, G., Becklin, E. E., Oke, J. B., and Searle, L. 1976, Ap. J., 205, 29.

Oke, J. B., and Goodrich, D. 1980, preprint.

Oke, J. B., and Schwartzschild, M. 1975, Ap. J., 198, 63.

Sandage, A. 1973, Ap. J., 183, 711.

Thuan, T. X. and Gunn, J. E. 1976, P. A. S. P., 88, 543.

Vaucouleurs, G. de 1961, Ap. J. Suppl, 5, 233.

Whitford, A. E. 1958, A. J., 63, 201.

Wyndham, J. D. 1966, Ap. J., 144, 459.

Yee, H. K. C. 1980, Ap. J., 241, in press (Nov).

Yee, H. K. C. and Oke, J. B. 1978, Ap. J., 226, 753.

---------- 1980, preprint, submitted to Ap. J..

Yoshizawa, M. and Wakamatsu, K. 1975, Astro. and Astrophys., 44, 363.

TABLE 1

Photometry

Object	Type	z	b_{II}	Date	r_G[a]	g_G	v_G	r_{GM}	g_{GM}	v_{GM}	r_M	g_M	v_M	Ref.[b]
MKN 1.....	Sy2	0.016	-29	Nov 1 1979	14.93	15.15	15.96	14.80	15.21	16.52	14.82	15.34	16,45	1
				Oct 31 1979	14.95	15.17	15.94	---	---	---	---	---	---	
MKN 9.....	Syl	0.0402	29	Oct 30 1979	14.46	14.59	14.52	14.32	14.65	15.03	14.32	14.75	15.06	3
MKN 79.....	Syl	0.0219	30	Nov 1 1979	14.03	14.35	14.44	13.90	14.42	14.96	13.67	14.28	14.58	4
				Oct 30 1979	14.05	14.33	14.42	---	---	---	---	---	---	
MKN 335....	Syl	0.025	-42	Oct 31 1979	13.51	13.50	13.28	13.36	13.54	13.78	13.64	13.60	13.72	2
MKN 348....	Sy2	0.014	-30	Oct 31 1979	14.52	14.94	15.68	14.40	15.02	16.24	14.40	15.06	16.23	2
MKN 352....	Syl	0.015	31	Oct 31 1979	14.54	14.85	14.85	14.41	14.92	15.36	14.33	13.83	15.15	2
MKN 358....	Syl	0.046	-31	Nov 1 1979	15.56	15.83	16.13	15.43	15.90	16.66	15.54	16.17	16.95	2
MKN 372....	Sy2?	0.029	-37	Nov 1 1979	14.87	15.47	16.15	14.75	15.56	16.71	14.82	15.64	16.90	2
MKN 374....	Syl	0.041	23	Nov 1 1979	14.83	14.14	15.27	14.69	14.21	15.78	14.66	15.16	15.56	2
MKN 376....	Syl	0.056	24	Nov 1 1979	14.30	15.55	15.54	14.17	14.62	15.05	14.07	14.46	14.83	2

Notes: a) Integrated magnitudes within a 10" aperture.
b) References for MCSP scans used for the integrated MCSP magnitudes: 1. Neugebauer et al. (1976), 2. de Bruyn and Sargent (1978), 3. Oke and Goodrich (1980), 4. Oke (private communication).

TABLE 2

Properties of the Underlying Galaxies

Object	r_o(kpc)	B_O(c)	M_V	Color of the underlying galaxy		Color of elliptical standard	
				$(g-r)_{GM}$	$(v-r)_{GM}$	$(g-r)_M$	$(v-r)_M$
MKN 1.....	3.0	21.5	-18.6	0.5	1.5	0.73	1.92
MKN 9.....	3.1	20.7	-21.5	0.7	1.5	0.75	2.06
MKN 79.....	6.1	21.4	-20.4	0.75	1.45	0.74	1.96
MKN 335....	---	--	>-20.5	—	--	--	--
MKN 348....	3.8	21.4	-18.8	0.6	1.5	0.73	1.91
MKN 352....	4.3	22.0	-18.5	0.6	1.3	0.73	1.91
MKN 358....	0.5	21.4	-23.0	0.4	1.4	0.76	2.10
MKN 372....	5.9	22.2	-20.8	0.75	1.9	0.74	2.00
MKN 374....	4.9	20.9	-22.0	—	--	--	--
MKN 376....	6.7	21.5	-22.3	0.6	1.2	0.77	2.15

TABLE 3

Parameters of Power-law Fit

Object	α	R_{ν_o}	R'_G	α	R_{ν_o}	R'_G	α	R_{ν_o}	R'_G
MKN 1.....	-1.0	0.30	0.39	0.0	0.20	0.15	+1.0	0.09	0.07
MKN 348....	-1.0	0.20	0.25	0.0	0.10	0.10	+1.0	0.05	0.05
MKN 352....	+1.5	0.55	0.07	+1.0	1.10	0.11	+0.5	1.70	0.16
MKN 358....	+1.0	0.20	0.11	+0.5	0.25	0.16	0.0	0.35	0.24
MKN 376....	+1.0	1.00	0.19	+0.5	1.60	0.30	0.0	>3.0	0.47

FIGURE CAPTIONS

Figure 1 - Examples of surface profiles of Markarian Seyfert galaxies. The ordinate is in units of magnitude per square arc second, and is marked in intervals of 1.0 magnitude with a reference surface brightness indicated for each object.

Figure 2 - Examples of color gradients of Markarian Seyfert galaxies. The ordinate is marked in intervals of 0.5 magnitude with red being upward. For each object, the +0.5 magnitude level is marked for reference.

Figure 3 - Estimated absolute magnitude of underlying galaxies versus nuclear continuum luminosity (L_{NT}) in units of ergs s^{-1} for radio galaxies and Markarian Seyfert galaxies.

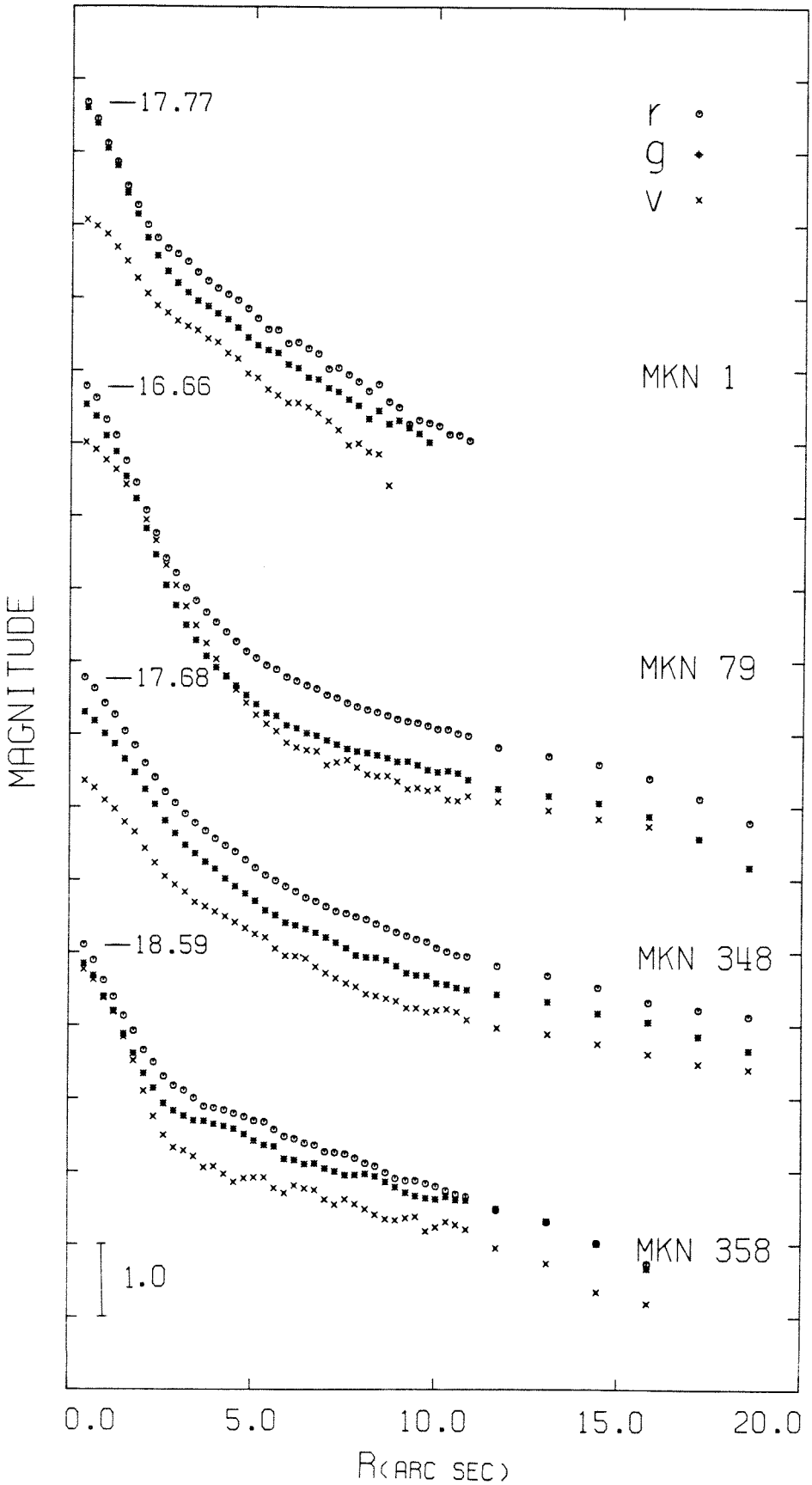
—17.77
r
g
V
MKN 1
—16.66
MKN 79
—17.68
MKN 348
—18.59
MKN 358
1.0
MAGNITUDE
0.0
5.0
10.0
15.0
20.0
R(ARC SEC)

Figure 1

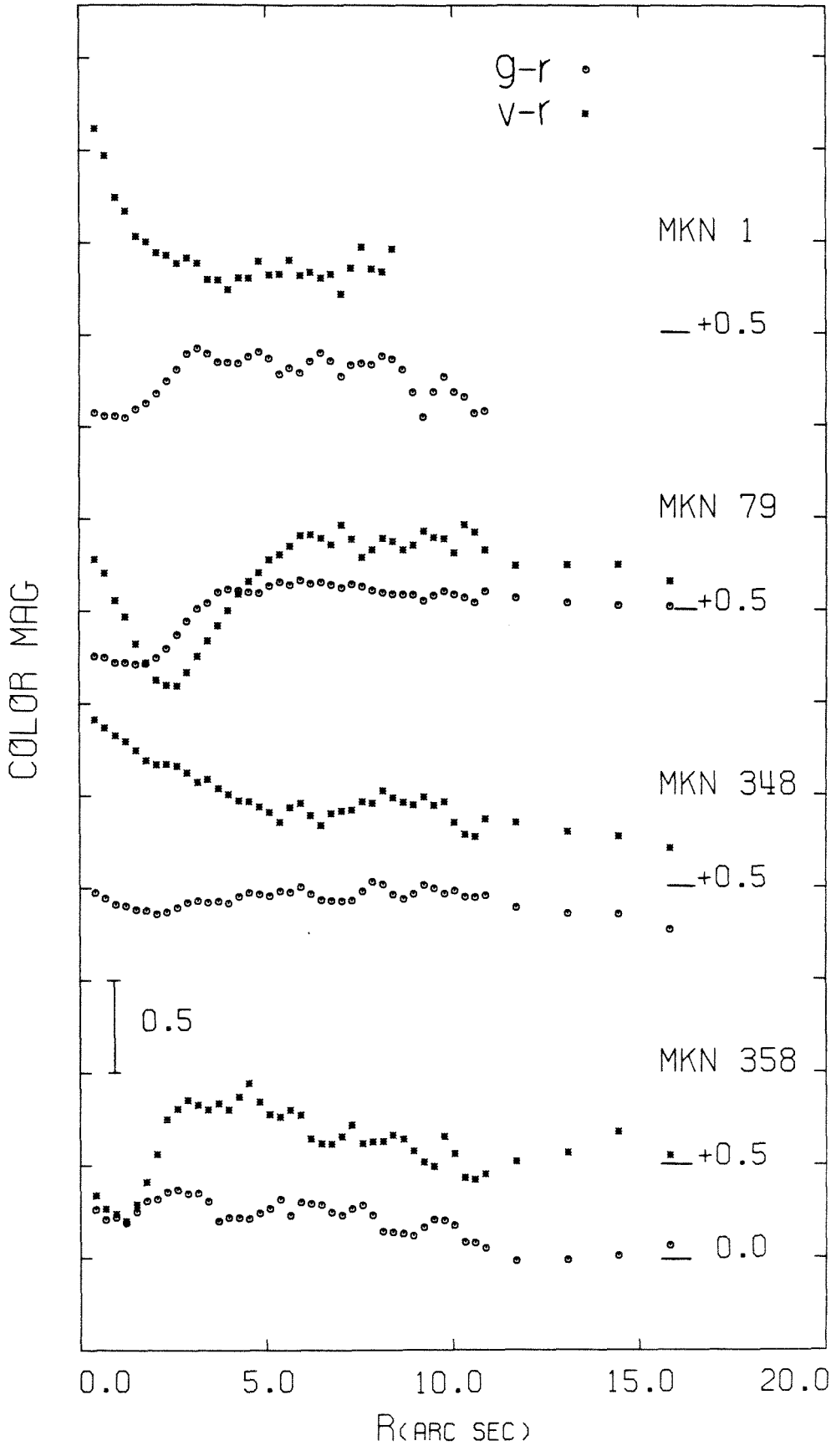
g-r
v-r
MKN 1
+0.5
MKN 79
+0.5
MKN 348
+0.5
0.5
MKN 358
+0.5
0.0
COLOR MAG
0.0
5.0
10.0
15.0
20.0
R(ARC SEC)

Figure 2

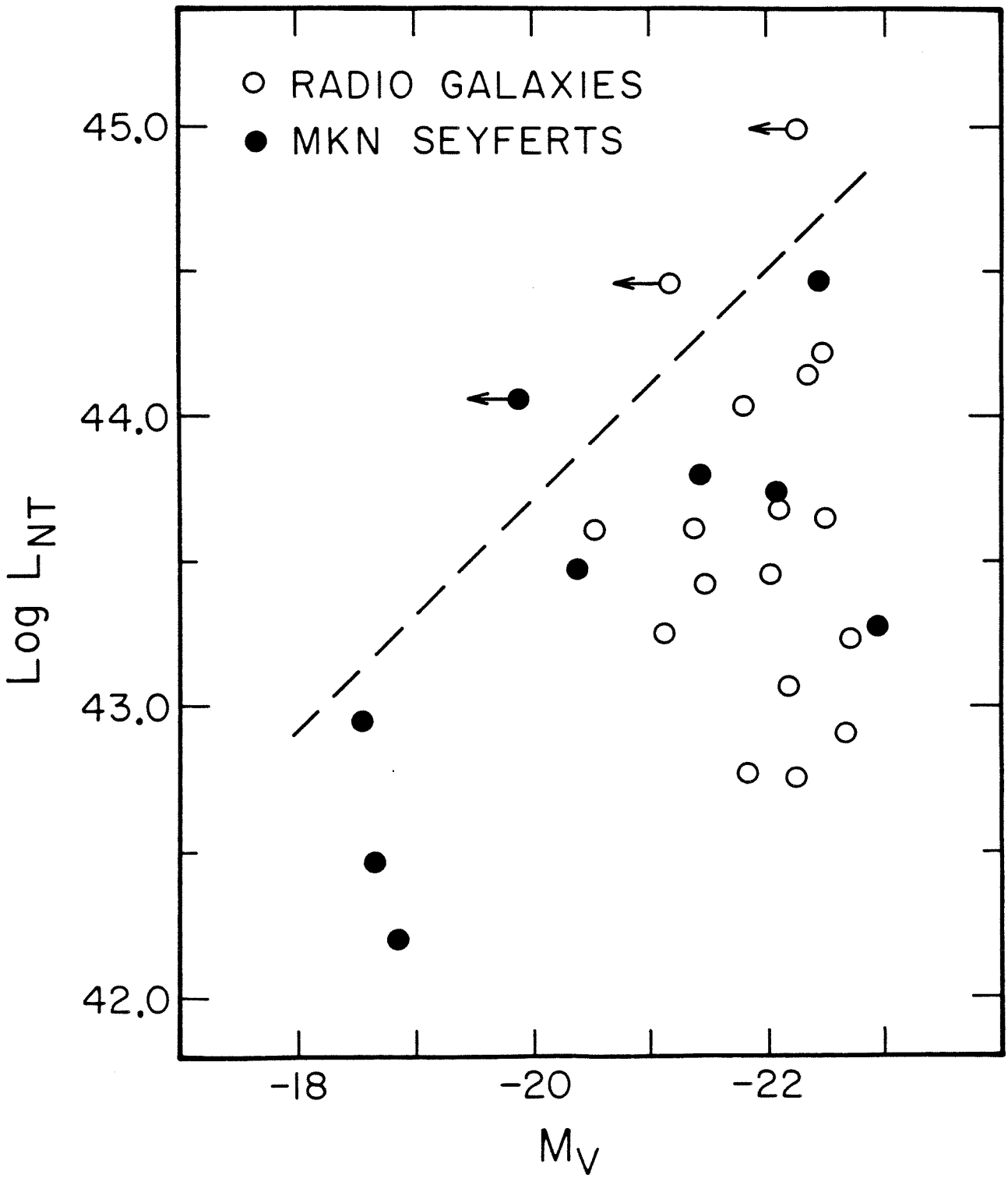
RADIO GALAXIES
MKN SEYFERTS
45.0
44.0
43.0
42.0
Log L_{NT}
-18
-20
-22
M_V

Figure 3